Critical Coupling and Synchronized Clusters in Arbitrary Networks of Kuramoto Oscillators

by

Brady Gilg

A Dissertation Presented in Partial Fulfillment
of the Requirements for the Degree
Doctor of Philosophy

Approved April 2018 by the
Graduate Supervisory Committee:

Dieter Armbruster, Chair
Hans Mittelmann
Anna Scaglione
Steven Strogatz
Bruno Welfert

ARIZONA STATE UNIVERSITY

May 2018

ABSTRACT

The Kuramoto model is an archetypal model for studying synchronization in groups of nonidentical oscillators where oscillators are imbued with their own frequency and coupled with other oscillators though a network of interactions. As the coupling strength increases, there is a bifurcation to complete synchronization where all oscillators move with the same frequency and show a collective rhythm. Kuramoto-like dynamics are considered a relevant model for instabilities of the AC-power grid which operates in synchrony under standard conditions but exhibits, in a state of failure, segmentation of the grid into desynchronized clusters.

In this dissertation the minimum coupling strength required to ensure total frequency synchronization in a Kuramoto system, called the critical coupling, is investigated. For coupling strength below the critical coupling, clusters of oscillators form where oscillators within a cluster are on average oscillating with the same long-term frequency. A unified order parameter based approach is developed to create approximations of the critical coupling. Some of the new approximations provide strict lower bounds for the critical coupling. In addition, these approximations allow for predictions of the partially synchronized clusters that emerge in the bifurcation from the synchronized state.

Merging the order parameter approach with graph theoretical concepts leads to a characterization of this bifurcation as a weighted graph partitioning problem on an arbitrary networks which then leads to an optimization problem that can efficiently estimate the partially synchronized clusters. Numerical experiments on random Kuramoto systems show the high accuracy of these methods. An interpretation of the methods in the context of power systems is provided.

I dedicate this work to my parents, Betty and Doug, and my brother Justin for all their love and support, as well as the support of all my friends and family.

Thank you to my advisor Dr. Armbruster for the many hours devoted to teaching me and for the opportunities I have been afforded. Thank you to Dr. Mittelmann for his helpful comments regarding optimization and the time he devoted to computing globally optimal solutions. Thank you to Dr. Scaglione and her students for the assistance in finding power systems test cases. Thank you to Dr. Welfert and Dr. Strogatz for their helpful comments on dynamical systems analysis. Thank to Dr. Kurths and the researchers at the Potsdam Institute for Climate Research for hosting me at their new facility. Thank you to Dr. Bullo and Dr. Jafarpour the invitation to visit UC Santa Barbara and for their insight into phase oscillator systems.

TABLE OF CONTENTS

CHAPTER Page

CHAPTER Page

LIST OF FIGURES

Figure Page

Chapter 1

INTRODUCTION

Synchronization is an emergent self-organizational phenomenon present in a variety of different natural systems. Metronomes, when set to different beats and placed on a movable surface will eventually synchronize to the same frequency (Strogatz, 2000). Pedestrians on a bridge may begin to walk in step with each other without any outside agent directing them. Fireflies will blink as a group even though they are without a leader. Electrical generators and loads will synchronize their operating frequencies when connected together by power lines. Some common characteristics between systems exhibiting synchronization are:

- Each agent in the system, when alone, exhibits periodic behavior. Metronomes beat, pedestrians walk with a consistent gait, fireflies blink, and AC electrical devices have a periodic voltage phase.

- The frequencies and phases of the periodic behavior can be different for each agent. Metronomes can be set to different rhythms, pedestrians have different preferred walking speeds, fireflies blink at different rates, and electrical devices operate at different power levels.

- There is some coupling mechanism by which information is transmitted between agents. Metronomes and pedestrians send vibrations through flexible surfaces, fireflies can see each other through line-of-sight, and electrical devices transmit power through transmission lines.

- Under appropriately high levels of similarity in agent's preferred behavior and

appropriately high amounts of coupling, agents will alter their behavior to match each other.

The example of a power grid has the additional property that coupling information is not transmitted between all agents simultaneously, but only through a network of power lines. Some nodes in the network may not have a direct connection to one another, but through an indirect path they may still be able to communicate and synchronize. In general, networks with a higher density of connections are more likely to lead to synchronization, but fascinatingly not all connections are created equal. Synchronization can occur with a remarkably sparse number of connections in a power grid if only the most important connections are chosen.

In power grid engineering, *frequency synchronization* is an important phenomenon in the study of faults and blackouts (Kundur *et al.*, 2004) because power grids operate using Alternating Current (AC). In an AC system, voltages of machines vary sinusoidally in time and the power flow between two machines is constrained by the phase difference between generator and load.

The Power-Angle equation is

$$P_e = \frac{|E^* V|}{x'_d} \sin(\phi - \psi)$$

where x'_d is the ransfer reactance between nodes, $V = |V|e^{i\psi}$ is the complex voltage at the terminal, and $E = |E^*|e^{i\phi}$ is the complex voltage at the transmitting node. Due to the $\sin(\phi - \psi)$ term, if the sending and receiving machines are not synchronized to the same frequency then the phase difference between them will be constantly changing from negative to positive and back again, and power cannot efficiently flow.

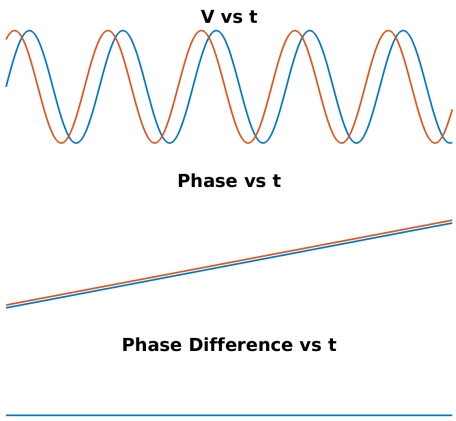

Figure 1.1: An example of frequency synchronization. The blue and orange voltage curves are frequency synchronized in time, so their phases grow at the same rate and the phase difference is constant.

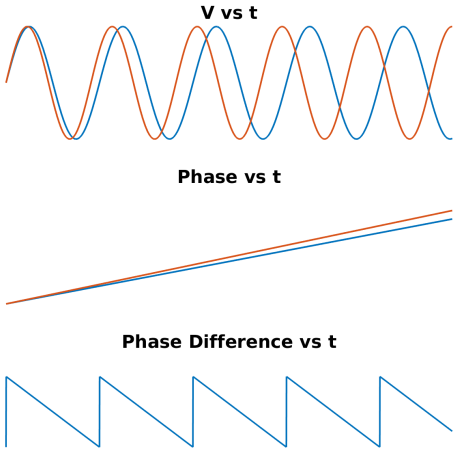

Figure 1.2: An example of unsynchronized frequencies. The blue and orange signals have phases that grow at different rates and so the phase difference grows also. The phase difference is shown modulo 2π, and repeatedly switches from positive to negative.

If two generators have a synchronized frequency as in figure 1.1 then power can

be transmitted between them. In normal operating conditions, every node in a power network should be synchronized to every other node so that power can freely flow to where it is needed. This ensures that there is no excess or lack of power at any particular location in the grid.

In this paper, we study the *network Kuramoto model*. The Kuramoto model is a simplified model of synchronizing phase oscillators with global coupling, and the networked version of the model restricts coupling to only occur between nodes in an associated graph. The model is significantly simpler than the true physics of a power grid, but it shares some essential similarities including the creation of islands of synchronized nodes when full synchronization of the entire system is not possible. We believe that a strong understanding of the network Kuramoto model is required before an equal level of understanding is possible in the power grid.

Chapter 2

THE NETWORK KURAMOTO MODEL

A network Kuramoto system is a collection of time-varying phase oscillators embedded in a network with coupling along edges. A given oscillator i has a constant internal driving frequency ω_i and a sinusoidal coupling to each of its neighbors in the network. The edge connections are represented through the symmetric network adjacency matrix A.

Definition 1. *A network Kuramoto system (A, ω) is a collection of phase oscillators with dynamics given by*

$$\dot{\phi}_i = \omega_i + \sigma \sum_j A_{ij} \sin(\phi_j - \phi_i) \tag{2.1}$$

Here $\phi_i \in \mathbb{R}$ is the phase of oscillator i, $\omega_i \in \mathbb{R}$ is the inherent driving frequency of node i, and $\sigma \in \mathbb{R}^+$ is the coupling strength.

The Kuramoto model is one of many models of synchronization on networks (Abrams *et al.*, 2016).

Definition 2. *The adjacency matrix $A \in \mathbb{R}_+^{N \times N}$ associated to a weighted graph is defined by*

$$A_{ij} = \begin{cases} w_{ij} & \text{if there exists an edge from node } i \text{ to node } j \\ 0 & \text{otherwise} \end{cases}$$

where w_{ij} is the weight of the edge from node i to node j. If A is symmetric, then we say the associated graph is undirected, and if all weights are 0 or 1, we say the graph is unweighted.

The network variant of the Kuramoto model has relevant applications to the electrical dynamics of power grids. In (Nishikawa and Motter, 2015), Nishikawa and Motter present a standardized description of power grid modeling techniques, and the key properties of their framework are that each generator or load in the system represents a node in an associated network, that each node is modeled by a phase variable, that the phase at each node has dynamics based on a combination of internal and external dynamics, and that the external dynamics are proportional to the phase difference across an edge in the network.

Under the Nishikawa/Motter modeling framework a network Kuramoto system can readily be seen as a simplified power grid model without any inertial term. With this interpretation of the network Kuramoto model, ϕ_i can be interpreted as the complex power angle of node i, ω_i as the internal power created or drawn by node i (positive for generators, negative for loads), and $\sigma * A_{ij}$ as the admittance of the electrical line between nodes i and j, if such a line exists.

2.1 Synchronization in the Kuramoto model

In the Kuramoto model, it is important to distinguish between different types of synchronization.

Definition 3. *Two nodes i and j are phase synchronized if their phases are asymptotically identical modulo 2π, i.e., given $\epsilon > 0$, there exists a time $T > 0$ such that*

$$|\phi_i - \phi_j| \pmod{2\pi} < \epsilon \quad \forall t > T.$$

We say that a Kuramoto system is phase synchronized if all nodes in the system are.

Definition 4. *Two nodes i and j are frequency synchronized if their phase difference is bounded in time, i.e.*

$$\limsup_{t\to\infty} |\phi_i - \phi_j| < \infty.$$

We say that a Kuramoto system is frequency synchronized if all nodes in the system are.

It is well known(Rodrigues *et al.*, 2016) that it is only possible for a Kuramoto system to fully phase synchronize if all oscillators have identical internal frequencies ω, or in the infinite coupling limit. We only study systems of nonidentical oscillators with finite coupling, so we will primarily refer to frequency synchronization. When discussing frequency synchronization it is convenient to define the long-term frequency of an oscillator (Ottino-Löffler and Strogatz, 2016).

Definition 5. *The long-term frequency of oscillator i is*

$$\lim_{t\to\infty} \frac{\phi_i}{t}.$$

It is a trivial observation that two oscillators have identical long-term frequencies if they are frequency synchronized. For intermediate levels of coupling the network Kuramoto model exhibits an islanding behavior, wherein some subsets of oscillators group together in frequency-synchronized clusters.

Definition 6. *A frequency-synchronized cluster is a maximal set of frequency-synchronized oscillators in a Kuramoto system.*

Our definition of a cluster is based on long-term frequencies rather than restrictions on the oscillator's phases (Favaretto *et al.*, 2017b) or their decay rates to equilibrium (Romeres *et al.*, 2013). Frequency synchronization can also be interpreted as an equivalence relation on the set of Kuramoto oscillators. Clusters are then the

equivalence classes of this relation and partition the set. It is important to recognize that the definitions of frequency synchronization and cluster synchronization are based on the trajectories of the oscillators in the system, and therefore vary when the initial conditions change, when the coupling strength σ changes, and ultimately depend on the solution curves for the dynamical system.

A similar concept occurs in a power grid when a fault occurs in a power grid. Initially, power grids are designed to be totally frequency synchronized and the entire network will be one large cluster. If the fault is not immediately corrected, phase instability can cause the grid to split into frequency-synchronized *islands*, where some parts of the system are electrically disconnected from others (FERC, 2012). The islands can still be connected physically, but without proper synchronization the amount of power that can flow between islands is severely limited and inconsistent. The network structure, power loads, and power generators all play a role in determining what islands will form. It is generally preferred that if a fault is unavoidable, the bulk of the network remain synchronized while a small section (possibly a single city, neighborhood, or even a single generator) form a separate cluster. However, it can happen that the clusters are the sizes of entire states or countries. If this occurs, it can be a major undertaking to re-synchronize the network. Predicting which clusters will form in a blackout is therefore a key planning step when preparing for future power blackouts. We believe that methods for determining synchronized clusters in the Kuramoto system could be useful in the future for performing the same task with power grids.

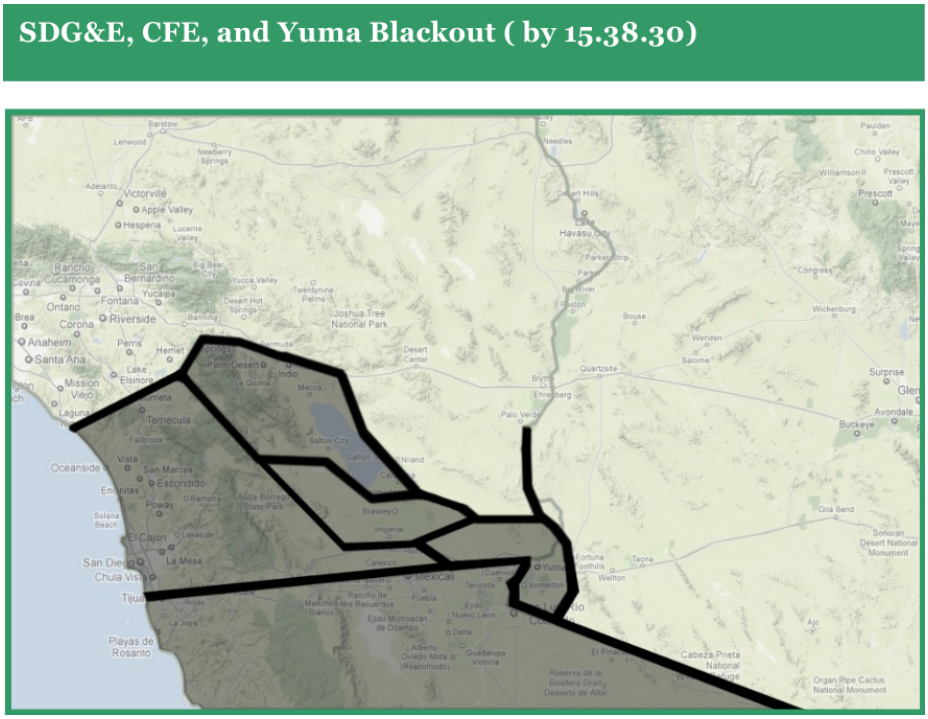

Figure 2.1: Frequency-synchronized islands in the 2011 southwest blackout FERC report (FERC, 2012).

To investigate the Kuramoto model's dependence on initial conditions, we created 1000 Kuramoto systems by generating a random connected Erdős–Rényi graph on 25 nodes and 40 edges and associated to each of them a uniformly randomly vector of frequencies. The critical coupling was computed for each system by iteratively running simulations at different values of σ. Finally, each system was simulated at a coupling 0.1% higher than the critical coupling with 1000 uniformly random initial conditions. We found that in 88.3% of systems, all 1000 initial conditions converged to the same fixed point. In the remaining systems an average of 86.0% of initial conditions converged to the same fixed point. This experiment provides strong evidence that when a stable fixed point exists in a Kuramoto sytem it is usually globally stable, and even when it isn't the stability basin occupies a majority of the

state space. However it is important to note that with other random graph structures such as ring graphs, the dependence on initial conditions can be much more severe (Wiley *et al.*, 2006) (Ottino-Löffler and Strogatz, 2016).

The bulk of this work will be to examine how frequency-synchronization in the network Kuramoto model varies with the coupling strength, and to attempt to predict the frequency-synchronized clusters without finding solution curves.

2.2 Example Systems

Consider a simple Kuramoto system on $N = 2$ nodes, with adjacency matrix $A = \begin{pmatrix} 0 & 1 \\ 1 & 0 \end{pmatrix}$ and frequencies $\omega = \begin{pmatrix} 1 \\ -1 \end{pmatrix}$. The dynamics of the system are given by

$$\dot{\phi_1} = 1 + \sigma \sin(\phi_2 - \phi_1)$$
$$\dot{\phi_2} = -1 + \sigma \sin(\phi_1 - \phi_2).$$

We will investigate the behavior of the system as the parameter σ varies. Set the initial conditions $\phi_1(0) = \phi_2(0) = 0$ and vary σ.

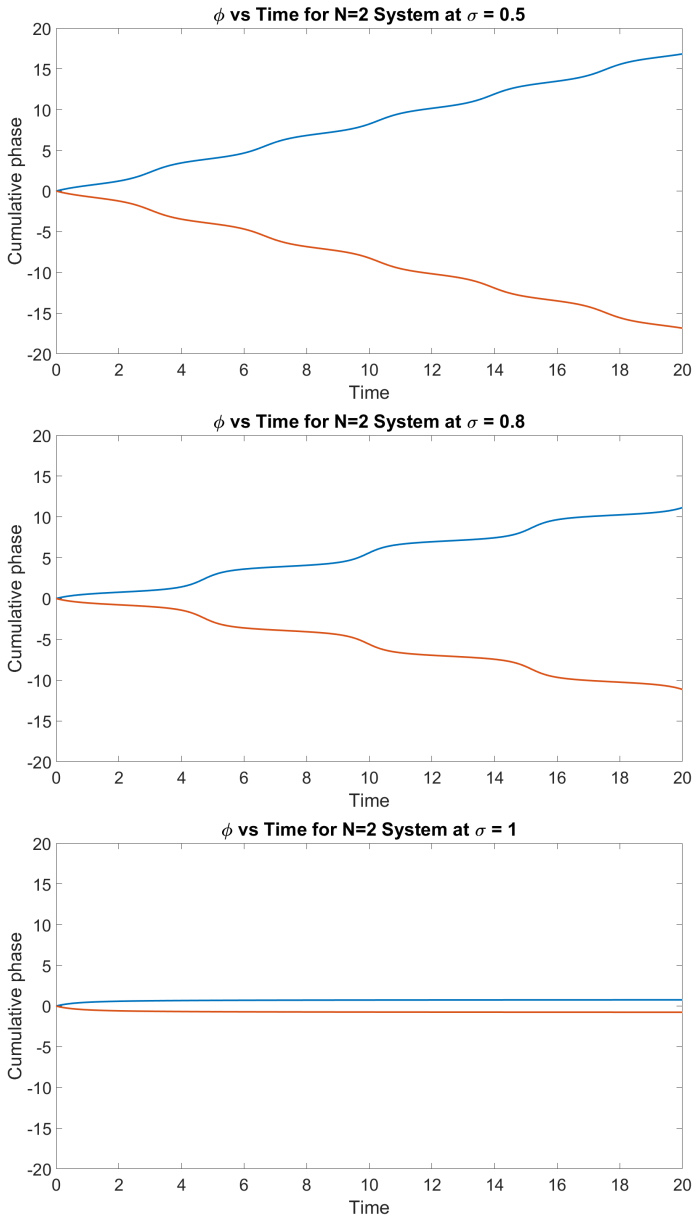

Figure 2.2: A comparison of the cumulative phase vs time for a Kuramoto system of two nodes at different coupling strengths. As the coupling increases, the long-term frequencies of each node converge. As σ approaches 1, the long-term frequencies approach 0. This is the onset of synchronization.

Simulations show that this system settles into a consistent periodic pattern. The

long-term behavior of the system is a mostly linear change in ϕ (equivalent to a mostly constant angular frequency) with fluctuations occurring as the phases mod 2π move past each other on the unit circle. The magnitudes of the long-term frequencies have a decreasing dependence on the coupling σ, and as σ approaches 1, the long-term frequencies for both nodes approach 0. For $\sigma \geq 1$, the system is totally synchronized and exhibits a fixed point. The fixed point corresponds to frequency synchronization but not phase synchronization, as the phases are still different for each node. This difference is again a function of σ.

The dependence on σ is more easily observed by plotting the long-term frequencies $\lim_{t\to\infty} \frac{\phi}{t}$ for each node vs. σ. We call this plot the *frequency bifurcation diagram.*

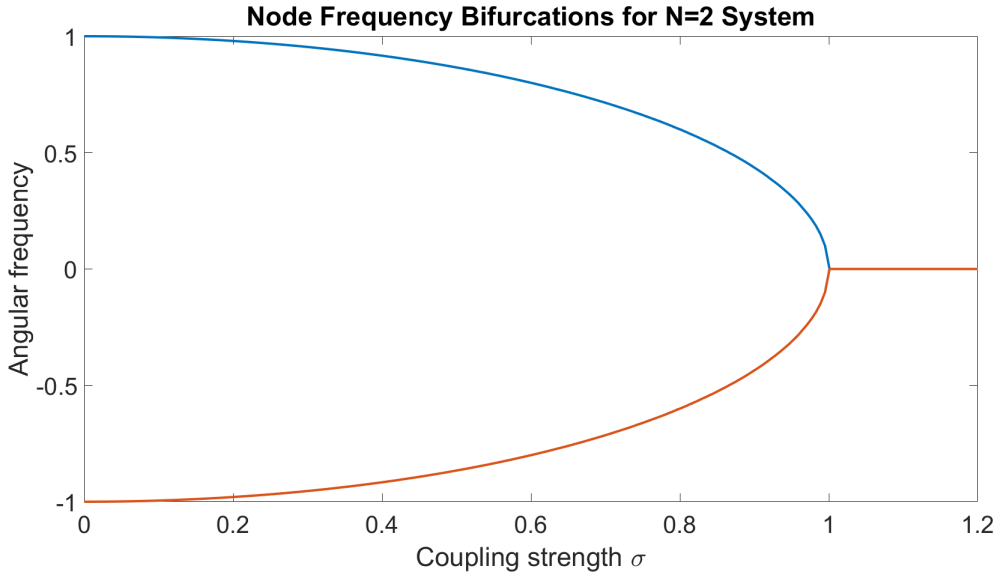

Figure 2.3: Frequency bifurcation diagram for a Kuramoto system with two nodes. For 1000 choices of σ the system was simulated numerically forward in time until a limit T, where T is sufficiently large such that all transients have decayed to zero. The first 50% of each simulation was thrown out to remove any remaining transient behavior and the ending 50% was used to estimate the long-term frequency of each oscillator, plotted on the vertical axis.

In figure 2.3 we see that the magnitudes of the long-term angular frequencies of both nodes in the $N = 2$ system decrease as σ increases, eventually achieving frequency synchronization at $\sigma = 1$, exactly as we observed from the phase plots.

Next consider a random connected Erdős–Rényi graph with $N = 25$ nodes, $M = 40$ edges, and uniformly random frequencies.

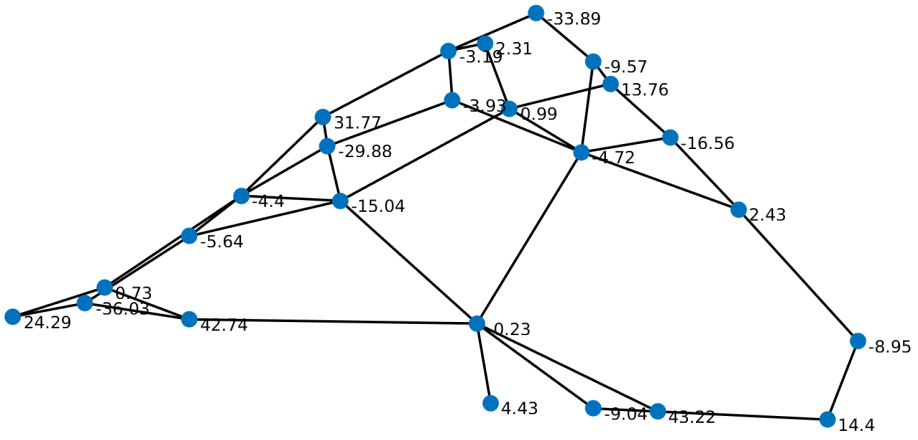

Figure 2.4: The randomly generated Kuramoto system on 25 nodes.

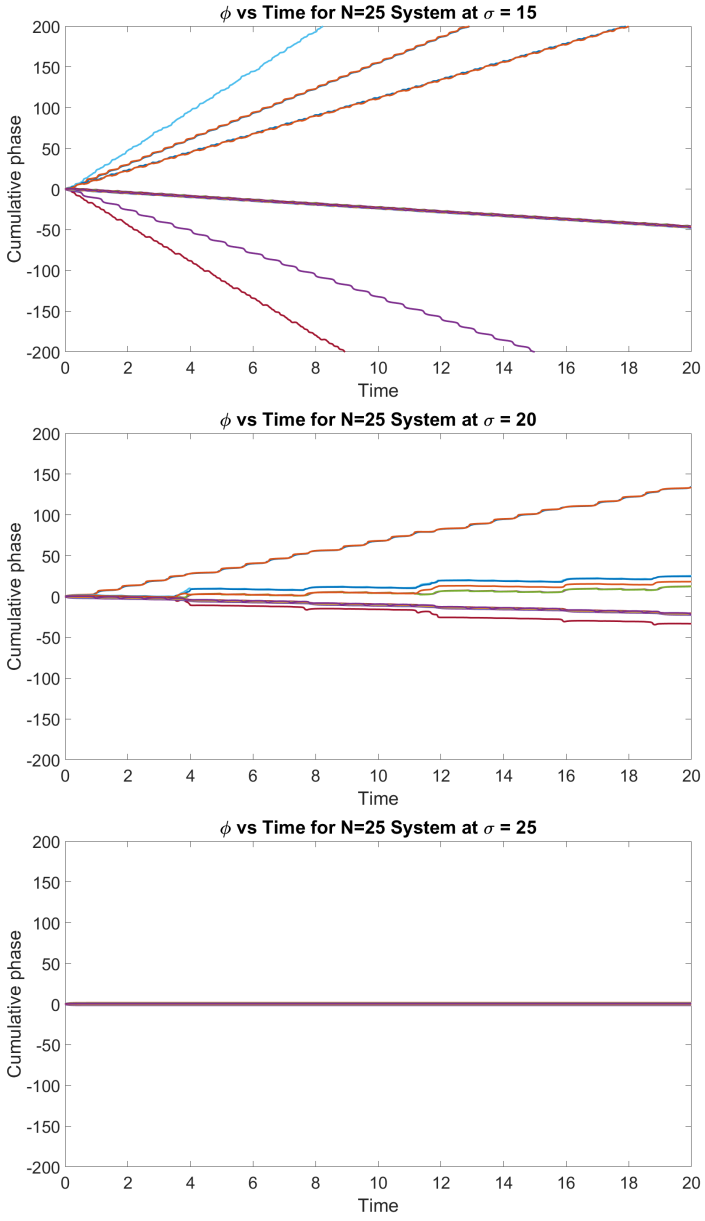

Figure 2.5: A comparison of the cumulative phase vs time for a Kuramoto system of 25 nodes at different coupling strengths. A cascade of synchronizing events as σ increases is more obvious here.

The same basic story is told by the system of 25 nodes. As σ increases, the average long-term angular frequencies of the nodes approach 0. Eventually, total frequency

synchronization occurs and a fixed point emerges. The 25 node system also showcases nontrivial cluster synchronization as σ changes. The cluster synchronization is most easily observed on the frequency bifurcation diagram for a Kuramoto system.

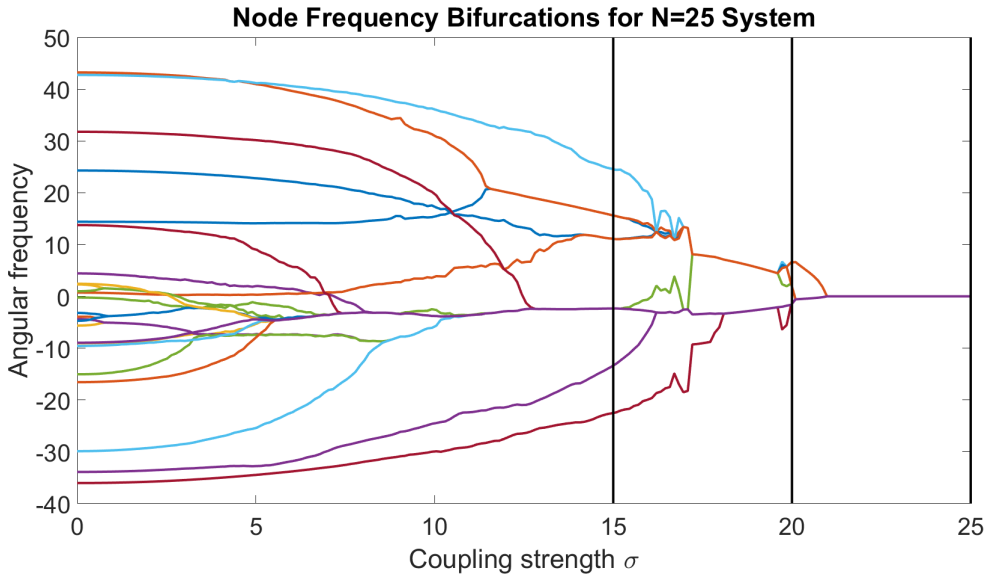

Figure 2.6: Bifurcation diagram for a Kuramoto system with 25 nodes. Vertical black lines correspond to σ values of 15, 20, and 25 respectively.

In figure 2.6 we see the complete bifurcation diagram for the $N = 25$ system. As σ increases, there is a cascade of cluster synchronization events before total synchronization occurs. At $\sigma = 0$, there are 25 distinct long-term frequencies corresponding to the 25 nodes in the system. With increasing σ the long-term frequencies begin to coalesce into fewer and fewer clusters until only one remains. At $\sigma = 15$ and $\sigma = 20$ there are six and three distinct frequencies, respectively, corresponding with the observations we made from the phase diagram. The clustering cascade is not purely monotone. As σ increases near 20 the number of clusters falls to two, briefly climbing back to three and then four before falling to one as total synchronization occurs.

2.3 The Critical Coupling and Saddle-Node Clusters

The transition to total frequency synchronization is the primary process we study in this dissertation. The coupling value for this event is significant and we give this value of σ a special name, the *critical coupling*.

Definition 7. *The critical coupling of a Kuramoto system, denoted σ_c, is the least such coupling such that a frequency synchronized solution exists.*

If ω has mean zero, then at the critical coupling a Kuramoto system undergoes a saddle-node bifurcation as a fixed point solution is created. The dynamics can easily be analyzed for the two-node case. Instead of studying each oscillator separately, instead examine the dynamics of the one-dimensional phase difference $\Psi := \phi_1 - \phi_2$,

$$\dot{\Psi} = \dot{\phi}_1 - \dot{\phi}_2 = 1 + \sigma \sin(\phi_2 - \phi_1) - [-1 + \sigma \sin(\phi_1 - \phi_2)]$$
$$\dot{\Psi} = 2 - 2\sigma \sin(\Psi).$$

The 2-node Kuramoto system is actually a one-dimensional dynamical system in Ψ. There is a saddle-node bifurcation when 2σ exceeds 2 in magnitude, so the critical coupling for the two node system is exactly $\sigma_c = 1$. There is a unique globally stable periodic orbit when $\sigma < 1$, and unique stable and unstable fixed points when $\sigma > 1$.

The exact critical coupling for the 25-node example system is unknown, and an exact explicit description probably does not exist. For this system, it has been computed numerically to be approximately 20.92.

We are also interested in the behavior of the system just below and just above the critical coupling. A thorough analysis of the bifurcation is performed in (Maistrenko *et al.*, 2005) for networks of size seven or less. Above the critical coupling there exists a steady state phase distribution satisfying $\dot{\phi} = 0$. The Kuramoto dynamics are

nonlinear so explicitly calculating or even approximating this distribution is nontrivial. Just below the critical coupling the phase oscillators self-organize into a set of frequency-synchronized clusters. These clusters have been observed to correlate with symmetries in the system's network structure (Sorrentino and Pecora, 2016).

Definition 8. *The saddle-node clusters of a Kuramoto system are the disjoint frequency-synchronized clusters that naturally form in a Kuramoto system for* $\sigma = \sigma_c - \epsilon$ *for arbitrarily small* ϵ*.*

Our definitions for the steady state phase distribution and the saddle-node clusters assume uniqueness, but this assumption need not be true for arbitrary Kuramoto systems. A change in initial conditions could lead to a different fixed point or different clusters. Much has been said about local and global stability results for Kuramoto systems as $\sigma \to \infty$ and often as $N \to \infty$, and our numerical experiments suggest that global stability is frequently true for systems of random size, structure, and coupling. For this reason, we will neglect considerations of stability and initial conditions for the remainder of this dissertation as they are largely unimportant for the type of statistical predictor results we seek. We wish to emphasize though that rigorous results must take stability into consideration, as one can easily construct Kuramoto systems which have multiple stable solution types at the same coupling, differing only in initial conditions (Ottino-Löffler and Strogatz, 2016).

2.4 The Influence of the Network Structure on Synchronized Clusters

In the 25 node bifurcation diagram of figure 2.6 it is apparent that clusters begin to form even at low coupling. There are several groups of nodes near zero angular frequency that cluster almost immediately. Intuitively, these nodes do not require much coupling to cluster because they have similar inherent frequencies. With similar fre-

quencies their phase difference is slowly varying, allowing a low coupling to overpower the separation what would ordinarily come from their small difference in angular frequency. This argument, while it carries some truth, quickly degrades when other pairs of nodes with similar frequencies are observed that do not synchronize until very high σ. An example is highlighted in figure 2.7.

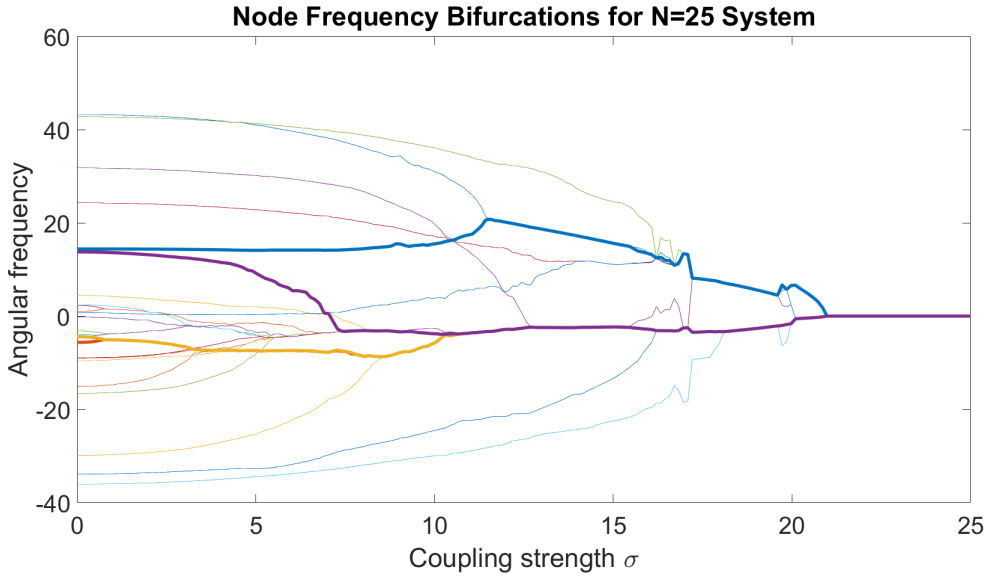

Figure 2.7: The same bifurcation data for the 25 node Kuramoto system, but with two pairs of nodes highlighted. Both pairs have similar inherent frequencies between them with no coupling, but the orange/red pair synchronizes at a very low σ while the blue/purple pair requires a very high σ before synchronization takes place.

Accurate clustering predictions cannot be achieved only from observations of similarities in inherent frequencies. The network structure plays a substantial role. In the figure 2.7 example, the orange/red pair is well connected in the network, but the blue/purple pair is not. Figure 2.8 demonstrates how the clustering in the system is biased towards nodes that have connectivity with each other in the network.

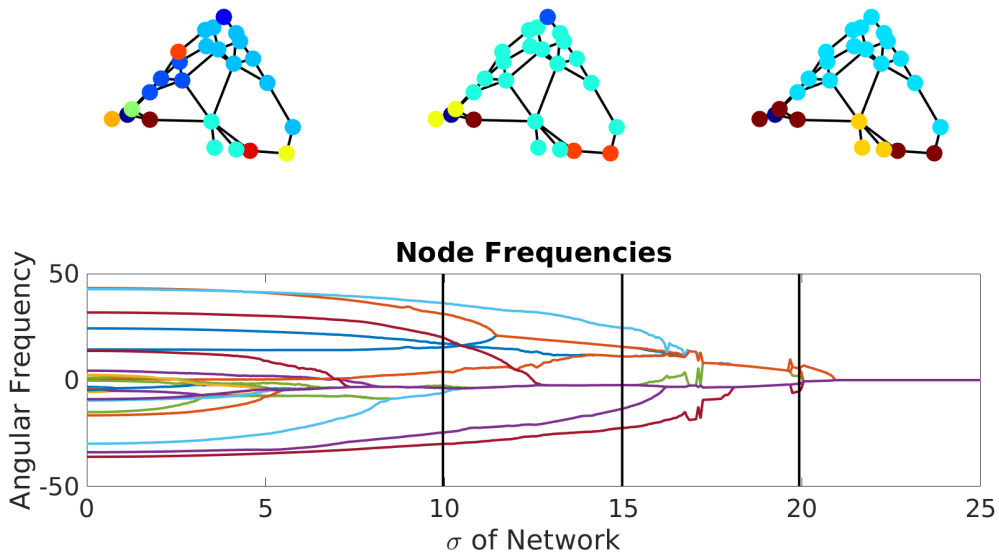

Figure 2.8: Three clusterings of the $N = 25$ node Kuramoto system at couplings of 10, 15, and 20. The nodes in the network are colored according to which clusters they belong. The color choices carry no meaning other than to assign nodes in the same cluster the same color. There are eleven clusters when $\sigma = 10$, six when $\sigma = 15$, four when $\sigma = 20$, and the data clearly demonstrates a high amount of network connectivity within the clusters that the Kuramoto system naturally forms. Notice, however, that it is possible for a cluster to be disconnected in the network. There is one such example when $\sigma = 20$.

Given a data set, statisticians have developed many techniques to partition the data points (Wikipedia, 2017). There is no one technique that is best; it is up to the statistician to identify what method most suits the data. Likewise, network researchers have developed clustering techniques for breaking a network into simple, well connected pieces(Newman, 2010). Most techniques rely on some definition of connectivity in a graph, and it is up to the mathematician to decide which choice best fits the network. In (Gómez-Gardenes *et al.*, 2007) it was observed that scale-free net-

works were relatively more likely to have a single dominant cluster while Erdős–Rényi networks often had groups of clusters similar in size. The Kuramoto oscillators have a self-organizational behavior that produces a hierarchical clustering through a combination of both the frequency data and the network structure (Sorrentino and Pecora, 2016) (Favaretto *et al.*, 2017b). To understand how their behavior works we require a method of prediction that does the same.

2.5 Questions to Answer About the Kuramoto System

As with most nonlinear dynamical systems, finding analytic solutions to the Kuramoto model is infeasible and likely impossible for many choices of system parameters. Instead we must ask more qualitative questions about the overall behaviour of the model and think about how changes in the system parameters affect this behaviour. Here we will collect some important questions and results about the network Kuramoto model, for a more complete study the review articles by Rodrigues et al.(Rodrigues *et al.*, 2016) and Dörfler et al. (Dörfler and Bullo, 2014) are recommended.

Problem 1. *Assuming that a Kuramoto model frequency synchronizes, to which frequency does it synchronize?*

Answer: If we adopt the stronger definition of frequency synchronization that the phase difference between two oscillators must be *constant*, not just bounded, then each connected component of the associated network synchronizes to the mean inherent frequency of that component.

Proof. Without loss of generality assume that a Kuramoto network has only one connected component. Assume that all oscillators synchronize to the same frequency $\tilde{\omega}$. Then, we must have

$$\dot{\phi}_i = \omega_i + \sigma \sum_j A_{ij} \sin(\phi_j - \phi_i) = \tilde{\omega}$$

for all oscillators. Compute the sum of all phase derivatives to get

$$\sum_i \dot{\phi}_i = \sum_i \left[\omega_i + \sigma \sum_j A_{ij} \sin(\phi_j - \phi_i) \right] = N * \tilde{\omega}.$$

Now observe that $\sum_i \sum_j A_{ij} \sin(\phi_j - \phi_i) = 0$, because we assume A to be a symmetric matrix, the i and j summations over over the same set, and sine is an odd function. Therefore, every term in the double summation will have a corresponding term to cancel it when i and j are flipped, and when i and j are equal the sine term is zero. So we have

$$\sum_i \omega_i + \sigma * 0 = N * \tilde{\omega}$$
$$\tilde{\omega} = \frac{1}{N} \sum_i \omega_i$$

and the synchronization frequency is the mean of all inherent oscillator frequencies, regardless of the network structure. □

Corollary 1. *We can always assume a reference frame in which* $\frac{1}{N} \sum_i \omega_i = 0$. *Then, strong frequency synchronization is equivalent to the existence of a stable fixed point.*

Proof. Simply apply the transformation $\tilde{\phi}_i = \phi_i - \left[\frac{1}{N} \sum_i \omega_i \right] * t$. Then,

$$\dot{\tilde{\phi}}_i = \dot{\phi}_i - \frac{1}{N} \sum_i \omega_i$$
$$\dot{\tilde{\phi}}_i = \omega_i + \sigma \sum_j A_{ij} \sin \left(\tilde{\phi}_j + \left[\frac{1}{N} \sum_i \omega_i \right] * t - \tilde{\phi}_i - \left[\frac{1}{N} \sum_i \omega_i \right] * t \right) - \frac{1}{N} \sum_i \omega_i$$
$$\dot{\tilde{\phi}}_i = \omega_i - \frac{1}{N} \sum_i \omega_i + \sigma \sum_j A_{ij} \sin \left(\tilde{\phi}_j - \tilde{\phi}_i \right).$$

Therefore we can instead consider the Kuramoto system $(A, \omega - \frac{1}{N}\sum_i \omega_i)$ on the $\tilde{\phi}$ phase variables as equivalent to the original system under a rotating reference frame. □

A rotating reference frame is useful because then the strong frequency synchronized state is equivalent to a fixed point, and the transition to synchronization is a saddle-node bifurcation in σ.

Problem 2. *Does every network Kuramoto system frequency synchronize as $\sigma \to \infty$?*

Answer: Yes.

Proof. First convert the network Kuramoto dynamics into vector form. Let $\phi \in \mathbb{R}^{N\times 1}$ be the phase vector and $\omega \in \mathbb{R}^{N\times 1}$ be the inherent frequency vector. Assign to each edge in the network an arbitrary orientation and choose an ordering of the edges from 1 to M. Let $B \in \mathbb{R}^{N\times M}$ be the oriented incidence matrix defined by

$$B_{ij} = \begin{cases} -1 & \text{if edge j leaves node i} \\ 1 & \text{if edge j enters node i} \\ 0 & \text{otherwise} \end{cases}$$

. Then the network Kuramoto dynamics become

$$\dot{\phi} = \omega - \sigma B \sin(B^T \phi).$$

Consider the σ-normalized version of the Kuramoto model by letting $\tilde{\phi}_i = \frac{\phi_i}{\sigma}$. Then,

$$\dot{\tilde{\phi}} = \frac{\omega}{\sigma} - B \sin(\sigma B^T \tilde{\phi}).$$

and in the limit as $\sigma \to \infty$, the $\tilde{\phi}$ system approaches an identical oscillator form of the Kuramoto model, where all oscillators are assumed to have inherent frequency zero.

Identical oscillator Kuramoto models are known to always exhibit an exponentially stable, phase synchronized fixed point where all phases are zero(Grabow *et al.*, 2010). Indeed, if $\frac{\omega}{\sigma} \to 0$ then $\tilde{\phi} = 0_N$ is clearly a fixed point, and for small perturbations we can linearize the sine function to get

$$\dot{\tilde{\phi}} \approx -\sigma B B^T \tilde{\phi} = -\sigma L \tilde{\phi}$$

where we have used the well known fact that $BB^T = L$, the network Laplacian, regardless of which oriented incidence matrix B is chosen. L is positive semidefinite and has non-negative eigenvalues, and the zero eigenvalue corresponds to the fact that $\sum_i \phi_i$ is a conserved quantity. In a rigorous sense the Kuramoto system is neutrally stable, but if we consider the dynamics only on the invariant set defined by $\sum_i \phi_i = 0$ then the zero vector is an asymptotically stable state of the $\tilde{\phi}$ system. Because the original ϕ system is a multiple of $\tilde{\phi}$, it must also have a linearly stable fixed point as $\sigma \to \infty$. □

These problems cover a few of the basic properties we are interested in for network Kuramoto systems and are integral for our analysis in the remainder of this dissertation. The questions we are most interested in going forward are

Problem 3. *Given a network Kuramoto system (A, ω), what is the critical coupling?*

Problem 4. *Given a network Kuramoto system (A, ω), what are the saddle-node clusters?*

2.6 Outline and Contributions

In this dissertation we address problems (3) and (4) simultaneously using a cluster order parameter optimization problem. In chapter 3 we review the standard order parameter and in section 3.3 we introduce a new order parameter based on clusters. In

section 3.4 we explain the analytical use of the cluster order parameter in Kuramoto systems, culminating in theorem 2. Theorem 2 establishes a lower bound on the critical coupling but the bound is unwieldy to calculate. In chapter 4 we show that the calculation of the bounds in theorem 2 and particularly in equation (3.22) are equivalent to a variation of the minimum isoperimetric ratio problem in spectral graph theory. We adapt an algorithm from the literature to approximately solve the problem and numerically test the accuracy for the estimates of the critical coupling and saddle-node clusters on random network Kuramoto systems. Finally in chapter 5 we interpret these results in the context of power systems.

The primary contributions of this dissertation are the generic order parameter intersection framework for estimating the critical coupling in chapter 3, the introduction of the cluster order parameter in 11 and its associated theorem 2 and conjecture 1 for bounding the critical coupling and identifying the saddle-node clusters respectively, and the observation in chapter 4 that the computation of the maximal cluster intersection for horizontally projected cluster order parameters is a variation of the isoperimetric problem in spectral graph theory.

2.7 Calculating the Steady State Phase Distribution

Problem 5. *Assuming that a Kuramoto system is frequency synchronized, what is the synchronized phase distribution? Equivalently, what is the fixed point in the Kuramoto system after the saddle-node bifurcation?*

Answer: Generally, finding the fixed point is a matter of finding the root of a system of nonlinear equations. Call the fixed point ϕ^*. ϕ^* satisfies

$$\omega_i + \sigma \sum_j A_{ij} \sin(\phi_j^* - \phi_i^*) = 0$$

for all i. Or, equivalently in vector notation,

$$\omega - \sigma B \sin(B^T \phi^*) = 0. \tag{2.2}$$

ϕ^* is not uniquely determined by this nonlinear condition because B^T has a nullspace equal to the span of 1_N and any vector in the space $\{0, 2\pi\}^N$ may be added to ϕ^* to also solve equation (2.2). To avoid these trivial solutions we define ϕ^* to be the vector in $(-\pi, \pi)^N$ with $1_N^T \phi^* = 0$. If ϕ^* is still not uniquely determined then we define ϕ^* to be the fixed point with the largest basin stability (Hellmann *et al.*, 2016). The basin stability of a fixed point is the probability that a trajectory will asymptotically return to the fixed point after a uniformly random perturbation in $(-\pi, \pi)^N$ orthogonal to 1_N is added.

ϕ^* can be found numerically through Newton's method or by simulating the system. Analytically, it is tempting to try to solve for ϕ^* as $\phi^* = (B^T)^{-1} \sin^{-1}\left(\frac{B^{-1}\omega}{\sigma}\right)$. Unfortunately, B is an $N \times M$ rectangular matrix, so B^{-1} does not exist. Even if $N = M$ and B is square, it is an oriented incidence matrix and will not have full rank. Summing the rows of B which correspond to a cycle in the graph will always yield 0. The number of elementary cycles in a connected graph with N nodes and M edges is $M - N + 1$, so B always has rank $N - 1$. See (Biggs, 1997) for more on the edge space and cycle space of a graph. Because the naive solution for ϕ^* is not correct, we have the following lemma due to (Dörfler *et al.*, 2013).

Lemma 1. *Given a Kuramoto system (A, ω), and a coupling $\sigma > \sigma_c$, the fixed point ϕ^* is well approximated as the solution to the linear system*

$$B^T \phi^* \approx \sin^{-1}\left(\frac{B^\dagger \omega}{\sigma}\right)$$
$$1_N^T \phi^* = 0$$

where $B^\dagger$ is the Moore-Penrose pseudoinverse of the oriented edge incidence matrix B. The error in the approximation decreases to zero as $\sigma \to \infty$. Moreover, the Dörfler estimate

$$\sigma_D = ||B^\dagger \omega||_\infty \tag{2.3}$$

is an estimate for the critical coupling.

Proof. Consider equation 2.2 in the edge space instead of the node space. Define the $M \times 1$ vector Ψ^* by $\Psi^* = \sin(B^T \phi^*)$. Then equation 2.2 is linear in Ψ^*, and Ψ^* is in the solution space to

$$B\Psi^* = \frac{\omega}{\sigma}. \tag{2.4}$$

Unfortunately this solution space is of dimension $M - N + 1$, so a unique solution cannot yet be determined. The shift from ϕ^* to Ψ^* was not a true change of coordinates because they are of different dimensions. Lost in transition was the Kirchoff condition that net change in phase around any cycle in the graph is zero. We must add this condition back in to Ψ^* by imposing

$$\sum_{k \in E} \sin^{-1}(\Psi_k^*) = 0 \tag{2.5}$$

for an oriented sequence of edges k in each elementary cycle E. As there are $M-N+1$ elementary cycles in a connected graph, these conditions reduce the solution space to zero degrees of freedom. It is likely that there exists a unique solution Ψ^* to both conditions, but the Kirchoff condition is nonlinear so this is not guaranteed. If a unique Ψ^* is found, ϕ^* can then be recovered by solving the linear equations $B^T \phi^* = \sin^{-1}(\Psi^*)$ and $1_N^T \phi^* = 0$, assuming that all elements of Ψ^* are less than or equal to 1 in magnitude.

Remarkably, if the nonlinear Kirchoff condition on Ψ^* is replaced by the first-order

linear approximation

$$\sum_{k \in E} \Psi_k^* = 0 \tag{2.6}$$

then Ψ^* is *exactly* solved by $\Psi^* = \frac{B^\dagger \omega}{\sigma}$. Assuming that this is a close approximation to the nonlinear solution, we have $B^T \phi^* \approx \sin^{-1}\left(\frac{B^\dagger \omega}{\sigma}\right)$. Additionally, for $\frac{B^\dagger \omega}{\sigma}$ to be in the domain of $\sin^{-1}$, we must have $\sigma \geq ||B^\dagger \omega||_\infty$. For a more extensive proof see the paper (Dörfler *et al.*, 2013). □

In (Dörfler *et al.*, 2013) it was observed that σ_D was an upper bound for the critical coupling in more than 99.9% of random Kuramoto systems, generated according to several different random graph models.

2.8 Terms and Definitions

$N \in \mathbb{N}$ is the number of oscillators in the system and $M \in \mathbb{N}$ is the number of edges in the embedded network. $\phi_i \in \mathbb{R}$ is the phase of oscillator i, $\omega_i \in \mathbb{R}$ is the inherent driving frequency of node i, $\sigma \in \mathbb{R}^+$ is the coupling strength, $A \in \mathbb{R}_+^{N \times N}$ is the symmetric adjacency matrix of the associated network, L is the graph Laplacian, and B is an oriented incidence matrix with arbitrary orientation. $A_{ij} = 1$ if nodes i and j are connected and 0 if they are not. $B \in \mathbb{R}^{N \times M}$ is defined by $B_{ij} = -1$ if edge j leaves node i, $B_{ij} = 1$ if edge j enters node i, and $B_{ij} = 0$ otherwise. The orientation is chosen by convention to point from the lower indexed node to the higher so that the edges are listed in lexicographic order. L is defined by $L = D - A$, where D is the diagonal matrix of node degrees. A, B, and L all contain complete information about the graph, so it is possible to convert from one to another with no loss. As a rule of thumb, A is more convenient to use when discussing properties of nodes, B when discussing edges, and L when discussing flows through the graph. $L^\dagger$ is the Moore-Penrose pseudoinverse of L. The Kuramoto dynamics can be equivalently stated in

vector form as

$$\dot{\phi} = \omega - \sigma B \sin(B^T \phi) \tag{2.7}$$

Chapter 3

ORDER PARAMETERS IN THE KURAMOTO MODEL

An *order parameter* is a real number that measures the degree of phase synchrony in a set of phase oscillators. Typically order parameters are defined to lie in some specified interval, with total phase synchronization occurring at the maximal value in that interval. Order parameters can be studied numerically as a way to *measure* phase cohesiveness, or analytically as an indicator to *prove* phase synchronization occurs. In chapter 3 we will review some of the order parameters that have previously been used to study the Kuramoto model and introduce new parameters to study cluster synchronization.

3.1 The Standard Order Parameter

Definition 9. *The standard order parameter r of a vector of phases $\phi \in \mathbb{R}^N$ is the magnitude of the complex order parameter O_s, defined by*

$$O_s := r_s e^{i\Psi} = \frac{1}{N} \sum_{i=1}^{N} e^{i\phi_i}. \tag{3.1}$$

The standard order parameter is most useful for analyzing a standard Kuramoto system. We define a standard Kuramoto system to be one where the underlying network is a complete graph.

O_s is the center of mass of all the phases in the vector ϕ when they are arranged on the complex unit circle, and r_s is the distance of O_s from the origin. The phase variable Ψ is the mean phase of all the oscillators in ϕ. Figure 3.1 gives an example of this interpretation.

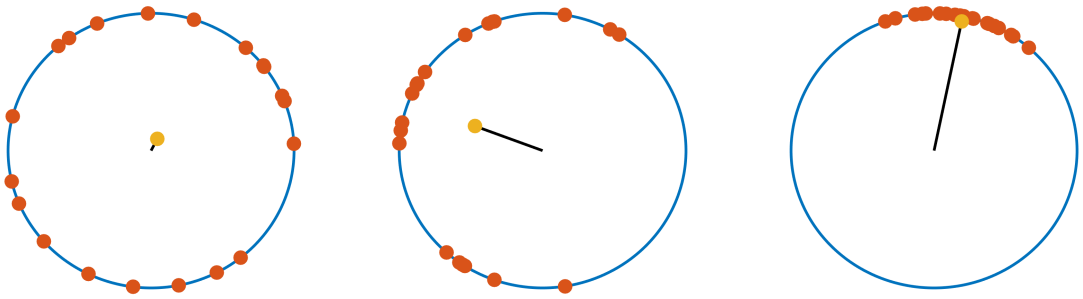

(a) $r_s = 0.095$, no phase cohesiveness.

(b) $r_s = 0.503$, partial phase cohesiveness.

(c) $r_s = 0.961$, high phase cohesiveness.

Figure 3.1: Three examples of phase distributions with varying levels of phase cohesiveness. The phases ϕ are arranged in orange around the complex unit circle while their center of mass O_s is shown in yellow. The order parameter r_s is the distance of the center of mass from the origin, shown in black.

If the phase vector ϕ is time-dependent as it is in the Kuramoto model, then O_s and the order parameter r_s will also be time-dependent. Studying how r_s changes in time gives insight towards the transition to synchrony as a Kuramoto system moves past a transient phase and into its long-term stable dynamics. In (Mirollo, 2012), Mirollo studies the time evolution of the standard order parameter in the $N \to \infty$ limit, and even in this limiting case the dynamics are nontrivial and rigorous analysis is dependent on initial conditions. Instead we observe the time-dependence numerically.

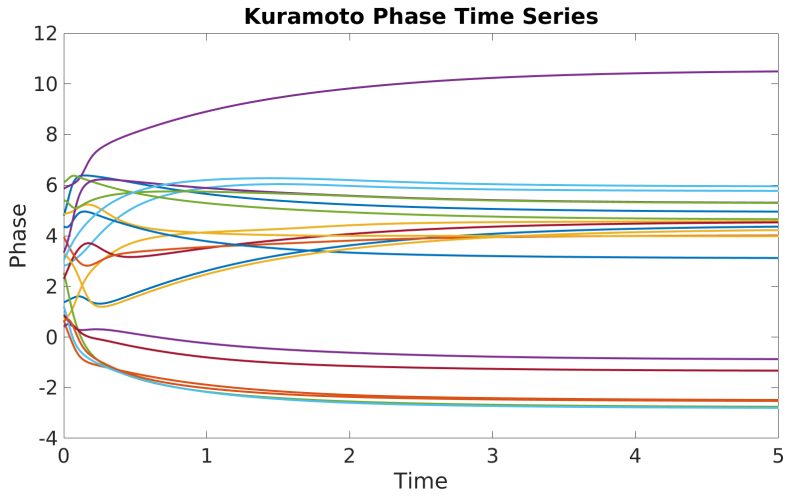

(a) The time evolution of a standard Kuramoto system above critical coupling. There is a transient period before total frequency synchronization and partial phase synchronization occurs.

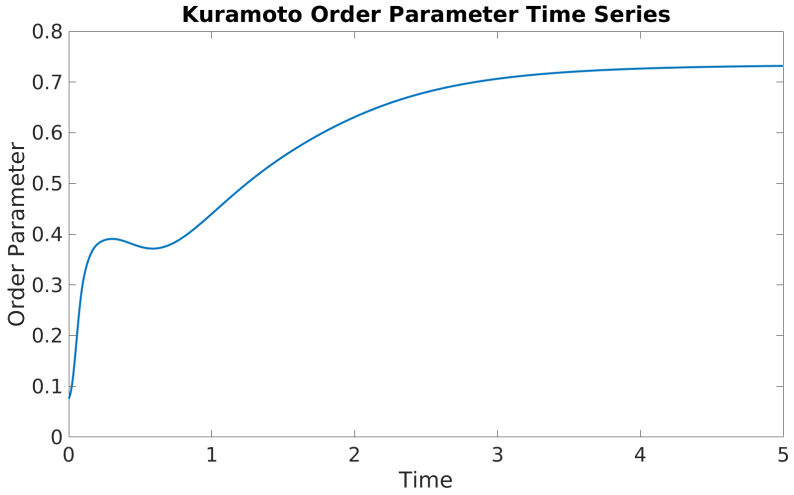

(b) The phase cohesiveness of the same system, tracked by its order parameter. The transition to synchrony is captured by the asymptotic increase in the order parameter.

Figure 3.2: An example Kuramoto system of twenty phase oscillators was simulated forward in time from a random initial distribution of phases. The order parameter is near zero for the random starting point, but increases through the transient region and asymptotically approaches a limit as time goes to infinity.

Above the critical coupling, we use the notation $r_s(\sigma)$ to refer to the $t \to \infty$ asymptotic limit of r_s for a Kuramoto system with coupling σ. Below the critical coupling, we define the *time-averaged* order parameter $\langle r_s \rangle_t$ to study how frequency synchronization changes with σ.

Definition 10. *The time-averaged order parameter $\langle r_s \rangle_t$ is defined by*

$$\langle r_s \rangle_t := \lim_{\tau \to \infty} \frac{1}{\tau} \int_0^\tau r_s(t) dt = \lim_{\tau \to \infty} \frac{1}{\tau} \int_0^\tau \left| \frac{1}{N} \sum_{i=1}^{N} e^{i\phi_i(t)} \right| dt. \tag{3.2}$$

Numerically, it is more convenient to average from T to $T + \tau$, where both T and τ are large.

Time-averaging of the order parameter gives a significant measurement of synchronization even at coupling strengths where total frequency synchronization doesn't occur.

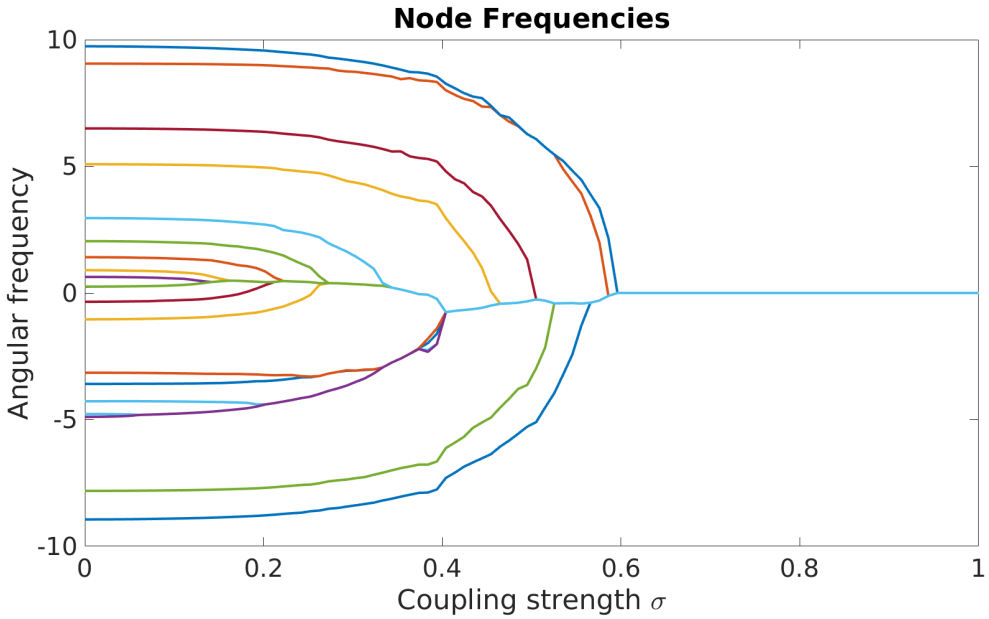

(a) The long-term frequency bifurcation plot for an all-to-all Kuramoto system.

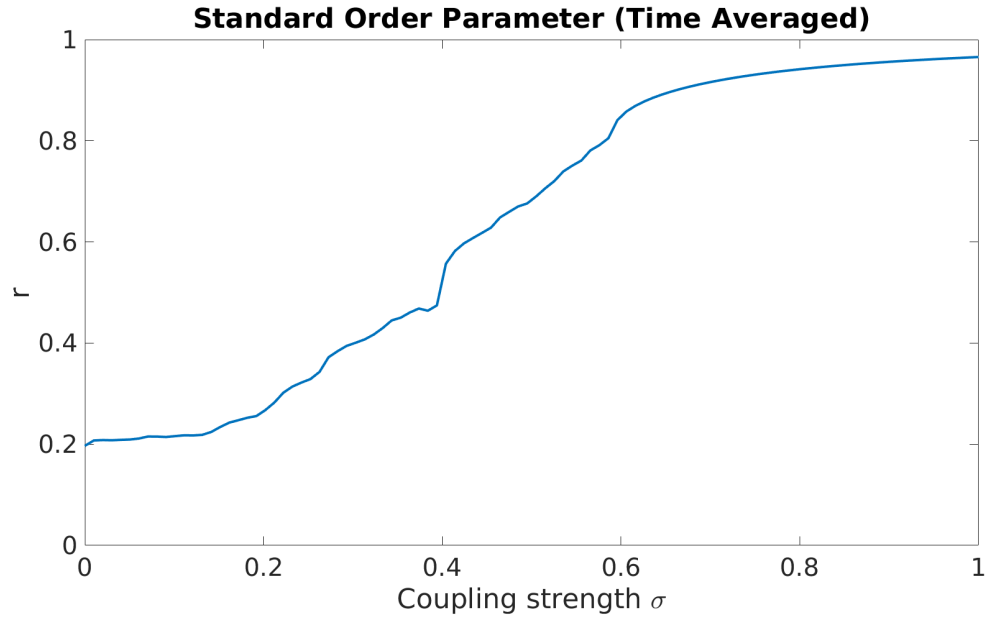

(b) The time-averaged order parameter as a function of σ.

Figure 3.3: An example Kuramoto system with the time-averaged order parameter used to measure frequency synchronization.

Kuramoto (Kuramoto, 1975) (Kuramoto, 2012) showed the importance of the

standard order parameter analytically using a mean-field approach. We will present his findings in a slightly different way than they are shown in (Strogatz, 2000), and instead follow (Almendral *et al.*, 2010) and make use of the trigonometric identity

$$\sum_j a_j \sin(x + z_j) = A \sin(x + Z) \tag{3.3}$$

where

$$A^2 = \sum_{p,q} a_p a_q \cos(z_p - z_q)$$
$$\tan(Z) = \frac{\sum_p a_p \sin(z_p)}{\sum_p a_p \cos(z_p)}.$$

The standard Kuramoto model is

$$\dot{\phi}_i = \omega_i + \sigma \sum_{j=1}^{N} \sin(\phi_j - \phi_i). \tag{3.4}$$

Apply identity (3.3) using $x = -\phi_i$, $z_j = \phi_j$ and $a_j = 1$ to get

$$\dot{\phi}_i = \omega_i + \sigma r \sin(\Psi - \phi_i). \tag{3.5}$$

where

$$r^2 = \sum_{p,q} \cos(\phi_q - \phi_p)$$
$$\tan(\Psi) = \frac{\sum_p \sin(\phi_p)}{\sum_p \cos(\phi_p)}.$$

Now equation 3.5 appears to show that oscillator ϕ_i is decoupled, its dynamics are influenced only by r, Ψ, σ, and its own internal properties. Of course, r and Ψ depend on the oscillator population, so the inter-dependencies are hidden in these two variables. Importantly though, r and Ψ are global variables and are not specific to the oscillator ϕ_i. To connect equation 3.5 with the standard order parameter, note

that $\sum_{p,q} \sin(\phi_q - \phi_p) = 0$ because sine is an odd function and both p and q range from 1 to N, so each term in the sum has a corresponding term that cancels it. Therefore,

$$
\begin{aligned}
r^2 &= \sum_{p,q} \cos(\phi_q - \phi_p) + i \sin(\phi_q - \phi_p) \\
r^2 &= \sum_{p,q} e^{i(\phi_q - \phi_p)} \\
r^2 &= \sum_{q} e^{i\phi_q} \sum_{p} e^{-i\phi_p} \\
r^2 &= \left| \sum_{q} e^{i\phi_q} \right|^2 .
\end{aligned}
$$

Now it is clear the r in equation (3.5) is the standard order parameter r_s multiplied by N. Likewise, Ψ is the phase of O_s. We will refer to r as "the order parameter".

Equation 3.5 has a simple one-dimensional saddle-node bifurcation if r is constant. A stable fixed point exists only if $\sigma r \geq |\omega_i|$. We can do the same analysis for every oscillator, so we would expect the critical coupling for the entire system to be given by $\sigma_c = \frac{||\omega||_\infty}{r}$, where $||\omega||_\infty$ is the largest magnitude component of the frequency vector ω.

Theorem 1. *Given a standard Kuramoto system with frequency vector ω and order parameter $r(\sigma)$ when the system is in steady state at coupling σ,*

$$\sigma \geq \frac{||\omega||_\infty}{r(\sigma)}. \tag{3.6}$$

In particular, $\sigma_c \geq \frac{||\omega||_\infty}{r(\sigma_c)}$.

Proof. For all i, the steady state solution is given by

$$\omega_i + \sigma \sum_{j=1}^{N} \sin(\phi_j^* - \phi_i^*) = 0.$$

Follow the same logic used to derive equation 3.5 to get

$$\omega_i + \sigma r(\sigma) \sin(\Psi - \phi_i^*) = 0. \tag{3.7}$$

Therefore $\sigma r(\sigma) \geq |\omega_i|$ for all i, or no root ϕ_i^* could exist. $\max_i(|\omega_i|) = ||\omega||_\infty$, so $\sigma > \frac{||\omega||_\infty}{r(\sigma)}$. □

Corollary 2. *For any choice of σ where a steady state solution exists to the Kuramoto system we have the bound*

$$\sigma_c \geq \frac{||\omega||_\infty}{r(\sigma)}. \tag{3.8}$$

Proof. The argument follows from the observation that r increases with σ. Because σ_c is the lowest coupling at which a steady state exists, we must have $\sigma \geq \sigma_c$. Therefore $r(\sigma) \geq r(\sigma_c)$ and $\frac{||\omega||_\infty}{r(\sigma_c)} \geq \frac{||\omega||_\infty}{r(\sigma)}$. □

r can only be constant in time when the system is in steady state, but its interpretation as the centroid of all phases on the complex circle (multiplied by N) provides some intuition that r can be nearly constant in time even outside of steady state. If the coupling is just below the critical value, then the steady state solution bifurcates and the system converges to a stable periodic orbit on the N-torus. Qualitatively, we expect the majority of the oscillators to remain frequency synchronized, with only a few drifting oscillators that deviate from the main pack. Because the bulk of oscillators stay grouped on the unit circle, their centroid magnitude stays high and nearly constant even as the oscillators rotate. The rogue oscillators contribute to some fluctuations, but should not significantly impact the order parameter over time. It should be noted that this argument breaks down when the drifting oscillators form a significant percentage of the entire system, and this is our motivation for introducing a *cluster* version of the order parameter in the next section.

Figure 3.3 shows that the time-averaged order parameter increases with σ, and is monotone increasing in the regime where a steady state solution exists. Rearranging

inequality 3.6, we have

$$r(\sigma) \geq \frac{||\omega||_\infty}{\sigma}.$$

The left hand side is increasing with σ while the right hand side is decreasing with σ. If the curves intersect, then the inequality becomes an equality for some value of σ, which must necessarily be a lower bound for σ_c.

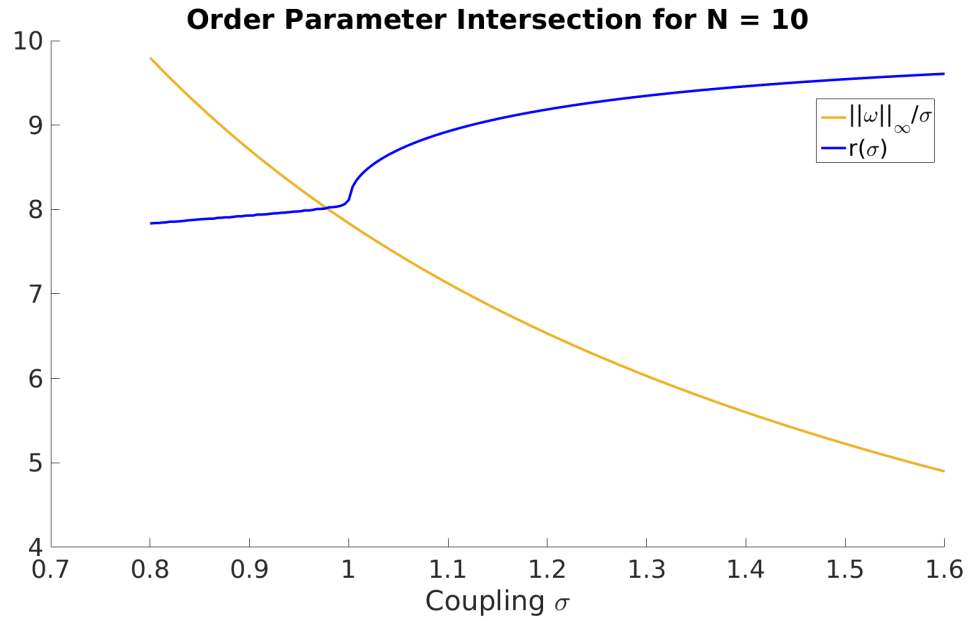

Figure 3.4: A demonstration of the intersection between the curves $r(\sigma)$ and $\frac{||\omega||_\infty}{\sigma}$ for an example Kuramoto system on ten nodes.

In actuality, we only define r above the critical coupling, so for lower values of σ we plot the time-averaged order parameter.

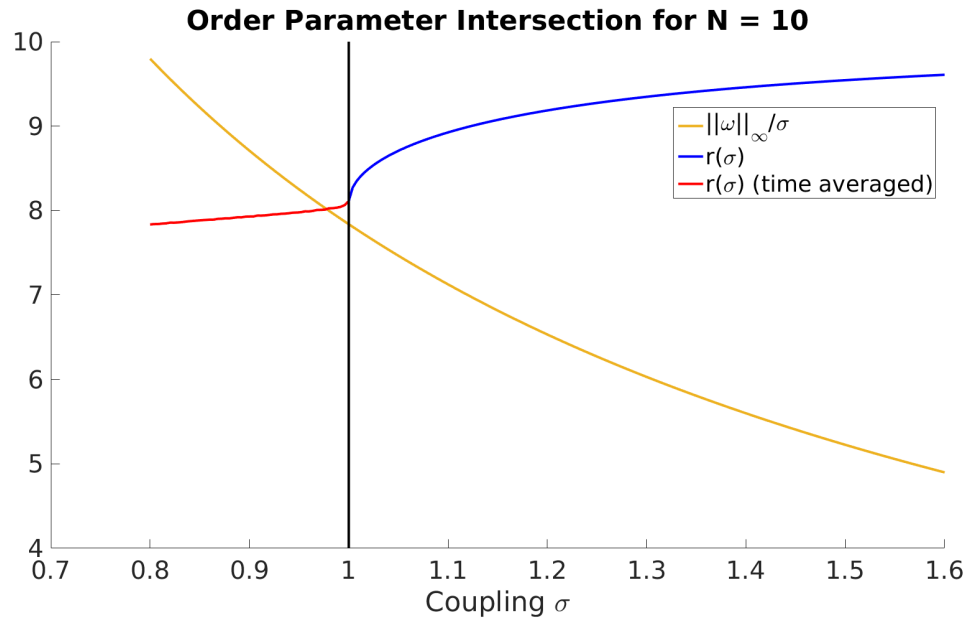

Figure 3.5: A demonstration of the intersection between the order parameter and $\frac{||\omega||_\infty}{\sigma}$ for an example Kuramoto system on ten nodes. The frequencies have been normalized such that the critical coupling σ_c is 1, indicated by a vertical black line. Below the critical coupling, r is replaced by its time-averaged version. The intersection point is clearly a lower bound for the critical coupling, as would be the intersection of any other projection of r below σ_c.

Our strategy for estimating the critical coupling is to approximate the curve r as a function of σ, and find where the approximation intersects $\frac{||\omega||_\infty}{\sigma}$. The intersection point is an estimate of σ_c, and depending on the method to estimate $r(\sigma)$ may be a strict lower bound.

3.2 Estimating the Order Parameter as a Function of σ

3.2.1 Bounding r by N

The simplest possible estimate of r is to assume it is constant. $r \to N$ as $\sigma \to \infty$ because the system phase synchronizes, and the approximation $r \approx N$ gives the bound

$$\sigma_c \geq \frac{||\omega||_\infty}{N}. \tag{3.9}$$

This is a trivial bound as mentioned in (Verwoerd and Mason, 2008) and (Dörfler and Bullo, 2011).

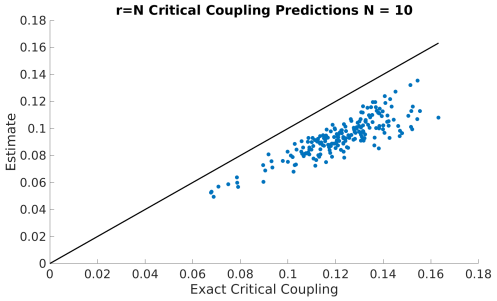

(a) Estimates using $r = N$ intersection for the critical coupling in systems of 10 nodes.

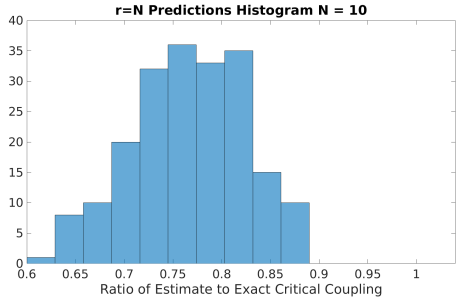

(b) Histogram of estimates as a percentage of the actual critical coupling.

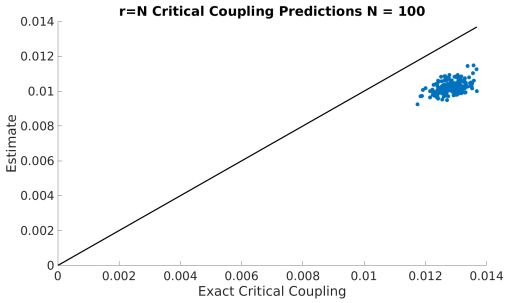

(c) Estimates using $r = N$ intersection for the critical coupling in systems of 100 nodes.

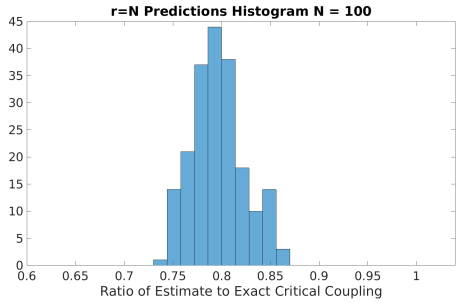

(d) Histogram of estimates as a percentage of the actual critical coupling.

Figure 3.6: We simulated 200 standard Kuramoto systems on 10 and 100 nodes with random frequencies and recorded their actual critical couplings in comparison to those predicted by the estimate in equation (3.9). The frequencies were generated uniformly on $[-1, 1]$ and the critical coupling was computed as the smallest σ Newton's method returned a fixed point of the system. The accuracy results show a clear gap on the order of 10-20% for the estimate, with a higher variance for lower N, but do confirm that eqation (3.9) is a strict lower bound in the experiment.

3.2.2 Sampling r at a Specified Coupling

A slightly more sophisticated approach is to compute r numerically at some finite σ^* above the critical coupling and assume r stays constant at that value.

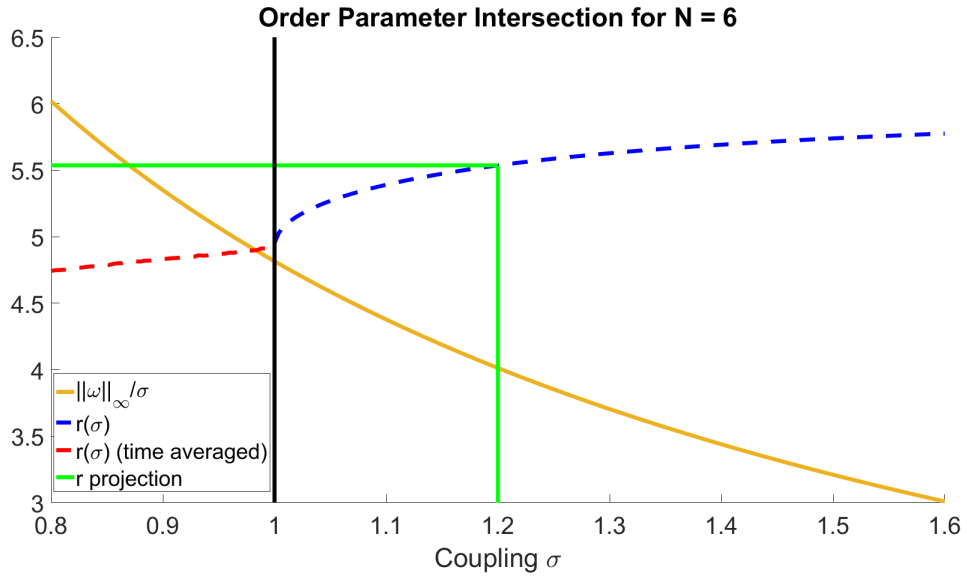

Figure 3.7: The intersection found by projecting r horizontally at a sampled point for an example system.

This leads to the bound

$$\sigma_c \geq \frac{||\omega||_\infty}{r(\sigma^*)} \tag{3.10}$$

where $r(\sigma^*)$ is found numerically. An attractive choice is the Dörfler estimate $\sigma^* = \sigma_D := ||B^T L^\dagger \omega||_\infty$, where B is an oriented incidence matrix of the complete graph, because σ_D is easily computed and is to our knowledge the tightest known upper bound for σ_c in greater than 99.9% of arbitrary Kuramoto systems (Dörfler *et al.*, 2013).

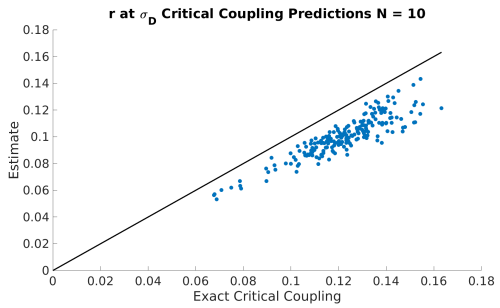

(a) Estimates using $r = r(\sigma_D)$ intersection for the critical coupling in systems of 10 nodes.

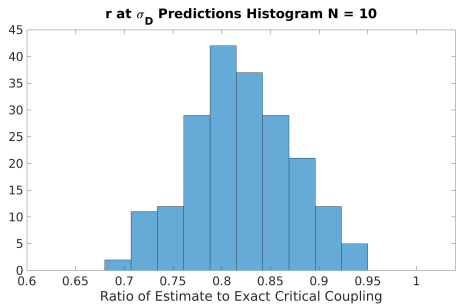

(b) Histogram of estimates as a percentage of the actual critical coupling.

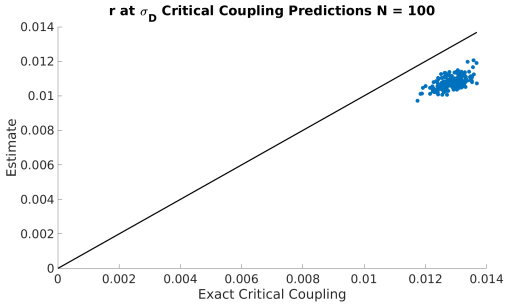

(c) Estimates using $r = r(\sigma_D)$ intersection for the critical coupling in systems of 100 nodes.

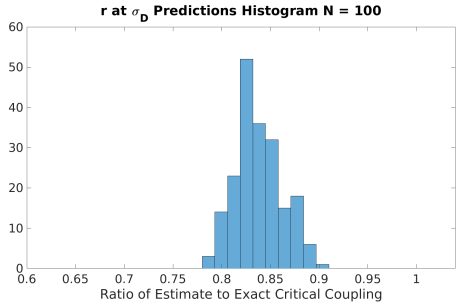

(d) Histogram of estimates as a percentage of the actual critical coupling.

Figure 3.8: The same 200 standard Kuramoto system critical couplings now compared to the estimate (3.10), with σ^* equal to the Dörfler estimate of σ_c. The accuracy is a strict improvement compared with figure (3.6), closing the gap somewhat. Eqation (3.10) is also a strict lower bound in the experiment.

Approaches (3.9) and (3.10) are equivalent to inequality 3.6, with $\sigma = \sigma^*$ or $\sigma \to \infty$ respectively.

3.2.3 First-Order Numerical Approximation for r

In figure 3.5, $r(\sigma)$ appears to be concave above the critical coupling. Therefore, any linear approximation of r in this regime will be an upper bound for r. Another strategy to estimate the critical coupling is to compute r at two points $r(\sigma^*)$ and $r(\sigma^* + \epsilon)$, and find the intersection of the linear interpolation of the two points with the curve $\frac{||\omega||_\infty}{r(\sigma^*)}$. Under the assumption that $r(\sigma)$ is concave, this intersection leads to the strict lower bound

$$\sigma_c \geq -b + \sqrt{b^2 + 4m||\omega||_\infty} \tag{3.11}$$

where $m = \frac{1}{\epsilon}[r(\sigma^* + \epsilon) - r(\sigma^*)]$ and $b = r(\sigma^*) - m\sigma^*$.

We tested this bound using $\sigma^* = \sigma_D$ and $\epsilon = \frac{1}{1000}\sigma_D$ on the same set of Kuramoto systems.

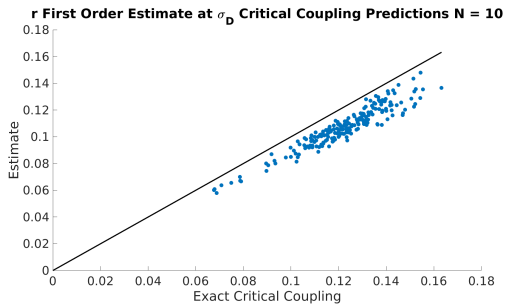

(a) Estimates using numerical first-order intersection for the critical coupling in systems of 10 nodes.

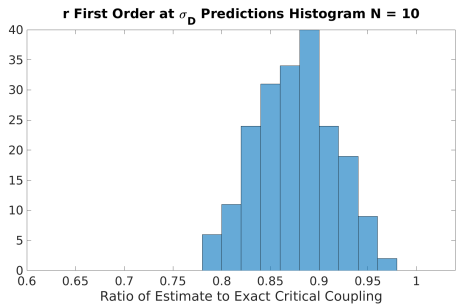

(b) Histogram of estimates as a percentage of the actual critical coupling.

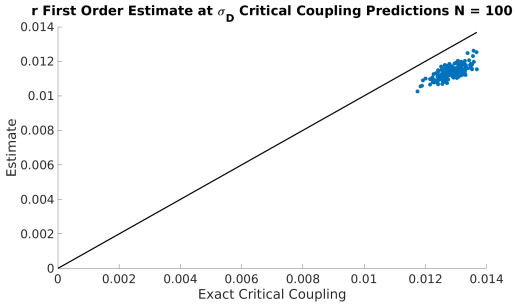

(c) Estimates using numerical first-order intersection for the critical coupling in systems of 100 nodes.

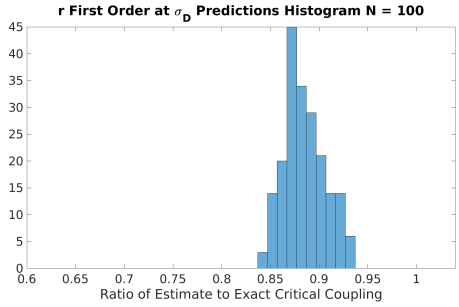

(d) Histogram of estimates as a percentage of the actual critical coupling.

Figure 3.9: The same 200 standard Kuramoto system critical couplings now compared to the estimate (3.11), with σ^* equal to the Dörfler estimate. The accuracy is improved over figure (3.8).

3.2.4 Approximating r by first approximating the steady state

We have

$$r^2 = \left| \sum_i e^{i\phi_i} \right|^2 = \sum_{i,j} e^{i(\phi_i - \phi_j)}$$

by definition. One strategy to approximate r is to first approximate the phases ϕ in

steady state and use them to evaluate the right-hand side. To our best knowledge, the strongest approximation of the steady state Kuramoto solution is the Dörfler estimate $B^T\phi^* \approx \sin^{-1}\left(\frac{B^\dagger\omega}{\sigma}\right)$ from lemma 1.

Unfortunately, this estimate is only well defined for $\sigma \geq ||B^\dagger\omega||_\infty \geq \sigma_c$, so we cannot use it to estimate r below the critical coupling. In fact the gap between $||B^\dagger\omega||_\infty$ and σ_c can be large if there is a significant regime where the steady state has phase differences greater than $\frac{\pi}{2}$ between adjacent oscillators. The best we can do is to estimate ϕ^* at the minimum possible $\sigma = ||B^\dagger\omega||_\infty = \sigma_D$ and assume r is constant below. This leads to the estimate

$$\sigma_c \approx \frac{||\omega||_\infty}{r_D} \tag{3.12}$$

where $r_D = \sum_{i,j} e^{i(\phi_i^* - \phi_j^*)}$ and ϕ^* is computed with lemma 1 using $\sigma = \sigma_D$. This bound should be comparable to (3.10) in accuracy, but is significantly faster to compute.

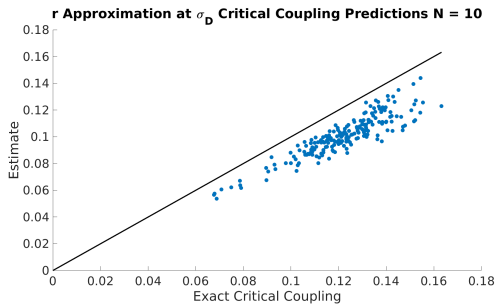

(a) Estimates using approximate $r(\sigma_D)$ intersection for the critical coupling in systems of 10 nodes.

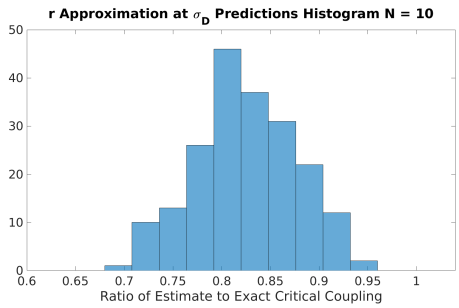

(b) Histogram of estimates as a percentage of the actual critical coupling.

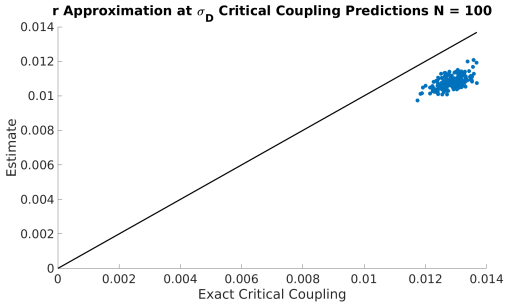

(c) Estimates using approximate $r(\sigma_D)$ intersection for the critical coupling in systems of 100 nodes.

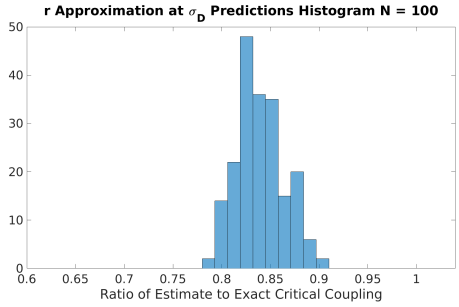

(d) Histogram of estimates as a percentage of the actual critical coupling.

Figure 3.10: The same 200 standard Kuramoto system critical couplings now compared to the estimate (3.12). There are only slight differences compared to figure (3.8), but this approach offers a substantial improvement in computation time and stability, especially for N large. This is because bound (3.10) requires an iterative scheme while estimate (3.12) is a system of linear equations. We can no longer prove that this estimate is a strict lower bound of the crtical coupling, but the experiment indicates that this is likely.

3.2.5 *Estimating the $r(\sigma)$ Curve Asymptotically*

A third option is to compute an asymptotic estimation of $r(\omega, \sigma)$ without relying on first computing the steady state solution. There are many such estimates in the literature (Verwoerd and Mason, 2008) (Dörfler *et al.*, 2013) (Jadbabaie *et al.*, 2004), the first of which was probably given by Kuramoto himself in (Kuramoto, 1975). However, Kuramoto's estimate and many which came later are asymptotic as $N \to \infty$ and as ω approaches a continuous frequency distribution. We instead seek estimates for which N is finite and ω is a constant, unchanging frequency vector.

As decribed in (Dörfler and Bullo, 2011), an implicit formula for $r(\omega, \sigma)$ is given in (Verwoerd and Mason, 2008). Additionally in (Dörfler and Bullo, 2011), Dörfler gives the bound

$$r \geq N\sqrt{\frac{1+\sqrt{1-(\sigma_c/\sigma)^2}}{2}}.$$

This bound is based on a geometric argument on the distribution of phases on the unit circle, and is only dependent on ω indirectly through the presence of the critical coupling term. At σ_c the bound becomes $r \geq N\frac{1}{\sqrt{2}}$, which leads to the bound

$$\sigma_c \geq \sqrt{2}||\omega||_\infty. \tag{3.13}$$

Another method is to use the steady state equations of the Kuramoto system to try and find a self-consistent requirement on the order parameter. The steady state solution ϕ_i^* to a Kuramoto system is given by

$$0 = \omega_i + \sigma \sum_{j=1}^{N} \sin(\phi_j^* - \phi_i^*)$$

Rewriting the right hand side in polar form, we have

$$0 = \omega_i + \sigma \frac{1}{2i} \left(e^{-i\phi_i^*} \sum_{j=1}^{N} e^{i\phi_j^*} - e^{i\phi_i^*} \sum_{j=1}^{N} e^{-i\phi_j^*} \right)$$

$$\frac{-2i\omega_i}{\sigma} = \left(e^{-i\phi_i^*} \sum_{j=1}^{N} e^{i\phi_j^*} - e^{i\phi_i^*} \sum_{j=1}^{N} e^{-i\phi_j^*} \right).$$

Recognizing that $r^2 = \sum_{i,j} e^{i(\phi_i - \phi_j)}$, we now multiply both sides by their respective complex conjugates.

$$\frac{2i\omega_i}{\sigma} \frac{-2i\omega_i}{\sigma} = \left(e^{-i\phi_i^*} \sum_{j=1}^{N} e^{i\phi_j^*} - e^{i\phi_i^*} \sum_{j=1}^{N} e^{-i\phi_j^*} \right) \left(e^{i\phi_i^*} \sum_{j=1}^{N} e^{-i\phi_j^*} - e^{-i\phi_i^*} \sum_{j=1}^{N} e^{i\phi_j^*} \right)$$

$$\frac{4\omega_i^2}{\sigma^2} = 2 \sum_{j=1}^{N} e^{i\phi_j^*} \sum_{k=1}^{N} e^{-i\phi_k^*} - e^{-2i\phi_i^*} \sum_{j=1}^{N} e^{i\phi_j^*} \sum_{k=1}^{N} e^{i\phi_k^*} - e^{2i\phi_i^*} \sum_{j=1}^{N} e^{-i\phi_j^*} \sum_{k=1}^{N} e^{-i\phi_k^*}$$

$$\frac{4\omega_i^2}{\sigma^2} = 2r^2 - \sum_{j=1}^{N} \sum_{k=1}^{N} e^{i(-2\phi_i^* + \phi_j^* + \phi_k^*)} + e^{i(2\phi_i^* - \phi_j^* - \phi_k^*)}$$

An equivalent expression can be found for every i, so sum up all such expressions.

$$\sum_{i=1}^{N} \frac{4\omega_i^2}{\sigma^2} = 2Nr^2 - \left(\sum_{j=1}^{N} e^{-i\phi_j^*} \sum_{k=1}^{N} e^{-i\phi_k^*} \sum_{i=1}^{N} e^{i\phi_i^*} e^{i\phi_i^*} + \sum_{j=1}^{N} e^{i\phi_j^*} \sum_{k=1}^{N} e^{i\phi_k^*} \sum_{i=1}^{N} e^{-i\phi_i^*} e^{-i\phi_i^*} \right)$$

$$\sum_{i=1}^{N} \frac{4\omega_i^2}{\sigma^2} = 2Nr^2 - (O_s^* O_s^* \sum_{i=1}^{N} e^{2i\phi_i^*} + O_s O_s \sum_{i=1}^{N} e^{-2i\phi_i^*})$$

Notice now that $\sum_{i=1}^{N} e^{2i\phi_i^*}$ is a complex order parameter corresponding to a distribution of phases twice as large as the steady state distribution. We now make the approximate assumption that this distribution corresponds to the steady state of a Kuramoto system with double the inherent frequencies.

$$\sum_{i=1}^{N} e^{2i\phi_i^*} \approx O_s(2\omega, \sigma)$$

This assumption is false, but is asymptotically correct as $\sigma \to \infty$.

$$\sum_{i=1}^{N} \frac{4\omega_i^2}{\sigma^2} \approx 2Nr^2 - (O_s^* O_s^* O_s(2\omega, \sigma) + O_s O_s O_s^*(2\omega, \sigma))$$

Assuming we shift the frame of reference such that the phase of the complex order parameter O_s is zero, we have $O_s = O_s^* = r$.

$$\sum_{i=1}^{N} \frac{4\omega_i^2}{\sigma^2} \approx 2Nr^2 - 2(r^2 r(2\omega, \sigma))$$
$$\frac{4||\omega||_2^2}{\sigma^2} \approx 2r^2(N - r(2\omega))$$

A standard perturbation analysis yields

$$r(\omega, \sigma) \approx N - \frac{1}{N^2}\frac{||\omega||_2^2}{\sigma^2} - \frac{1}{N^5}\left(\frac{||\omega||_2^2}{\sigma^2}\right)^2 - \frac{5}{4N^8}\left(\frac{||\omega||_2^2}{\sigma^2}\right)^3 - \frac{25}{16N^{11}}\left(\frac{||\omega||_2^2}{\sigma^2}\right)^4 - ...$$

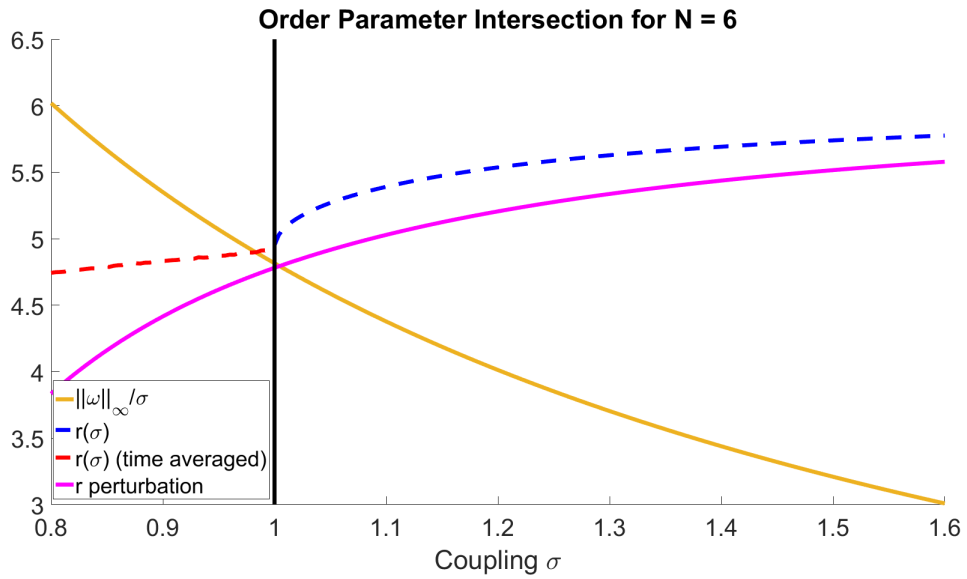

Figure 3.11: The intersection found by asymptotically estimating r.

Utilizing only the first-order approximation and finding the intersection with the curve $\frac{||\omega||_\infty}{\sigma}$ yields an estimate for the critical coupling.

$$\sigma_c \approx \frac{1}{N}||\omega||_\infty + \frac{1}{2}\sqrt{\frac{||\omega||_\infty^2}{N^2} + \frac{4||\omega||_2^2}{N^3}}. \tag{3.14}$$

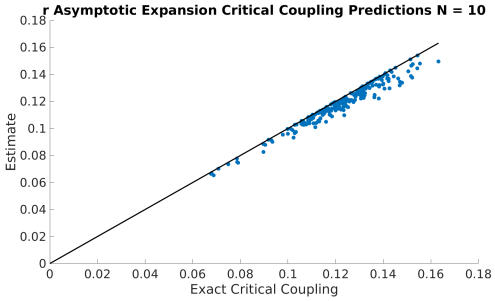

(a) Estimates using asymptotic intersection for the critical coupling in systems of 10 nodes.

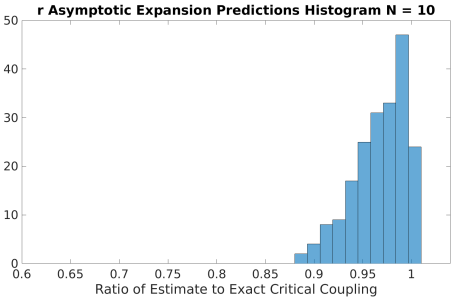

(b) Histogram of estimates as a percentage of the actual critical coupling.

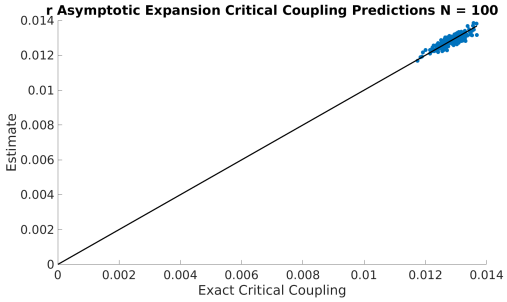

(c) Estimates using asymptotic intersection for the critical coupling in systems of 100 nodes.

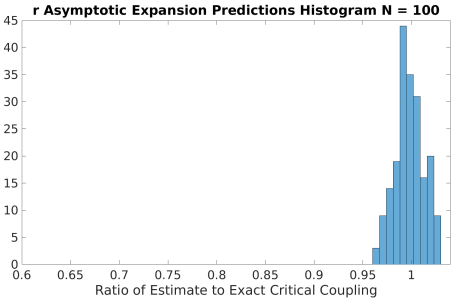

(d) Histogram of estimates as a percentage of the actual critical coupling.

Figure 3.12: The same 200 standard Kuramoto system critical couplings now compared to the estimate (3.14). The estimates are closest in mean to the actual critical coupling of any we have tried, but are not strict lower bounds as in many of the previous cases.

3.3 A New Order Parameter on Clusters

The σ_c prediction histograms exhibit a variance in accuracy from one Kuramoto system to another. We would like to better understand what properties of the system lead our approximations to be stronger or weaker.

One obvious problem with analysis of equation (3.5) is that it is specific to a single oscillator ϕ_i. When we use equation (3.5) to form the bound in equation (3.6), we are implicitly assuming that at the critical coupling bifurcation the oscillator with maximum magnitude inherent frequency decouples alone from the rest of the system. However, numerical studies have shown that frequently in random Kuramoto systems the bifurcation is into two or more synchronized *clusters* which contain multiple oscillators. This is particularly common in the network variation of the Kuramoto model. In (Gómez-Gardenes *et al.*, 2007), the qualitative paths of cluster synchronization were investigated in Kuramoto systems on random Erdős–Rényi(ER) and Barabási-Albert(BA) network topologies and further analysis was conducted in (Stout *et al.*, 2011). It was found that cluster growth in a network Kuramoto model followed two basic paradigms; there could be one dominant giant cluster to which more and more oscillators attach as the coupling increases (Lee, 2005), or there could be a coalescent effect in which small clusters form throughout the network and synchronize to form medium and then large clusters. It was found that BA scale-free networks had comparatively more affinity for the first paradigm, while ER networks had more for the second.

To investigate how this clustering behavior affects our estimates, we repeated the experiment from figure 3.8 and applied a color coding to identify which systems exhibited a nonstandard bifurcation (either into more than two clusters or into two clusters of size greater than one).

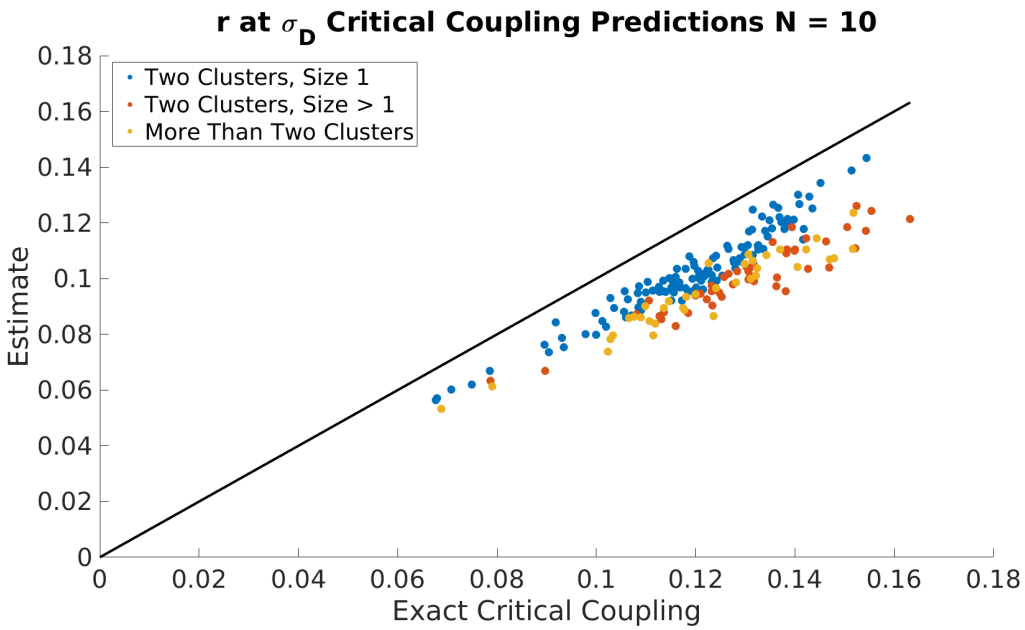

Figure 3.13: 200 standard Kuramoto system critical couplings compared to the estimate (3.10), but now color coded to show the systems with nonstard bifurcation behaviour. A standard bifurcation is into two clusters of size 1 and $N-1$, these systems are shown in blue. Systems which bifurcated into clusters of nonstard size or into more than two clusters are shown in red and orange, respectively. There is a clear bias in accuracy for the nonstandard bifurcation systems. The estimates for those systems are almost universally worse than the estimates for the standard bifurcations, because the standard bifurcations are the ones which equation (3.6) was designed to approximate.

We propose a new order parameter r_C to better study the bifurcations of Kuramoto systems into clusters of nonstandard size. Additionally, we define our new order parameter on the network variant of the Kuramoto model.

Definition 11. *The cluster order parameter r_C is defined on a network Kuramoto*

system (A, ω) *and a nonempty, strict subset of nodes* C *by*

$$r_C := \left| \sum_{i \in C, j \notin C} A_{ij} e^{i(\phi_j - \phi_i)} \right|. \tag{3.15}$$

Note that any subset C *partitions the nodes of a Kuramoto system into two clusters, the nodes in* C *and nodes not in* C*.*

The standard order parameter is not a very useful tool for analyzing network Kuramoto systems because it contains no information about the network structure. Many other order parameters have been defined (Schröder *et al.*, 2017) as tools to study synchronization in network systems, but most are defined as a single quantity over the entire set of oscillators. It is important to recognize that equation (3.15) defines a separate order parameter for each and every nonempty strict subset of nodes C. For a Kuramoto system of size N, there are $2^{N-1} - 1$ possible distinct ways to partitions the nodes of the system into two groups, and therefore the same number of choices for the subset C. This is a significant departure from the standard order parameter (3.1) which is defined only once per Kuramoto system. Even in the case where C is a single oscillator, r_C still depends on the choice of oscillator and is distinct from r. Like the standard order parameter, the cluster order parameter changes with σ, and above σ_c we define $r_C(\sigma)$ to be the cluster order parameter for cluster C when the system is in steady state at coupling σ. The cluster order parameter shares a resemblance with the universal order parameter defined in (Schröder *et al.*, 2017), which was proven to be strictly increasing in σ in steady state. We conjecture that the same is true for the cluster order parameter.

In the case that A is a complete graph, we have $r_C = \left|\sum_{i \in C} e^{i\phi_i}\right| \left|\sum_{j \notin C} e^{i\phi_j}\right|$, and we can interpret r_C as the product of standard order parameters of each cluster in the system. If A is not a complete graph, then r_C cannot be factored in this way. Rather than attempting to capture the phase cohesiveness of an entire Kuramoto system,

the cluster order parameter measures the phase cohesiveness of the phase *differences* along the subset of edges between clusters.

Definition 12. *The time-averaged cluster order parameter* $\langle r_C \rangle_t$ *is defined by*

$$\langle r_C \rangle_t := \lim_{\tau \to \infty} \frac{1}{\tau} \int_0^\tau r_C(t) dt = \lim_{\tau \to \infty} \frac{1}{\tau} \int_0^\tau \left| \sum_{i \in C, j \notin C} A_{ij} e^{i(\phi_j(t) - \phi_i(t))} \right| dt. \tag{3.16}$$

3.4 Mean Field Formulation Using the Cluster Order Parameter

In section 3.4 we establish the usefulness of the cluster order parameter in analyzing network Kuramoto systems. Assume that the oscillators of a Kuramoto system are partitioned into those belonging to a subset C and those that do not. Define the cluster averages γ_1 and γ_2 by

$$\dot{\gamma}_1 = \frac{1}{|C|} \sum_{i \in C} \dot{\phi}_i$$
$$\dot{\gamma}_2 = \frac{1}{N - |C|} \sum_{i \notin C} \dot{\phi}_i.$$

Then the dynamics for the cluster averages are given by

$$\dot{\gamma}_1 = \frac{1}{|C|} \sum_{i \in C} \left[\omega_i + \sigma \sum_j A_{ij} \sin(\phi_j - \phi_i) \right]$$
$$\dot{\gamma}_2 = \frac{1}{N - |C_p|} \sum_{i \notin C} \left[\omega_i + \sigma \sum_j A_{ij} \sin(\phi_j - \phi_i) \right]$$

Let

$$\tilde{\omega} = \frac{1}{|C|} \sum_{i \in C} \omega_i$$

for simplification purposes. We will restrict ourselves to the dynamics for γ_1 from here on, the analysis for γ_2 is similar. It is convenient now that any terms in the

double sums between nodes of the same cluster will cancel out (assuming the graph A is undirected). We therefore only need to consider the cross-cluster connections.

$$\dot{\gamma}_1 = \tilde{\omega} + \frac{\sigma}{|C|} \sum_{i \in C, j \notin C} A_{ij} \sin(\phi_j - \phi_i)$$

We want to rewrite the right hand side in terms of γ_1 and γ_2 as much as possible. Add and subtract γ terms within the argument of the sine function to get

$$\dot{\gamma}_1 = \tilde{\omega} + \frac{\sigma}{|C|} \sum_{i \in C, j \notin C} A_{ij} \sin\left(\phi_j - \phi_i + \gamma_2 - \gamma_1 - \gamma_2 + \gamma_1\right)$$

$$\dot{\gamma}_1 = \tilde{\omega} + \frac{\sigma}{|C|} \sum_{i \in C, j \notin C} A_{ij} \sin\left(\phi_j - \phi_i + \gamma_2 - \gamma_1 - \frac{1}{N - |C|} \sum_{k \notin C} \phi_k + \frac{1}{|C|} \sum_{k \in C} \phi_k\right)$$

$$\dot{\gamma}_1 = \tilde{\omega} + \frac{\sigma}{|C|} \sum_{i \in C, j \notin C} A_{ij} \sin\left(\gamma_2 - \gamma_1 - \frac{1}{N - |C|} \sum_{k \notin C} [\phi_k - \phi_j] + \frac{1}{|C|} \sum_{k \in C} [\phi_k - \phi_i]\right).$$

Let $Y_{ij} = -\frac{1}{N-|C|} \sum_{k \notin C} [\phi_k - \phi_j] + \frac{1}{|C|} \sum_{k \in C} [\phi_k - \phi_i]$. Then,

$$\dot{\gamma}_1 = \tilde{\omega} + \frac{\sigma}{|C|} \sum_{i \in C, j \notin C} A_{ij} \sin\left(\gamma_2 - \gamma_1 + Y_{ij}\right).$$

Now we can use the trigonometric identity (3.3) to write

$$\sum_{i \in C, j \notin C} A_{ij} \sin\left(\gamma_2 - \gamma_1 + Y_{ij}\right) = r_C \sin(\gamma_2 - \gamma_1 + Z)$$

where

$$r_C^2 = \sum_{i \in C, j \notin C, r \in C, s \notin C} A_{ij} A_{rs} \cos(Y_{ij} - Y_{rs})$$

$$\tan(Z) = \frac{\sum_{i \in C, j \notin C} A_{ij} \sin(Y_{ij})}{\sum_{i \in C, j \notin C} A_{ij} \cos(Y_{ij})}.$$

To see that this definition of r_C is equivalent to (3.15), first simplify $Y_{ij} - Y_{rs}$.

$$Y_{ij} - Y_{rs} = \frac{1}{N - |C|} \sum_{k \notin C} [\phi_k - \phi_s - \phi_k + \phi_j] + \frac{1}{|C|} \sum_{k \in C} [\phi_k - \phi_i - \phi_k + \phi_r]$$

$$Y_{ij} - Y_{rs} = \phi_j - \phi_s + \phi_r - \phi_i$$

So $r_C^2 = \sum_{i \in C, j \notin C, r \in C, s \notin C} A_{ij} A_{rs} \cos(\phi_j - \phi_s + \phi_r - \phi_i)$. Use the complex representation of cosine to get

$$r_C^2 = \sum_{i \in C, j \notin C, r \in C, s \notin C} A_{ij} A_{rs} \frac{1}{2} [e^{i(\phi_j - \phi_s + \phi_r - \phi_i)} + e^{-i(\phi_j - \phi_s + \phi_r - \phi_i)}]$$

$$r_C^2 = \frac{1}{2} \sum_{i \in C, j \notin C, r \in C, s \notin C} A_{ij} A_{rs} e^{i(\phi_j - \phi_s + \phi_r - \phi_i)} + \frac{1}{2} \sum_{i \in C, j \notin C, r \in C, s \notin C} A_{ij} A_{rs} e^{-i(\phi_j - \phi_s + \phi_r - \phi_i)}$$

Recognize that the two sums are equivalent under the change of indices $i \leftrightarrow r$ and $j \leftrightarrow s$. Then,

$$r_C^2 = \sum_{i \in C, j \notin C, r \in C, s \notin C} A_{ij} A_{rs} e^{i(\phi_j - \phi_s + \phi_r - \phi_i)}$$

and the summation is now separable.

$$r_C^2 = \left[\sum_{i \in C, j \notin C} A_{ij} e^{i(\phi_j - \phi_i)} \right] \left[\sum_{r \in C, s \notin C} A_{rs} e^{-i(\phi_s - \phi_r)} \right] = \left| \sum_{i \in C, j \notin C} A_{ij} e^{i(\phi_j - \phi_i)} \right|^2$$

This is equivalent to the definition of the cluster order parameter given in 3.15, and leads to a mean-field representation for the dynamics of γ_1 similar to how the standard order parameter did for each oscillator.

$$\dot{\gamma}_1 = \tilde{\omega} + \frac{\sigma}{|C|} r_C \sin(\gamma_2 - \gamma_1 + Z) \tag{3.17}$$

The analogous expression for γ_2 is

$$\dot{\gamma}_2 = -\frac{|C|}{N-|C|}\tilde{\omega} + \frac{\sigma}{N-|C|} r_C \sin(\gamma_1 - \gamma_2 - Z) \tag{3.18}$$

and the dynamics for their difference is

$$\dot{\gamma}_1 - \dot{\gamma}_2 = \left(1 + \frac{|C|}{N-|C|}\right)\tilde{\omega} - \sigma\left(\frac{1}{|C|} + \frac{1}{N-|C|}\right) r_C \sin(\gamma_1 - \gamma_2 - Z). \tag{3.19}$$

This allows us to prove a theorem for clusters analogous to Theorem 1.

Theorem 2. *Given a network Kuramoto system (A, ω), a subset of oscillators C, and the respective cluster order parameter $r_C(\sigma)$ when the system is in steady state at coupling σ,*

$$\sigma \geq \frac{|\sum_{i\in C}\omega_i|}{r_C(\sigma)}. \tag{3.20}$$

In particular, $\sigma_c \geq \frac{|\sum_{i\in C}\omega_i|}{r_C(\sigma_c)}$ for all possible clusters C.

Proof. If a steady state solution exists for the Kuramoto system, one must also exist for equation (3.19).

$$\left(1 + \frac{|C|}{N-|C|}\right)\tilde{\omega} - \sigma\left(\frac{1}{|C|} + \frac{1}{N-|C|}\right) r_C \sin(\gamma_1 - \gamma_2 - Z) = 0 \tag{3.21}$$

Therefore $\sigma\left(\frac{1}{|C|} + \frac{1}{N-|C|}\right) r_C \geq \left(1 + \frac{|C|}{N-|C|}\right)|\tilde{\omega}|$ or no root could exist. We have $\frac{1}{|C|} + \frac{1}{N-|C|} = \frac{N}{|C|(N-|C|)}$ and $\left(1 + \frac{|C|}{N-|C|}\right)|\tilde{\omega}| = \left(\frac{N-|C|+|C|}{N-|C|}\right)\left|\frac{1}{|C|}\sum_{i\in C}\omega_i\right| = \frac{N}{|C|(N-|C|)}\left|\sum_{i\in C}\omega_i\right|$. Cancellation leads to $\sigma r_C \geq \left|\sum_{i\in C}\omega_i\right|$. □

Corollary 3. *For any choice of σ where a steady state solution exists and for any subset of oscillators C we have the bound*

$$\sigma_c \geq \frac{|\sum_{i\in C}\omega_i|}{r_C(\sigma)}. \tag{3.22}$$

Proof. The argument follows from the observation that r_C increases with σ. Because σ_c is the lowest coupling at which a steady state exists, we must have $\sigma \geq \sigma_c$. Therefore $r_C(\sigma) \geq r_C(\sigma_c)$ and $\frac{|\sum_{i\in C}\omega_i|}{r_C(\sigma_c)} \geq \frac{|\sum_{i\in C}\omega_i|}{r_C(\sigma)}$. □

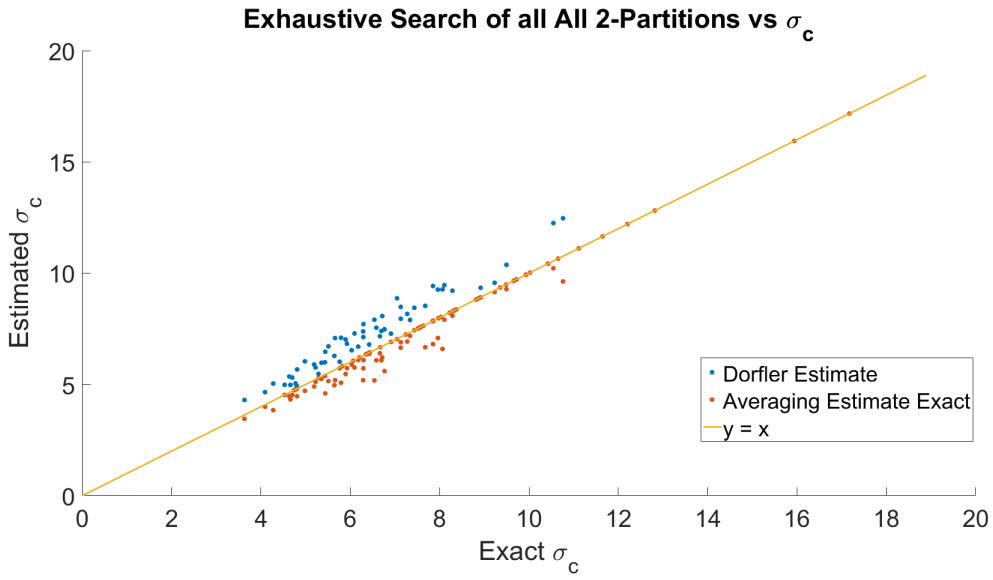

Figure 3.14: Random network Kuramoto systems of size $N = 16$ on ER graphs with uniformly random frequencies were generated. An exhaustive search of all 2^{15} possible choices for C in each systems was performed. The maximal lower bound for each system is plotted, with the line indicating perfect approximation of σ_c and the Dörfler estimate σ_D shown for reference.

Theorem 2 invites a method to estimate σ_c similar to that introduced in section 3.1. Estimate the curve $r_C(\sigma)$, and find the intersection point with the curve $\frac{|\sum_{i\in C}\omega_i|}{\sigma}$. The intersection will be an estimate for σ_c, and possibly a strict lower bound depending on how $r_C(\sigma)$ is approximated. A conceptual barrier is to choose the cluster C. In principle, any choice of C leads to a lower bound on σ_c though equation (3.22), but in practice the vast majority of bounds produced in this manner are extremely poor. Only a few choices lead to a lower bound which is a substantial percentage of σ_c. This

can be seen as both a curse and blessing. On one hand, there are exponentially many $(2^{(N-1)} - 1)$ choices for C, so an exhaustive search through each of their respective bounds to find the maximum is infeasible unless N is less than 20 or 30. On the other hand, if the cluster with the maximum bound *is* found, this gives us great insight into the behavior of the Kuramoto system just below the critical coupling. Sufficient conditions on cluster synchronization combining frequencies and edge weights were introduced in (Favaretto *et al.*, 2017b) (Favaretto *et al.*, 2017a), but a predictive result was not obtained. In this dissertation we investigate the predictive power of theorem 2.

Conjecture 1. *Assume that a network Kuramoto system (A, ω) has a critical coupling σ_c and bifurcates into exactly two clusters for $\sigma \approx \sigma_c - \epsilon$. We conjecture that the clusters that form maximize the intersection point between $r_C(\sigma)$ and $\frac{\left|\sum_{i \in C} \omega_i\right|}{\sigma}$ (either cluster can be taken to be C due to symmetry).*

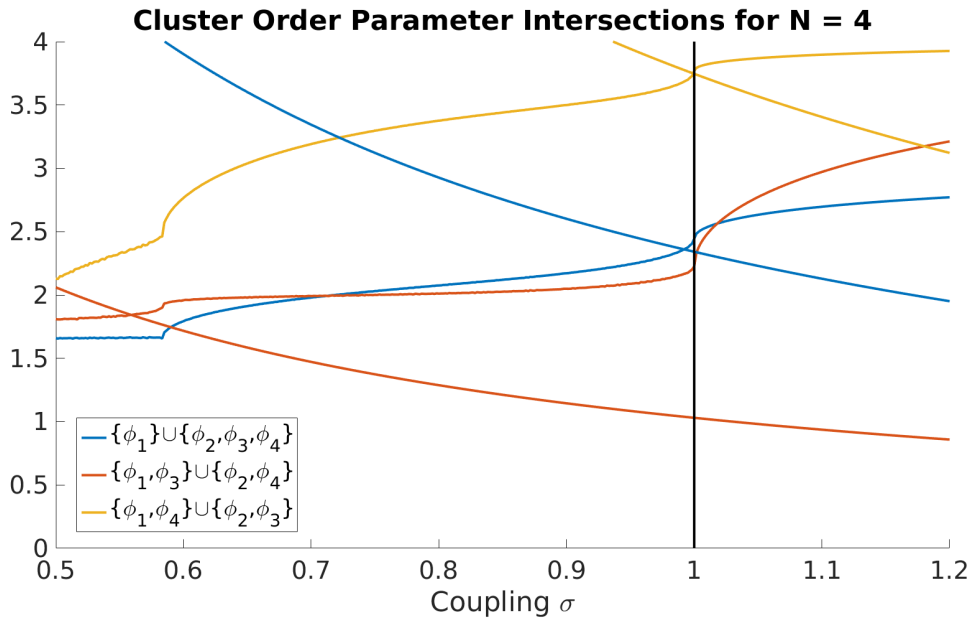

Figure 3.15: A demonstration of the intersections between the $r_C(\sigma)$ and $\frac{|\tilde{\omega}|}{\sigma}$ curves for three possible choices of C. We simulated a Kuramoto system on a complete graph of 4 nodes, with random inherent frequencies normalized such that the critical coupling is 1 (shown in black). For three of the seven possible partitions of a set of four oscillators into two clusters, we computed the $r_C(\sigma)$ curves and the $\frac{|\tilde{\omega}|}{\sigma}$ curves and identified their intersection points. Below the critical coupling we replaced r_C with its time-average. The three clusters are color coded, and for each cluster choice the increasing curve is $r_C(\sigma)$ and the decreasing curve is $\frac{|\tilde{\omega}|}{\sigma}$. Each of the three intersection points gives a lower bound on the critical coupling, but the intersection corresponding to $C = \{\phi_1, \phi_4\}$ is the largest. We surveyed all seven possible choices for C and found that this cluster had the maximum lower bound, and that the Kuramoto system naturally split into these two clusters just below the critical coupling.

3.5 More Than Two Clusters

Kuramoto systems can have more than two synchronized clusters for certain ranges of the coupling strength, as seen in figure 2.8. Some systems do not even have values of the coupling where exactly two clusters exist and instead bifurcate from total synchronization directly to three or more clusters. A statistical study is seen in figure 3.16. These observations provide motivation to find an extension of theorem 2 for more than two clusters.

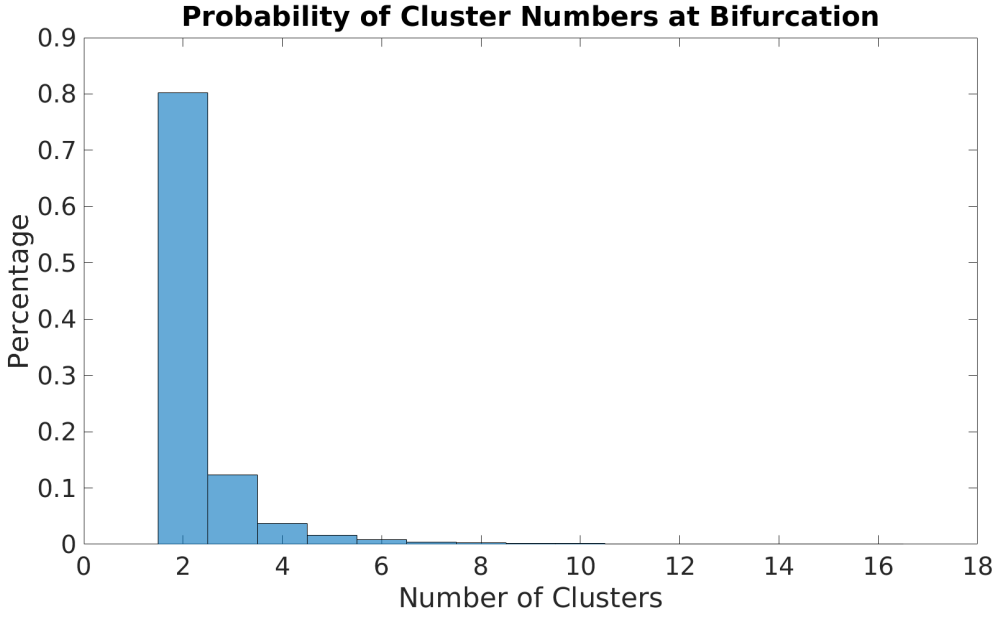

Figure 3.16: A histogram of the number of clusters at bifurcation for random Kuramoto systems. 86,000 random ER networks with 20 nodes and random numbers of edges were generated and oscillators were embedded into the network with inherent frequencies chosen uniformly at random. The critical coupling for each system was computed and the number of clusters just below critical coupling was recorded.

In appendix A, we have derived expressions based on identity (3.3 for Kuramoto systems of more than two clusters. Assume that the oscillators of a Kuramoto system

are partitioned into sets $C_1, C_2, C_3, ...$ and define γ_p to be the mean of phases of nodes in C_p. Then,

$$\dot{\gamma}_p = \tilde{\omega}_p + \frac{\sigma}{|C_p|} \sum_{l \neq p} r_{lp} \sin(\gamma_l - \gamma_p + Z_{lp}) \tag{3.23}$$

where

$$\tan(Z_{lp}) = \frac{\sum_{i \in C_p, j \in C_l} A_{ij} \sin(Y_{ij})}{\sum_{i \in C_p, j \in C_l} A_{ij} \cos(Y_{ij})} \tag{3.24}$$

and r_{lp} is the multicluster order parameter between clusters C_l and C_p.

Definition 13. *The multicluster order parameter r_{lp} on a network Kuramoto system (A, ω) with disjoint subsets C_l and C_p is*

$$r_{lp} := \left| \sum_{i \in C_l, j \in C_p} A_{ij} e^{i(\phi_j - \phi_i)} \right|. \tag{3.25}$$

With more than two clusters we then have a multicluster order parameter *matrix* r and a phase offset matrix Z, which are respectively symmetric and anti-symmetric. An extension of theorem 2 applies.

Theorem 3. *Given a network Kuramoto system (A, ω) partitioned into sets $C_1, C_2, C_3, ...$, let $\gamma_p = \frac{1}{|C_p|} \sum_{i \in C_p} \phi_i$ and $\tilde{\omega}_p = \frac{1}{|C_p|} \sum_{i \in C_p} \omega_i$. Define r_{lp} and Z_{lp} by equations (3.25) and (3.24). If the coupling σ is chosen such that the Kuramoto system has a steady state solution, then there must also exist a solution to*

$$\tilde{\omega}_p + \frac{\sigma}{|C_p|} \sum_{l \neq p} r_{lp} \sin(\gamma_l - \gamma_p + Z_{lp}) = 0 \tag{3.26}$$

for all p.

Proof. Equation (3.26) is the fixed point condition for equation (3.23). Most of the work in the proof comes from the derivation of equation (3.23) found in appendix A.

Then because each γ_p term is a linear combination of ϕ variables, a fixed point for the ϕ system exists only if a fixed point for the γ system exists. $\square$

If we assume both r and Z to be constant, then equation 3.23 shows that the γ variables form a lower-dimensional network Kuramoto system with weighted, directed edge couplings and phase offsets. Theorem 3 states that the critical coupling of γ system is a lower bound for the critical coupling of the ϕ system.

Theorem 3 is an extension of theorem 2, but the usefulness of the extension to more than two clusters is limited. With only two clusters, the phase difference dynamics in equation (3.19) are a one-dimensional dynamical system with an easy to calculate saddle-node bifurcation. With systems of three or more clusters the presences of cycles complicate matters and an explicit formula for the critical coupling is not currently known.

3.5.1 Multiple Cluster Example

Take the 25 node system from figure 2.4 at coupling $\sigma = 15$.

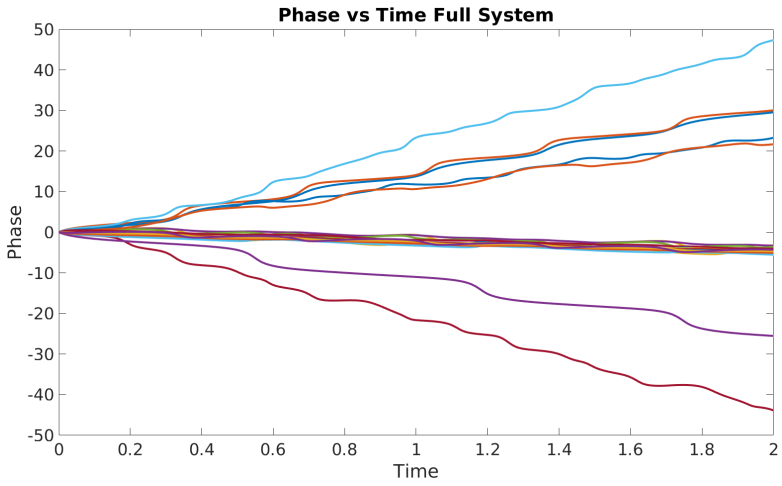

(a) Phase time series for $N = 25$ example.

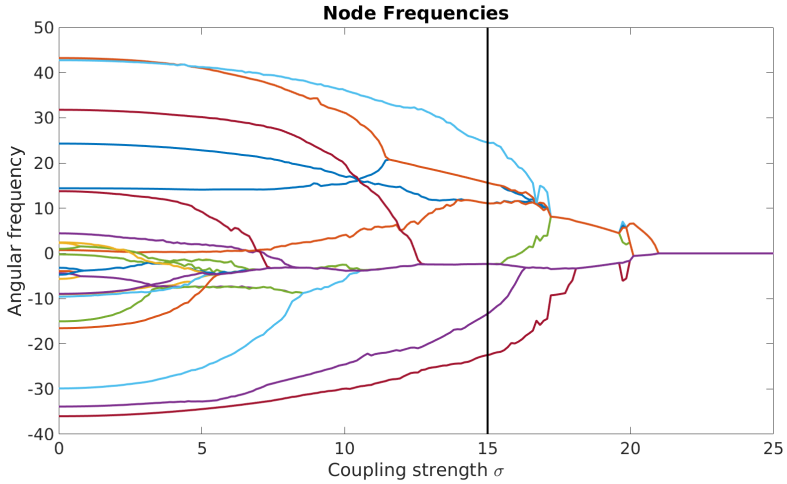

(b) Bifurcation diagram for $N = 25$ example with $\sigma = 15$ marked.

Figure 3.17: There are six clusters for the $N = 25$ example system at $\sigma = 15$. They can be readily seen in either the time-series plot or the bifurcation diagram.

To form a reduced system of size six from these six clusters, we computed the fixed point ϕ^* at $\sigma = 20.92$ very near the bifurcation point and used it to compute matrices r and Z.

$$r = \begin{pmatrix} 0 & 0 & 1 & 1 & 0 & 1 \\ 0 & 0 & 1.97 & 0 & 0 & 0 \\ 0.06 & 0.11 & 0 & 0.07 & 0.16 & 0.06 \\ 0.5 & 0 & 0.5 & 0 & 0 & 0.5 \\ 0 & 0 & 1.43 & 0 & 0 & 0 \\ 1 & 0 & 1 & 1 & 0 & 0 \end{pmatrix}, Z = \begin{pmatrix} 0 & 0 & -0.10 & 0.12 & 0 & 0 \\ 0 & 0 & -0.82 & 0 & 0 & 0 \\ 0.10 & 0.82 & 0 & -0.14 & -1.07 & -1.23 \\ -0.12 & 0 & 0.14 & 0 & 0 & 0.12 \\ 0 & 0 & 1.07 & 0 & 0 & 0 \\ 0 & 0 & 1.23 & -0.12 & 0 & 0 \end{pmatrix}.$$

Next we constructed the reduced system given by equation 3.23 and assumed r and Z were constant matrices with no dependence on time or σ. This is clearly a false assumption but it allows us to compare the reduced system to the full one.

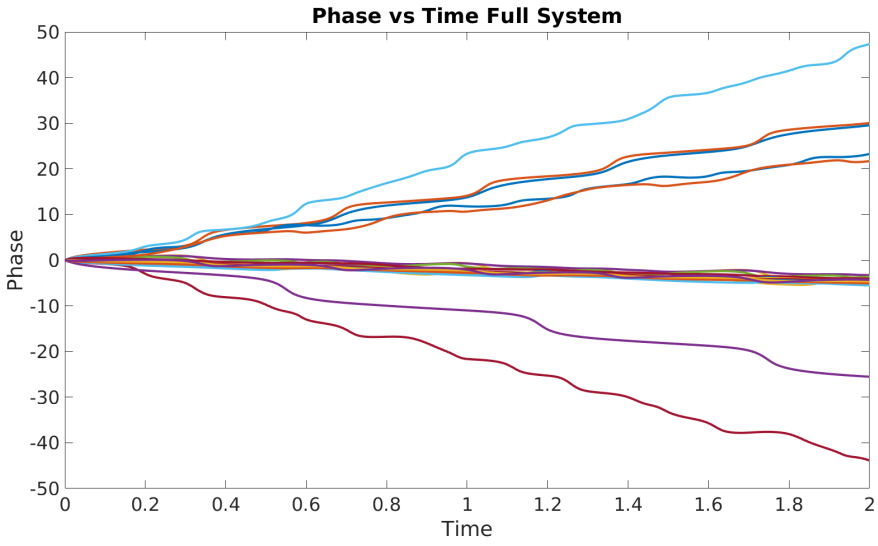

(a) Full

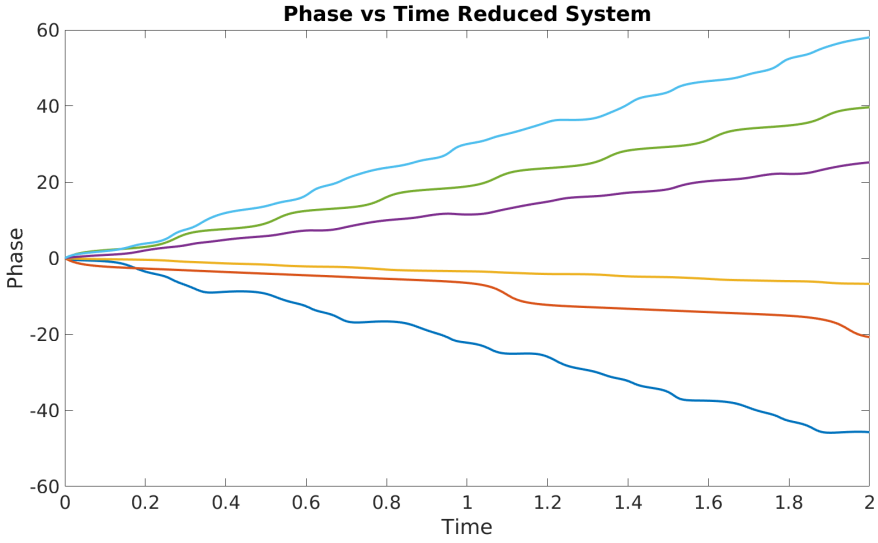

(b) Reduced

Figure 3.18: A comparison of the phase time series for the full and reduced systems.

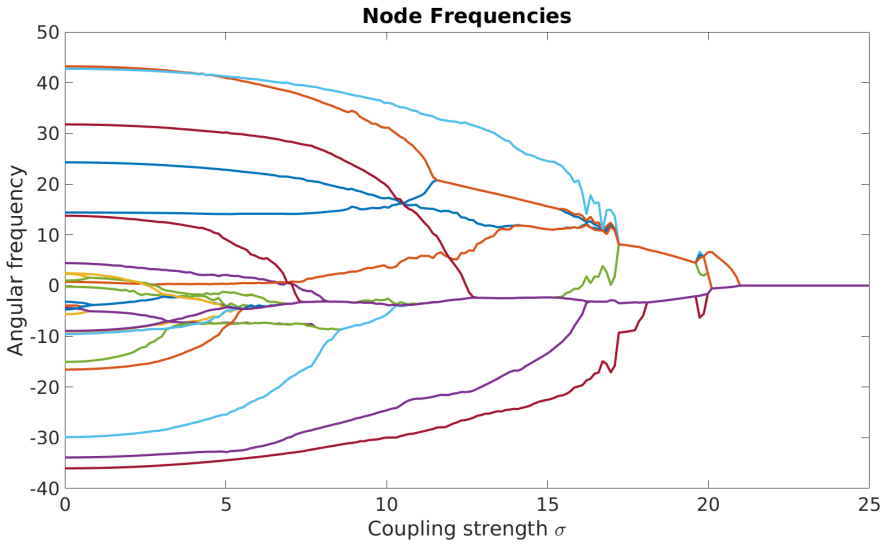

(a) Full

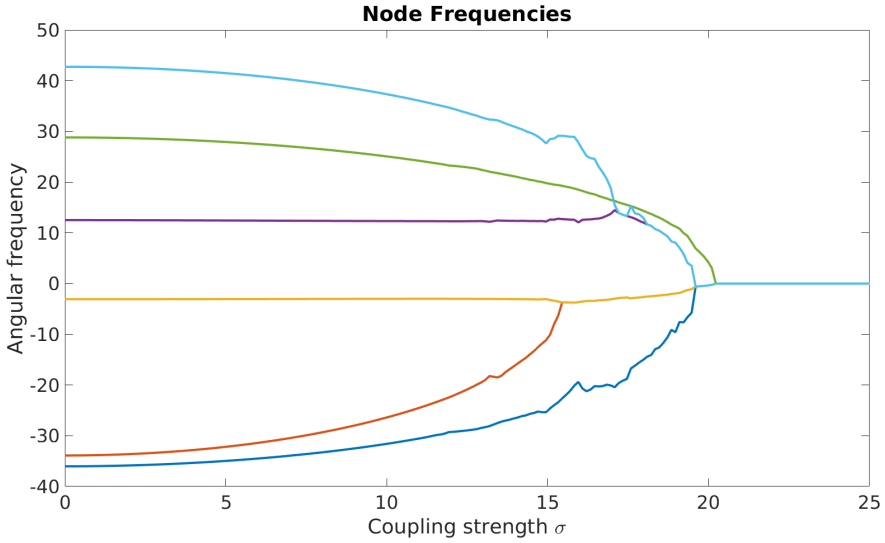

(b) Reduced

Figure 3.19: A comparison of the bifurcation diagrams for the full and reduced systems.

In this example figure 3.19 shows that the critical coupling for the reduced system is a lower bound for the critical coupling of the full system.

3.5.2 Relation to External Equitable Partitions

Definition 14. *An External Equitable Partition (EEP) of a graph is a partition of the graph into clusters such that all nodes within one cluster have the same number of neighbors in each respective external cluster. Additionally, if the graph is associated to a Kuramoto system and all nodes within each cluster have identical frequencies, then the Kuramoto system is said to respect the EEP.*

In (Schaub *et al.*, 2016) it was observed that Kuramoto systems which respect an External Equitable Partition have an exact dimensional reduction to a lower dimensional manifold. This can be seen with even small examples. Consider an $N = 3$ node triangular graph with adjacency matrix $A = \begin{pmatrix} 0 & 1 & 1 \\ 1 & 0 & 1 \\ 1 & 1 & 0 \end{pmatrix}$ and frequencies $\omega = \begin{pmatrix} -1 \\ -1 \\ 2 \end{pmatrix}$. The system is 3-dimensional, but there exists a 2-dimensional invariant subspace where $\phi_1 = \phi_2$ for all time. Assuming that the initial conditions for ϕ_1 and ϕ_2 are identical, we can replace ϕ_1 and ϕ_2 by a single variable $\phi_{12} := \phi_1 = \phi_2$ and recompute the dynamics on the invariant subspace. The full dynamics for this system are

$$\begin{aligned}
\dot{\phi}_1 &= -1 + \sigma\left[\sin(\phi_2 - \phi_1) + \sin(\phi_3 - \phi_1)\right] \\
\dot{\phi}_2 &= -1 + \sigma\left[\sin(\phi_1 - \phi_2) + \sin(\phi_3 - \phi_2)\right] \\
\dot{\phi}_3 &= +2 + \sigma\left[\sin(\phi_1 - \phi_3) + \sin(\phi_2 - \phi_3)\right]
\end{aligned}$$

which when simplified form the reduced system

$$\begin{aligned}
\dot{\phi}_{12} &= -1 + \sigma \sin(\phi_3 - \phi_{12}) \\
\dot{\phi}_3 &= 2 + 2\sigma \sin(\phi_{12} - \phi_3).
\end{aligned}$$

We can view the dynamics on the invariant subspace as the dynamics for a *weighted*, *directed* $N = 2$ Kuramoto system with adjacency matrix $r = \begin{pmatrix} 0 & 1 \\ 2 & 0 \end{pmatrix}$ and frequencies $\tilde{\omega} = \begin{pmatrix} -1 \\ 2 \end{pmatrix}$. An eight node example from (Schaub *et al.*, 2016) of an EEP and its respective quotient graph is seen in figure 3.20. If all like-colored nodes in the system have the same inherent frequency, then the Kuramoto system respects the EEP, and the quotient graph forms a reduced system exactly matching the dynamics on the full system's stable manifold.

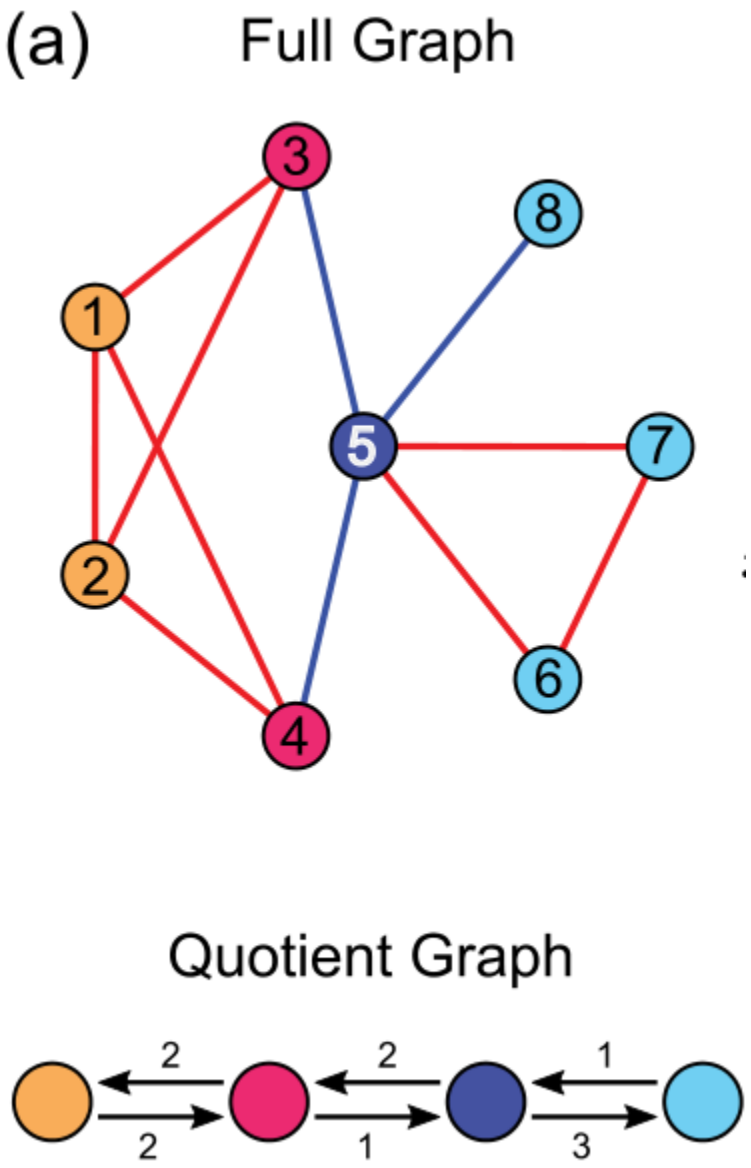

Figure 3.20: An example due to Schaub (Schaub *et al.*, 2016) of an eight node system with a nontrivial External Equitable Partition of four clusters. Every node within a cluster has the same number of neighbors in every other external cluster. The quotient graph of the partition reproduces the exact dynamics on the stable invariant subspace of the original system.

If a Kuramoto system respects an EEP, then the dynamics in equation 3.23 are equivalent to the reduction process shown in (Schaub *et al.*, 2016).

Chapter 4

NETWORK OPTIMIZATION PROBLEMS AND SPECTRAL GRAPH THEORY

4.1 The Cluster Optimization Problem

In chapter 4 we will investigate the implications of theorem 2 and its corollary 3.22. The corollary states that if σ is a fixed value above the critical coupling, ϕ^* is the steady state solution vector corresponding to that σ, and C is a cluster of nodes in the Kuramoto network, then there is an associated lower bound on the critical coupling for that cluster. The lower bound is given by

$$\sigma_c \geq \frac{|\sum_{i\in C}\omega_i|}{\left|\sum_{i\in C, j\notin C} A_{ij}e^{i(\phi_j^*-\phi_i^*)}\right|}. \tag{4.1}$$

It's natural to ask which choice of cluster C produces the *maximal* lower bound.

Problem 6. *Given a Kuramoto network (A,ω) on a set of oscillators V and a fixed coupling $\sigma \geq \sigma_c$, the cluster optimization problem is to find*

$$\max_{C\in\mathbb{P}(V)} \frac{|\sum_{i\in C}\omega_i|}{\left|\sum_{i\in C, j\notin C} A_{ij}e^{i(\phi_j^*-\phi_i^*)}\right|}. \tag{4.2}$$

In other words, given a fixed vector of phases ϕ we wish to find the subset of nodes C which maximizes the ratio $L(C)$, defined by

$$L(C) = \frac{|\sum_{i\in C}\omega_i|}{\left|\sum_{i\in C, j\notin C} A_{ij}e^{i(\phi_j^*-\phi_i^*)}\right|}.$$

In chapter 4 we will explore methods for finding solutions to problem 6 and expand on the problem's physical relevance to a Kuramoto system. We convert the ratio

$L(C)$ into a standardized form and show that problem 6 is related to the well-known problem of graph partitioning in spectral graph theory. We utilize the isoperimetric method of (Grady and Schwartz, 2006) to find approximate solutions to the cluster optimization problem and compare these solutions to the clusters that form naturally in a Kuramoto system. Additionally we perform numerical experiments to compare the maximal lower bound found in problem 6 to the true value of the critical coupling.

4.2 The Network Cut Interpretation

In conjecture 1, we conjectured that the cluster C which maximizes the intersection point between the curve $r_C(\sigma)$ and the curve $\frac{|\sum_{i\in C}\omega_i|}{\sigma}$ would correspond to a frequency-synchronized cluster of oscillators in the Kuramoto system just below critical coupling. Problem 6 asks to find the cluster which maximizes $L(C)$, an approximate guess for the intersection point. Therefore we should expect that the solution to problem 6 should also resemble the sort of cluster we would expect to find in a Kuramoto system.

Numerical simulations of Kuramoto systems suggest a few properties we expect to find in synchronized clusters. Typically, a cluster is formed from oscillators of similar inherent frequency and there are relatively fewer network connections to oscillators outside of the cluster. The structure of $L(C)$ suggests that the solution to problem 6 is likely to have similar properties, so we are looking for a subset of oscillators C with high *internal consistency* (similar frequencies) and low *external baggage* (edges connecting to non-cluster oscillators).

Maximizing $L(C)$ is a combination of maximizing $|\sum_{i\in C}\omega_i|$ and minimizing r_C. Maximizing $|\sum_{i\in C}\omega_i|$ alone would be accomplished by placing all positive frequency nodes in one cluster and all negative frequency nodes in the other, and corresponds with our observation that similar frequency nodes tend to cluster together. Minimiz-

ing r_C alone is equivalent to finding the minimum cut in a complex-weighted graph, where the minimum cut is defined to be the one which minimizes the sum total magnitude of edge weights cut. This corresponds well to our observation that Kuramoto clusters tend to have fewer edges connecting to external oscillators. Maximizing $L(C)$ is accomplished by finding a good balance in these two quantities.

Quantities related to $L(C)$ are frequently studied in graph theory in efforts to quantify community structures in networks. The *isoperimetric ratio* of a graph cut is defined to be the number of edges severed by that cut divided by the number of nodes in the smaller of the two components separated by that cut. It's reasonable that a component formed by a cut with a small isoperimetric ratio matches our intuitive concept of a network community. We will expand more on this concept when we introduce the isoperimetrc algorithm. For a good survey of graph partitioning concepts and the isoperimetric ratio, we recommend (Shewchuk, 2016).

4.3 Standardized Vector Formulation of the Cluster Optimization Problem

To utilize the base of knowledge of optimizing nonlinear functions we seek to rewrite equation 4.2 in vector form.

Lemma 2. *The choice of cluster that maximizes $L(C)$ simultaneously minimizes the ratio*

$$\Lambda(x) := \left| \frac{x^T L_w x}{\omega^T x} \right| \tag{4.3}$$

where x is the characteristic vector of C and L_w is a weighted Laplacian matrix of the Kuramoto network with weights defined below.

Let x be the $N \times 1$ characteristic vector for cluster C, defined element-wise as

$$x_i = \begin{cases} 1 & \text{if node } i \in C \\ 0 & \text{otherwise} \end{cases}.$$

Then $1_N - x$ is the characteristic vector of the complement of C, where 1_N is the $N \times 1$ vector of all ones. Using this vector notation, we can rewrite

$$\sum_{i \in C} \omega_i := \text{Total frequency of cluster } C = \omega^T x$$

Let the weighted Laplacian matrix L_w be defined by

$$L_w(i,j) = \begin{cases} A_{ij} \cos(\phi_j^* - \phi_i^*) & i \neq j \\ -\sum_{k \neq i} L_w(i,k) & \text{otherwise} \end{cases}$$

Then $x^T L_w x$ is the sum of edge weights from nodes in C to nodes outside of C, with weight $\cos(\phi_j^* - \phi_i^*)$.

Proof. To see the connection between r_C and $x^T L_w x$, first convert the complex exponential to Cartesian form.

$$r_C = \left| \sum_{i \in C, j \notin C} A_{ij} e^{i(\phi_j^* - \phi_i^*)} \right| = \left| \sum_{i \in C, j \notin C} A_{ij} [\cos(\phi_j^* - \phi_i^*) + i \sin(\phi_j^* - \phi_i^*)] \right|$$
$$= \sqrt{\left[\sum_{i \in C, j \notin C} A_{ij} \cos(\phi_j^* - \phi_i^*) \right]^2 + \left[\sum_{i \in C, j \notin C} A_{ij} \sin(\phi_j^* - \phi_i^*) \right]^2}$$

The first double summation is exactly $x^T L_w x$. The second can be simplified, because

$$\sum_{i \in C, j \notin C} A_{ij} \sin(\phi_i^* - \phi_j^*) = \sum_{i \in C, j} A_{ij} \sin(\phi_i^* - \phi_j^*) - \sum_{i \in C, j \in C} A_{ij} \sin(\phi_i^* - \phi_j^*)$$

When i and j both index over the same cluster C_1, then for each (i,j) term in the sum there will be a corresponding (j,i) term. Because A is symmetric and sine is odd, these terms will be inverses, cancel out, and the entire sum will equal zero. Therefore,

$$\begin{aligned}\sum_{i\in C, j\notin C} A_{ij}\sin(\phi_i^* - \phi_j^*) &= \sum_{i\in C, j} A_{ij}\sin(\phi_i^* - \phi_j^*) \\ &= \frac{1}{\sigma}\sum_{i\in C}\omega_i + \sum_{i\in C, j} A_{ij}\sin(\phi_i^* - \phi_j^*) - \frac{1}{\sigma}\sum_{i\in C}\omega_i \\ &= \frac{1}{\sigma}\sum_{i\in C}\left[\omega_i + \sigma\sum_{j=1}^{N} A_{ij}\sin(\phi_i^* - \phi_j^*)\right] - \frac{1}{\sigma}\sum_{i\in C}\omega_i.\end{aligned}$$

The term in brackets is exactly the right hand side of the Kuramoto model, and because ϕ^* is a fixed point of the system it evaluates to zero. So $\sum_{i\in C, j\notin C} A_{ij}\sin(\phi_i^* - \phi_j^*) = -\frac{1}{\sigma}\omega^T x$. Therefore we have

$$r_C = \sqrt{\left[x^T L_w x\right]^2 + \left[\frac{1}{\sigma}\omega^T x\right]^2}$$

and

$$L(C) = \left|\frac{\omega^T x}{\sqrt{\left[x^T L_w x\right]^2 + \left[\frac{1}{\sigma}\omega^T x\right]^2}}\right| = \left|\frac{1}{\sqrt{\left[\frac{x^T L_w x}{\omega^T x}\right]^2 + \left[\frac{1}{\sigma}\right]^2}}\right|$$

With this simplification, we can see that the choice of x which maximizes $L(C)$ is the same choice which minimizes the quantity

$$\Lambda(x) := \left|\frac{x^T L_w x}{\omega^T x}\right|. \tag{4.4}$$

□

The simplified form of $\Lambda(x)$ admits a corresponding optimization problem

Problem 7. *Given a weighted Laplacian matrix $L_w \in \mathbb{R}^{N\times N}$ and a mass vector $\omega \in \mathbb{R}^N$ with $1_N^T\omega = 0$, find*

$$\min_x \Lambda(x) = \min_x \left|\frac{x^T L_w x}{\omega^T x}\right| \tag{4.5}$$

among all possible nonzero characteristic vectors $x \in \{0,1\}^N$.

4.4 The Cheeger Constant

Quantities similar in form to that of $\Lambda(x)$ are studied in spectral graph theory. The Cheeger constant (Spielman, 2017) h of an unweighted, undirected graph with Laplacian matrix L is defined as the minimum of all isoperimetric ratios (Chung, 2007) (Shewchuk, 2016) (Chung, 1996), i.e.

$$h = \min_x \left| \frac{x^T L x}{1_N^T x} \right|. \tag{4.6}$$

(the elements of x are chosen such that 1 represents membership in the *smaller* cluster) For a standard Laplacian matrix, $x^T L x$ is the number of edges between the two clusters, and $1_N^T x$ is the number of nodes in the smaller cluster. The Cheeger constant is a measurement of the amount of bottlenecking in a network. Take for example a network formed by joining two equally large, dense networks by a single edge. Almost certainly the minimum isoperimetric ratio will correspond to the cut across the edge, and the Cheeger constant will be $\frac{2}{N}$, quite a small number if N is large. On the other hand, a complete graph on N nodes has Cheeger constant $\frac{N}{2}$, corresponding to a bisection into two equal pieces. The Cheeger constants indicate that the first graph has a more significant bottleneck than the second.

We can then interpret equation (4.5) by noting that $x^T L_w x$ is the sum of the *weights* of the edges between the two clusters and $|\omega^T x|$ is the *frequency-weighted mass* of the nodes in one cluster. Because we assume that $\omega^T 1_N = 0$ for a Kuramoto system, we no do not need to specify whether x is the smaller or larger cluster. Both will have the same frequency-weighted mass.

The Cheeger constant is of particular interest in spectral graph theory due to the existence of the two Cheeger inequalities (Chung, 1996) (Chung, 2007), upper and lower bounds relating the the Cheeger constant to the spectrum of L. They can be

stated compactly as

$$\frac{\lambda_2}{2} \leq h \leq \sqrt{2\lambda_2}$$

where λ_2 (sometimes called the algebraic connectivity) is the smallest nonzero eigenvalue of L (all Laplacian matrices have at least one zero eigenvalue). For proofs of the Cheeger inequalities see (Chung, 1996) or (Shewchuk, 2016). The inequalities establish a link between a *physical* property of a network (a bottleneck), and a *spectral* property of one of the network's associated matrices. λ_2 is a proxy measurement for the how bottlenecked a graph is, and its corresponding eigenvector (often called the Fiedler vector) is a useful tool for categorizing which nodes belong together in a community structure. This is the primary topic of study in spectral graph theory, and we can piggyback on their results to analyze the network Kuramoto model. We have not been able to precisely define an analogue of the Cheeger inequalities for the solution to 4.5, but we believe that many of the methods used to analyze Kuramoto systems based on the eigenvalues or eigenvectors of graph Laplacians (Izumida and Kori, 2013) (Jadbabaie *et al.*, 2004) (Arenas *et al.*, 2008) can be explained because $\Lambda(x)$ is a weighted isoperimetric ratio.

4.5 The Isoperimetric Algorithm

To find the vector x which minimizes $\Lambda(x)$, we employ the isoperimetric algorithm first described in (Grady and Schwartz, 2006) and summarized in (Shewchuk, 2016). The isoperimetric algorithm is a heuristic for estimating the minimum isoperimetric ratio of a graph, and we have found that a slightly modified version is useful for approximation the solution to problem 7.

First, note that if the graph L_w is disconnected, then any choice of x which is a characteristic vector of a component of the graph will be in the null space of the

matrix L_w and therefore will give $\Lambda(x) = 0$. This corresponds to the observation that in a disconnected Kuramoto network, the clusters that form will naturally be the corresponding components of the graph. If the graph is connected, then the problem of minimizing $\Lambda(x)$ with a characteristic vector x is equivalent to finding the corner of the N-cube in the first quadrant of $\mathbb{R}^N$ which minimizes the function $\Lambda(x) : \mathbb{R}^N \to \mathbb{R}$. As with many questions about community detection in networks, this discrete version of the problem is known to be NP-complete.

The isoperimetric method is based on the assumption that the discrete solution is in some sense "nearby" to the relaxed continuous solution. Consider the relaxed problem of minimizing the function $\Lambda(x)$ not on the corners of the N-cube, but instead on the surface of a smooth $(N-1)$-dimensional surface. The advantage of working on a smooth surface is that the calculus technique of the Lagrange multiplier can be utilized. Round the relaxed solution to determine which corner of the N-cube is "closest" to the location of the relaxed minimum. The assumption is that the corner which is closest will with high likelihood be the discrete solution.

Choose a surface by imposing a scaling value $k \in \mathbb{R} \setminus \{0\}$ and enforcing the constraint $\omega^T x = k$. This transforms the expression for $\Lambda(x)$ into the more tractable form

$$\Lambda(x) := \left| \frac{x^T L_w x}{k} \right|.$$

Each choice of k then gives a distinct surface with no intersection with any other surface given by a different value of k. Minimizing $\Lambda(x)$ is equivalent to minimizing the expression $x^T L_w x$ subject to the constraint $\omega^T x = k$. As described in (Grady and Schwartz, 2006), this is accomplished by introducing a Lagrange multiplier y and minimizing the function

$$Q(x) = x^T L_w x - y(\omega^T x - k).$$

Differentiate Q with respect to x and set the derivative to be zero in each component to get the system of linear equations

$$\frac{dQ}{dx} = 2L_w x - y\omega = 0_N.$$

The continuous choice of x that minimizes $\Lambda(x)$ is given by the solution to

$$2L_w x = y\omega. \tag{4.7}$$

Choose y so that the solution x to equation 4.7 satisfies the constraint $\omega^T x = k$. To choose y, first solve the system for $y = 1$. Call this solution x^1. Then, solve the system for $y = \frac{k}{\omega^T x^1}$.

$$2L_w x = \frac{k}{\omega^T x^1}\omega \tag{4.8}$$

The solution x to equation 4.8 will satisfy $\omega^T x = k$.

It was observed in (Grady and Schwartz, 2006) that the choice of scaling k along with the leading 2 in equation 4.8 only serve to scale the solution x linearly. The criterion cut rounding we use is independent of linear scaling so take simplest possible relaxed solution x_r, defined as the solution to

$$L_w x_r = \omega. \tag{4.9}$$

To convert the relaxed solution $x_r \in \mathbb{R}^N$ into a binary solution $x_b \in \{0,1\}^N$, employ the criterion cut process as described in (Grady and Schwartz, 2006). For each element x_r^i in the vector x_r, let x_{bi} be the binary cut defined as

$$x_{bi}^j = \begin{cases} 1 & \text{if } x_r^j \leq x_r^i \\ 0 & \text{otherwise} \end{cases}.$$

Excluding the cut which places all nodes in a single cluster, there are $N-1$ possible cuts to consider. Do a brute force search to find the one which minimizes $\Lambda(x)$, and call the solution x_b. x_b is the prediction of the saddle-node clusters in the system.

This method requires only rudimentary linear algebra to compute x_r, and from there only $O(N)$ function calculations to find x_b. This is a great improvement from the $O(2^N)$ candidates we started with. A disadvantage is that the criterion cut process is not guaranteed to find the global minimum of $\Lambda(x)$.

4.5.1 A Note on the Computation of x_r

L_w is a (weighted) graph Laplacian, and is therefore singular with null space span$\{1_N\}$. For any solution x_r to equation 4.9, $x_r + a1_N$ will also be a solution, for any $a \in R$. As a convention we choose $a = -\min(x_r)$ so that the elements of x_r will be nonnegative, with at least one zero.

Computationally, finding x_r can be accomplished by choosing a node and removing the row and column corresponding to that node from L_w and the frequency corresponding to that node from ω. This will form the nonsingular $(N-1) \times (N-1)$ matrix $\hat{L}_w$, and the $(N-1) \times 1$ vector $\hat{\omega}$. Then, we can solve the system $\hat{L}_w \hat{x} = \hat{\omega}$ with normal methods. x_r can be formed by adding the element 0 back to the vector $\hat{x}$ to replace the element that was previously removed and adding the linear multiple of 1_N as described.

It should be noted that whatever linear multiple of 1_N is chosen has no effect on quantities such as $L_w x_r$ or $\omega^T x_r$, because 1_N is in the null space of L_w and is orthogonal to ω by assumption.

4.5.2 An Illustrative Example

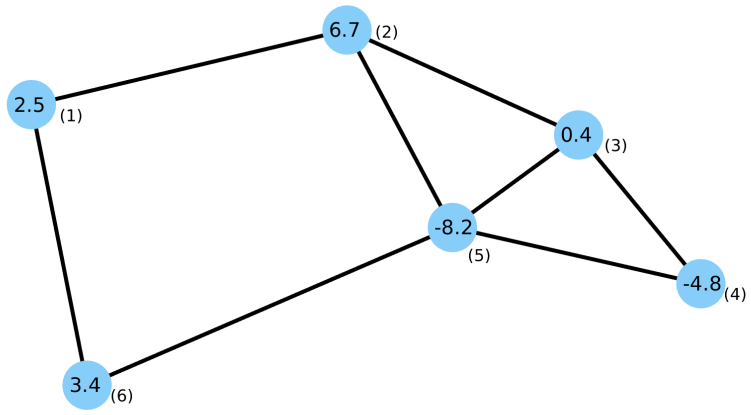

Figure 4.1: An example Kuramoto system with 6 nodes and 8 edges. The node frequencies were generated randomly and are labeled inside. The node indices are in parentheses.

Consider the randomly generated Kuramoto system pictured in figure 4.1. The system has $N = 6$ nodes and 8 edges. The system has adjacency matrix A and frequencies ω given by

$$A = \begin{pmatrix} 0 & 1 & 0 & 0 & 0 & 1 \\ 1 & 0 & 1 & 0 & 1 & 0 \\ 0 & 1 & 0 & 1 & 1 & 0 \\ 0 & 0 & 1 & 0 & 1 & 0 \\ 0 & 1 & 1 & 1 & 0 & 1 \\ 1 & 0 & 0 & 0 & 1 & 0 \end{pmatrix} \qquad \omega = \begin{pmatrix} 2.5 \\ 6.7 \\ 0.4 \\ -4.8 \\ -8.2 \\ 3.4 \end{pmatrix}$$

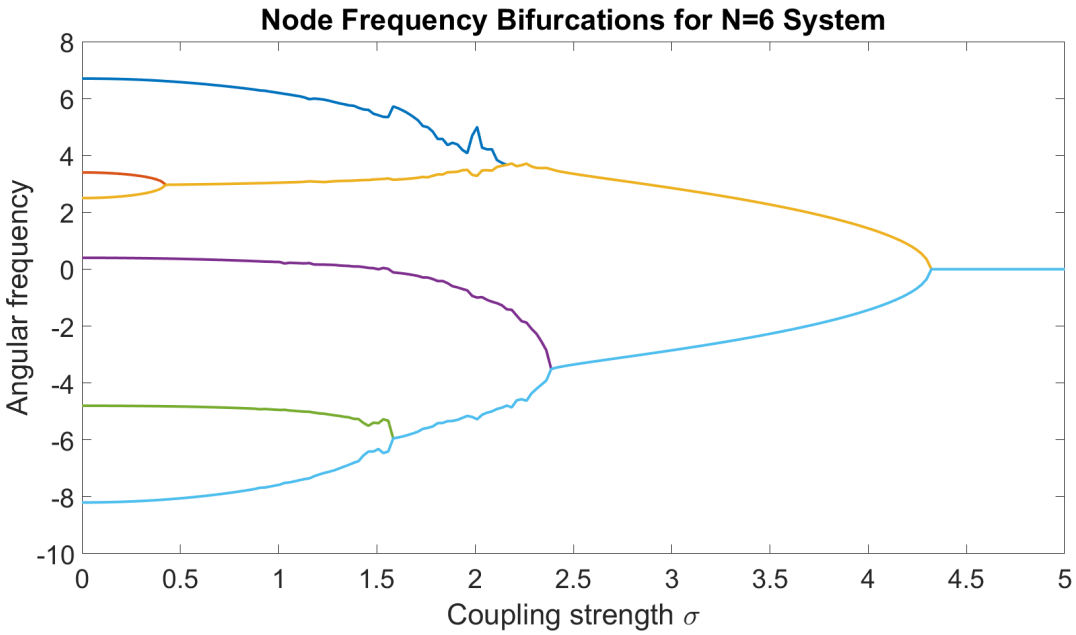

Figure 4.2: The frequency bifurcation plot clearly shows a split into two clusters of three nodes each.

The bifurcation plot in figure 4.2 for this system reveals that the clusters which form just below the critical coupling are composed of nodes $\{1, 2, 3\}$ and $\{4, 5, 6\}$. Our goal is to compute these clusters without relying on the slow process of simulating the system at many values of σ.

Begin by identifying a value of σ which is *definitely* above the critical coupling, so that a fixed point will exist. A good choice is the Dörfler estimate $\sigma_D = ||B^{\dagger}\omega||_{\infty}$ as described in (Dörfler *et al.*, 2013). $B^{\dagger}$ is the pseudo-inverse of the oriented edge incidence matrix B of the graph. For this system we have

$$B = \begin{pmatrix} -1 & -1 & 0 & 0 & 0 & 0 & 0 & 0 \\ 1 & 0 & -1 & -1 & 0 & 0 & 0 & 0 \\ 0 & 0 & 1 & 0 & -1 & -1 & 0 & 0 \\ 0 & 0 & 0 & 0 & 1 & 0 & -1 & 0 \\ 0 & 0 & 0 & 1 & 0 & 1 & 1 & -1 \\ 0 & 1 & 0 & 0 & 0 & 0 & 0 & 1 \end{pmatrix},$$

$$B^{\dagger}\omega = \begin{pmatrix} -1.3 \\ -1.2 \\ -3.5 \\ -4.5 \\ -2.9 \\ -1 \\ 1.9 \\ 4.6 \end{pmatrix},$$

so $\sigma_D = 4.6$. Next we compute the fixed point ϕ^* for the system with $\sigma = \sigma_D$ iteratively using Newton's method. For this system, the fixed point is

$$\phi^* \approx \begin{pmatrix} 0.895 \\ 0.577 \\ -0.389 \\ -1.081 \\ -0.664 \\ 0.662 \end{pmatrix}.$$

Note that we are working in a reference frame in which $\phi^T 1_N = 0$. Now, compute the weighted Laplacian L_w evaluated at ϕ^* (L_w is equivalent to the Jacobian divided by

σ_D),

$$L_w \approx \begin{pmatrix} -1.92 & 0.95 & 0 & 0 & 0 & 0.97 \\ 0.95 & -1.84 & 0.57 & 0 & 0.32 & 0 \\ 0 & 0.57 & -2.30 & 0.77 & 0.96 & 0 \\ 0 & 0 & 0.77 & -1.68 & 0.91 & 0 \\ 0 & 0.32 & 0.96 & 0.91 & -2.44 & 0.24 \\ 0.97 & 0 & 0 & 0 & 0.24 & -1.22 \end{pmatrix}.$$

As with all rescaled Kuramoto system Jacobians the weights of each off-diagonal term are less than or equal to 1 in magnitude. Additionally, for this graph all off diagonal terms are nonnegative. This is common but not a guaranteed property, as it is possible for some nodes at the fixed point to have phase differences greater than $\frac{\pi}{2}$ across edges. When this happens the cosine of the phase difference is negative.

Now we solve the system $L_w x_r = \omega$ which has as a solution the one-dimensional space

$$x_r \approx \begin{pmatrix} -13.41 \\ -10.85 \\ -1.54 \\ 2.68 \\ 0.99 \\ -13.33 \end{pmatrix} + a \begin{pmatrix} 1 \\ 1 \\ 1 \\ 1 \\ 1 \\ 1 \end{pmatrix},$$

and we choose $a = 13.41$ by convention so that each element of x_r is nonnegative, so

$$x_r \approx \begin{pmatrix} 0 \\ 2.55 \\ 11.87 \\ 16.09 \\ 14.40 \\ 0.08 \end{pmatrix}.$$

Next we define the six x_{bi} vectors according to the criterion cut.

$$x_{b1} = \begin{pmatrix} 1 \\ 0 \\ 0 \\ 0 \\ 0 \\ 0 \end{pmatrix}, x_{b2} = \begin{pmatrix} 1 \\ 1 \\ 0 \\ 0 \\ 0 \\ 1 \end{pmatrix}, x_{b3} = \begin{pmatrix} 1 \\ 1 \\ 1 \\ 0 \\ 0 \\ 1 \end{pmatrix}, x_{b4} = \begin{pmatrix} 1 \\ 1 \\ 1 \\ 1 \\ 1 \\ 1 \end{pmatrix}, x_{b5} = \begin{pmatrix} 1 \\ 1 \\ 1 \\ 0 \\ 1 \\ 1 \end{pmatrix}, x_{b6} = \begin{pmatrix} 1 \\ 0 \\ 0 \\ 0 \\ 0 \\ 1 \end{pmatrix}.$$

x_{b4} is a degenerate solution and is discarded. For the other five choices, we compute the values of $\Lambda(x)$ and $L(C)$,

$$\Lambda(x_{b1}) = 0.7692, \Lambda(x_{b2}) = 0.09, \Lambda(x_{b3}) = 0.1768, \Lambda(x_{b5}) = 0.3508, \Lambda(x_{b6}) = 0.2021,$$

$$L(x_{b1}) = 1.2511, L(x_{b2}) = 4.2499, L(x_{b3}) = 3.5688, L(x_{b5}) = 2.4229, L(x_{b6}) = 3.3690.$$

$\Lambda(x)$ and $L(x)$ are inversely related, so minimizing $\Lambda(x)$ is equivalent to maximizing $L(x)$ and either choice can be made. The conclusions we reach are that x_{b2} is the most likely set of saddle-node clusters and that $\sigma_c \geq L(x_{b2}) = 4.2499$. An exhaustive

search of all 31 possible distinct and non-degenerate partitions of the six nodes into two clusters reveals that $L(x_{b2})$ is the global maximum among the corners of the N-cube.

Additionally, figure 4.2 shows that x_{b2} is the correct prediction for the clusters that form, and the true value of σ_c is approximately 4.303. The binary σ_c and Dörfler σ_c approximations of 4.2499 and 4.6 respectively are lower and upper bounds for the true value of σ_c. For the remainder of this example we will refer to x_{b2} as just x_b, the binary solution to the optimization problem. Due to the symmetry of the problem we could just as easily consider the solution $1_N - x_b$, as all relevant quantities are orthogonal to the vector 1_N.

For this example, we have $\omega^T x_b = 12.6$. This suggests that in this example, the "correct" scaling choice should be $k = 12.6$. If we scale our relaxed solution vector x_r so that $\omega^T x_r = \omega^T x_b = 12.6$, we get the linearly scaled vector

$$x_r \approx \begin{pmatrix} 1.171 \\ 0.985 \\ 0.307 \\ 0 \\ 0.123 \\ 1.165 \end{pmatrix}.$$

The interesting thing about this rescaled vector x_r is that $L(x_r) = 4.3623$. In theorem 2 we proved that $L(x_b)$ is a lower bound for σ_c, and in this example $L(x_r)$ appears to be an upper bound. If this is true in general, then we we have

$$L(x_b) \leq \sigma_c \leq L(x_r) \leq \sigma_D.$$

Presently we are unable to prove that $L(x_r)$ is an upper bound for the critical coupling.

If it is, then to the best of our knowledge $L(x_r)$ is the tightest known upper bound on the critical coupling σ_c for a general networked Kuramoto system, and $L(x_b)$ is the tightest known lower bound. Figure 4.3 shows the steps in this example graphically.

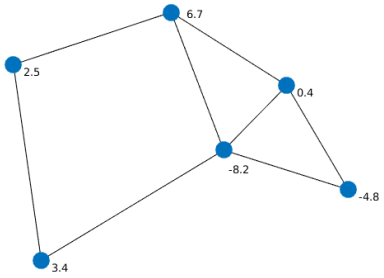

(a) A 6 node Kuramoto system with graph A and frequencies ω. Nodes are labeled with their respective frequencies.

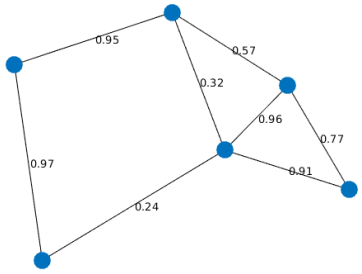

(b) Edge weights determined by the scaled Jacobian matrix L_w of a fixed point ϕ^*.

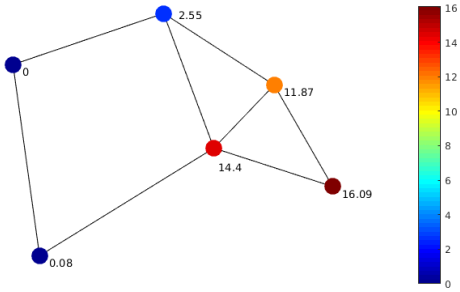

(c) Node weights determined by calculating the relaxed optimization solution. The nodes are colored according to their weights in the relaxed vector x_r.

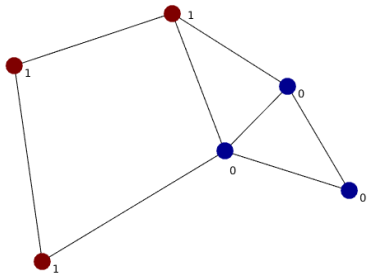

(d) Of the 5 possible cuts on the relaxed vector, the one with the minimum value of $\Lambda(x)$ is displayed.

Figure 4.3: Steps in the isoperimetric algorithm to identify the most likely saddle-node clusters that will form for a 6 node example system.

4.5.3 *Applying Fixed Point Estimation to the Optimization Problem*

The algorithm as described so far for determining clusters is considerable faster than iterative simulation of the system. However one disadvantage is that it requires calculation of a fixed point ϕ^*, which requires iterative applications of Newton's method. It would be nice to replace this step with a direct linear algebra calculation so that the entire algorithm could be only matrix and vector calculations. In fact, the work of Dörfler in (Dörfler *et al.*, 2013) gives us methods to approximate ϕ^* in just this way. We have the approximations

$$B^T\phi^* \approx \sin^{-1}\left(\frac{B^\dagger\omega}{\sigma}\right)$$

and

$$B^T\phi^* \approx \frac{B^\dagger\omega}{\sigma},$$

both of which are uniquely defined when combined with the assumption $\text{mean}(\phi^*) = 0$.

Of course what we really seek for our method is the Laplacian matrix L_w. Given a fixed point ϕ^* or an approximation of ϕ^*, we have defined L_w as

$$L_w(i,j) = \begin{cases} A_{ij}\cos(\phi_j^* - \phi_i^*) & i \neq j \\ -\sum_{k\neq i} L_w(i,k) & \text{otherwise} \end{cases}$$

Noting that L_w is a graph Laplacian, it can be equivalently written as

$$L_w = Bdiag(\cos(B^T\phi^*))B^T$$

Given that ϕ^* satisfies $\omega - \sigma B\sin(B^T\phi^*) = 0$ we can form the approximations

$$\sin(B^T\phi^*) \approx \frac{B^\dagger\omega}{\sigma}$$

and

$$\cos(B^T\phi^*) \approx \sqrt{1_M - \left(\frac{B^\dagger\omega}{\sigma}\right)^2}$$

where $B^\dagger$ is the psuedoinverse of B and vector squaring is done component-wise. Using this approximation for $\cos(B^T\phi^*)$, we can form the approximation for L_w

$$L_w \approx Bdiag\left(\sqrt{1_M - \left(\frac{B^\dagger\omega}{\sigma}\right)^2}\right)B^T. \tag{4.10}$$

This approximation can be calculated directly and is not dependent on the unknown quantity ϕ^*, nor any simulations of any kind. However, the approximate L_w is not guaranteed to produce a lower bound for σ_c, merely an estimate.

4.5.4 Summary of the Isoperimetric Method for Predicting Kuramoto Clusters

The goal of the isoperimetric algorithm for graph reduction is to provide upper and lower bounds for the critical coupling, and to estimate what clusters form when a Kuramoto system desynchronizes. The technique is

1. Choose a reference coupling σ^* at which the Kuramoto system is guaranteed to have a fixed point ϕ^*. A good choice is $\sigma^* = ||B^\dagger\omega||_\infty$, as Dörfler has shown that this value is an upper bound to the critical coupling in most systems. Therefore, a fixed point will exist.

2. Compute the rescaled Jacobian matrix L_w at ϕ^*. L_w is a weighted Laplacian, so it can be expressed in the form $L_w = Bdiag\left(\cos(B^T\phi^*)\right)B^T$, where $\cos(B^T\phi^*)$ is the vector of edge weights, and ϕ^* is the fixed point or an approximate fixed

point of the system at σ^*. We always assume that $1_N\phi^* = 0$, but this still leaves several options to approximate ϕ^*.

Some options for ϕ^* are:

- The actual, true fixed point of the system.
- The least squares approximation to the inconsistent system $B^T\phi^* = \sin^{-1}(\frac{B^\dagger\omega}{\sigma^*})$.
- The solution to the consistent but approximate system $B^T\phi^* = \frac{B^\dagger\omega}{\sigma^*}$. With this choice, we get $L_w = Bdiag\left(\cos(\frac{B^\dagger\omega}{\sigma^*})\right)B^T$.
- Rather than approximate ϕ^*, we can approximate L_w directly as $L_w = Bdiag\left(\sqrt{1_M - (\frac{B^\dagger\omega}{\sigma^*})^2}\right)B^T$, the matrix obtained under the assumption that $B^T\phi^* = \sin^{-1}(\frac{B^\dagger\omega}{\sigma^*})$ is consistent.

We will refer to these as ϕ^* approximations (1) through (4) respectively. In theory, (1) should provide the best results, but it is the most computationally expensive to compute. (2), (3), and (4) each have about the same computation cost, but their effectiveness as an estimation tool varies. Additionally, it may be that any of these four choices could be more susceptible to analysis.

3. Solve $L_w x_r = \omega$ to compute the relaxed solution vector x_r. Note that L_w is rank deficient, as the span of 1_N is always in its null space. To work around this issue, choose an arbitrary reference node i, and delete the ith row and ith column from L_w and the ith element of ω to form $\hat{L}_w$ and $\hat{\omega}$, then solve the system $\hat{L}_w\hat{x}_r = \hat{\omega}$. Obtain a solution for x_r from $\hat{x}_r$ by adding the 0 element reference node which was deleted back in, and then adding any multiple of 1_N which is desired.

   Alternatively, solve the augmented system with $1_N x_r = 0$, and then add any multiple of 1_N to x_r.

4. Find x_b by iteration through x_r. Sort the entries of x_r, then compute the minimum value of $x^T L_w x$ for each of $N-1$ binary roundings of x_r. x_b is an estimate of the characteristic vector of the final two clusters prior to total synchronization.

5. $$L(x_b) = \frac{1}{\sqrt{\left[\frac{x_b^T L_w x_b}{\omega^T x_b}\right]^2 + \frac{1}{\sigma*^2}}}$$
is the binary estimate of the critical coupling.

6. To get the second estimate, replace x_b with a linear multiple of x_r that has an equivalent weight to x_b with respect to the vector ω. The choice $\frac{\omega^T x_b}{\omega^T x_r} x_r$ accomplishes this, and leads to the approximation

$$L(x_r) = \frac{1}{\sqrt{\left[\frac{\omega^T x_b x_r^T L_w x_r}{(\omega^T x_r)^2}\right]^2 + \frac{1}{\sigma*^2}}}.$$
$L(x_r)$ is the relaxed estimate of the critical coupling.

4.6 Numerical Experiments on Predictions of Critical Coupling and Saddle-Node Clusters

The isoperimetric heuristic solution to problem (7) is a fast computation and an estimate of the critical coupling for an arbitrary Kuramoto system. In section 4.6 we test the accuracy of this estimate through numerical experiments. We also compute Adjusted Rand Index (ARI) scores (Rand, 1971) to test the accuracy of the predictions for the saddle-node clusters.

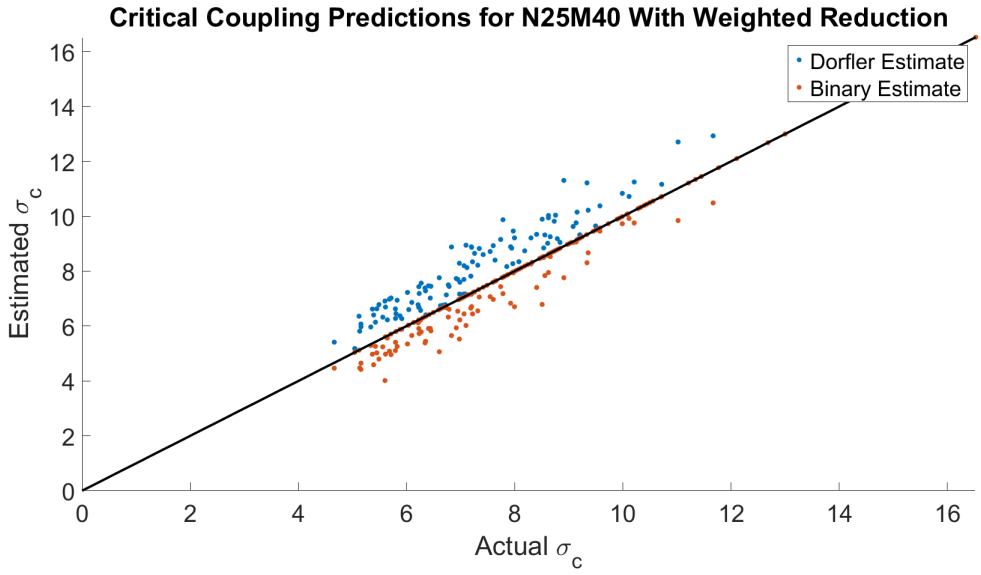

(a) Isoperimetric bounds using the weighted Laplacian at the true fixed point.

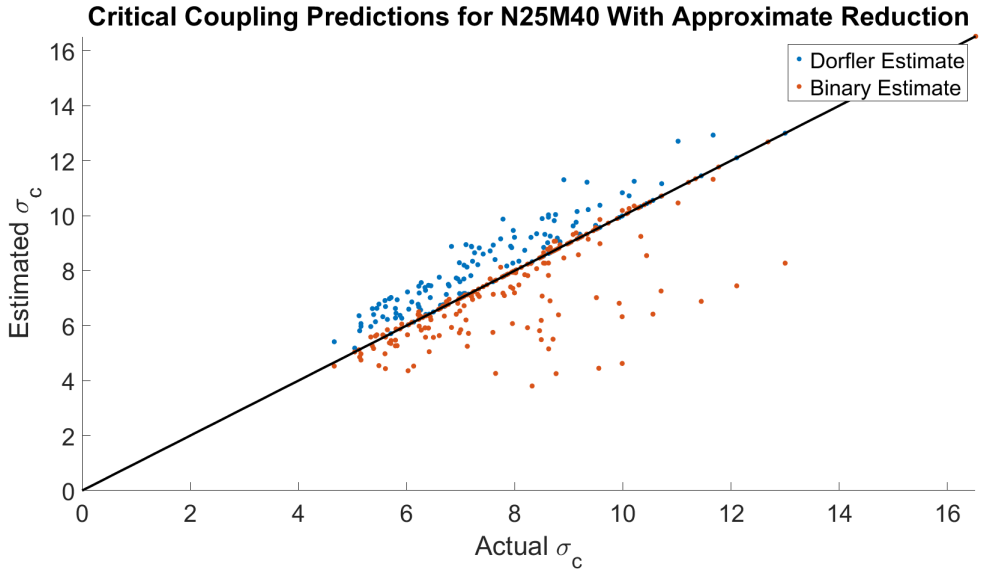

(b) Isoperimetric estimates using the weighted Laplacian with asymptotic estimates for the fixed point.

Figure 4.4: Distributions of estimates for the critical coupling in randomly generated Kuramoto systems.

In figure 4.4 we produced random connected Erdős–Rényi graphs with 25 nodes

and 40 edges and assigned uniformly random frequencies to the nodes. We used the isoperimetric algorithm to approximately solve the optimization problem 6 with the true weighted Laplacian (a) and an approximate weighted Laplacian (b). Additionaly we compared the critical coupling predictions with the Dörfler estimate in (Dörfler *et al.*, 2013). When the Laplacian is weighted with the true steady state phases in (a), the isoperimetric predictions are strict lower bounds with accuracy comparable to the Dörfler estimate. When an approximate Laplacian is used in (b), the accuracy is lowered and the lower boundedness is lost, but computation is sped up significantly.

To compare the accuracy of cluster predictions to those that actually occur at bifurcation in Kuramoto systems, we simulated a large number of random systems and assigned each prediction an ARI score (Rand, 1971). The ARI is a statistical measurement of how well one clustering assignment matches another, adjusted for the probability that elements would be assigned correctly by chance. An ARI of one indicates perfect predictions, while a negative score or a score near zero indicates a prediction indistinguishable from a random guess. Scores in between zero and one are effective predictions with errors.

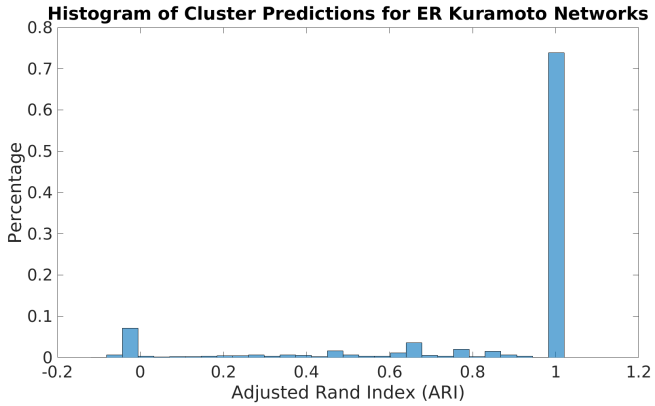

(a) Distribution of ARI for estimates on Erdős–Rényi graphs.

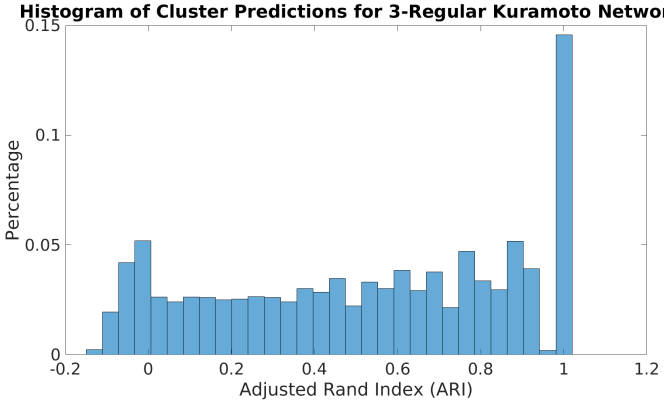

(b) Distribution of ARI for estimates on regular graphs.

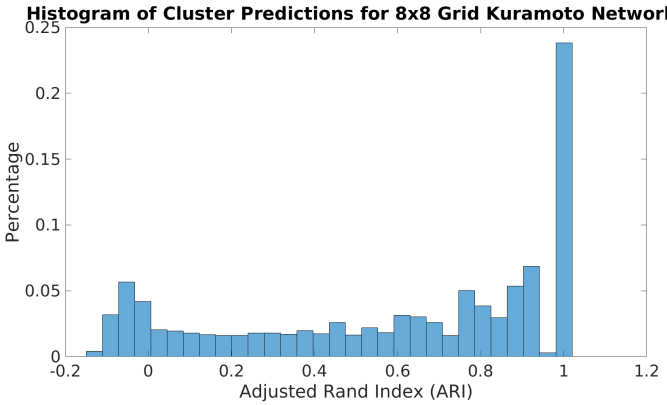

(c) Distribution of ARI for estimates on random regular graphs.

Figure 4.5: Distributions of ARI scores for cluster predictions on assorted network types. 12,000 random systems were created for each type of network and frequencies were chosen uniformly at random.

Figure 4.5 contains data on cluster predictions for 36,000 total random Kuramoto systems of three different network types. Each system had 64 nodes and oscillators were embedded into random Erdős–Rényi, regular graphs of constant degree 3 (Kim and Vu, 2003), or 8x8 rectangular grid networks. The intention of figure 4.5 is to assess the accuracy of the saddle-node cluster predictions using the isoperimetric algorithm and to study how the accuracy depends on the network type. For all network types the most common ARI result was one, indicating a perfect prediction. Predictions were easiest for ER networks, mostly because of the chance that ER networks would have a high bottleneck. Regular and grid networks tend to not have bottlenecks. ARI scores from 0.2 to one are still good and indicate that most of the nodes were assigned to the correct clusters with a low percentage of errors. There were some systems with an ARI score near 0 indicating that the isoperimetric prediction was completely wrong. Some of these were due to systems that had multiple potential bottlenecks of relatively similar severity.

Chapter 5

POWER SYSTEMS

In this dissertation we have imagined the network Kuramoto system as a simplified model for power flow in AC electrical grids. We have used the power grid interpretation as motivation for deciding which analogous questions to ask about the Kuramoto system. Namely, calculating the critical coupling is the analogue of determining if a power grid is in steady state, and identifying synchronized clusters is the analogue of predicting islanding behavior in the event of a blackout. In reality, the network Kuramoto model is far too simple to produce real predictive results for actual power systems, but a second-order model is much closer (Grzybowski *et al.*, 2016).

In chapter 5, we introduce a more advanced second-order power system model based on the swing equation (Anderson and Fouad, 2008). Following the work in(Nishikawa and Motter, 2015) the swing equation is converted into a second-order phase oscillator network model. We show that the second-order model can also be expressed through an order parameter, and see a glimpse of how our methods for analyzing the Kuramoto system can be adapted. We give an interpretation of the optimization program in chapter 4 as a restriction on balanced power flow. Finally, we show numerical clustering predictions for a selection of Kuramoto systems with networks taken from test cases in the MATPOWER software package, and we compare the results of the isoperimetric heuristic to a globally optimal solver.

5.1 The Swing Equation and Nishikawa and Motter's Second-Order Model

In (Nishikawa and Motter, 2015), Nishikawa and Motter converted the swing equation into a unified second-order phase oscillator dynamical system for simulating

power systems.

$$\frac{2H_i}{\omega_R}\ddot{\delta}_i + \frac{D_i}{\omega_R}\dot{\delta}_i = \mathcal{A}_i - \sum_{j\neq i} K_{ij}\sin(\delta_i - \delta_j - \gamma_{ij}) \tag{5.1}$$

Here, each oscillator i represents a generator or load in the power system. For each oscillator, δ_i is the phase angle, H_i and D_i are inertia and damping constants, $\mathcal{A}_i$ is the net power created or used, K is a network admittance matrix, and γ_{ij} is an inductive phase shift along a power line, and ω_R is a reference system frequency. In their paper, Nishikawa and Motter cover many of the pros and cons of different options for calculating each of these parameters, but for our purposes we will just assume that each parameter is specified and constant. If we make the variable changes $\phi_i = \delta_i$, $B_i = \frac{2H_i}{D_i}$, $\omega_i = \frac{\mathcal{A}_i\omega_R}{D_i}$, $A_{ij} = \frac{\omega_R}{D_i}K_{ij}$, then equation (5.1) can be rewritten as

$$B_i\ddot{\phi}_i + \dot{\phi}_i = \omega_i + \sum_{j\neq i} A_{ij}\sin(\phi_j - \phi_i + \delta_{ij}). \tag{5.2}$$

If we assume that the damping constant D_i is identical for all oscillators then A is a symmetric adjacency matrix, and if we assume that the phase shift along power lines is symmetric then $\delta_{ij} = \delta_{ji}$. Under these assumptions, equation 5.2 is a second-order network Kuramoto system on an undirected graph with $\sigma = 1$ and we can again assume a reference frame in which $1_N^T\omega = 0$.

Many of the questions we have about second-order Kuramoto systems can be answered by studying the first-order model. Crucially, the fixed point equation is identical for both models, and thus so is the critical coupling. Near a fixed point, the second-order model is asymptotic to a first-order model and shares the same local stability properties. For a lower bound on the critical coupling and a study of what synchronized clusters are likely below the bifurcation, we perform an analysis analogous to the derivation of equation (3.17). If we take C to be an arbitrary subset

of oscillators in the system and define $\dot{\gamma}_1 = \frac{1}{|C|}\sum_{i\in C}\dot{\phi}_i$, then we can derive the dynamics

$$\beta_1\ddot{\gamma}_1 + \dot{\gamma}_1 = \tilde{\omega} + \frac{\sigma}{|C|}r_C\sin(\gamma_2 - \gamma_1 + Z) \tag{5.3}$$

where

$$\begin{aligned}
\beta_1 &= \left[\sum_{i\in C} B_i\right] \\
r_C^2 &= \sum_{i\in C, j\notin C, r\in C, s\notin C} A_{ij}A_{rs}\cos(\phi_j - \phi_s + \phi_r - \phi_i + \delta_{ij} - \delta_{rs}) \\
\tan(Z) &= \frac{\sum_{i\in C, j\notin C} A_{ij}\sin\left(\frac{1}{|C|}\sum_{k\in C}[\phi_k - \phi_i] - \frac{1}{N-|C|}\sum_{k\notin C}[\phi_k - \phi_j] + \delta_{ij}\right)}{\sum_{i\in C, j\notin C} A_{ij}\cos\left(\frac{1}{|C|}\sum_{k\in C}[\phi_k - \phi_i] - \frac{1}{N-|C|}\sum_{k\notin C}[\phi_k - \phi_j] + \delta_{ij}\right)}.
\end{aligned}$$

Bounds on the critical coupling similar to those in chapter 3 can then be derived, but we omit them in this dissertation. A power systems engineer would be interested in whether the critical coupling is greater than or less than one, because we have $\sigma = 1$ in equation (5.2). We have investigated the second-order Kuramoto model numerically and found that in addition to having identical fixed points to the first-order model, identical cluster-synchronization partitions frequently exist in both models when fixed points do not. The second-order inertial term has a strong effect on the trajectories of periodic orbits and on global stability results, so initial conditions are much more significant in the second-order model.

5.2 Power Grid Interpretation of Critical Coupling Bounds

In steady state power system, not all sections of the grid carry an equal amount of power. Larger, more central lines are built to accommodate a higher capacity of power flow to a larger proportion of users while smaller peripheral lines carry small

amounts of power to fewer people. Additionally, an uneven distribution of demand dictates an uneven distribution of power flow, so even lines of equal quality there may carry radically different amounts of power. Given a single power line and the demand of power through that line, it is relatively trivial to calculate if there is enough capacity to meet the demand. In a power *network*, deciding if the demand can be met is much trickier, because a required amount of power could be drawn from multiple parts of the network. We are interested in identifying the sections of a given power grid which have the most power flow demand relative to their capacity. The function $\Lambda(x)$ in equation 4.4 can be interpreted as a power flow ratio which measures the ratio between capacity and demand for an arbitrary cut x in the grid. If we interpret the cut set as a variable we can optimize the power flow ratio over the entire grid. The cut set which minimizes the ratio is the one closest to capacity in the system.

We can study cluster synchronization in power grids by comparing the required power flow across a set of lines to the total capacity of those lines. It's obvious that for any given set of of power lines the total power flowing through them cannot exceed the sum of their capacities, and if the lines are at capacity then power must be rerouted to other parts of the grid. However if we consider a set of lines which *cut* the grid then there is nowhere else to reroute excess power.

Definition 15. *A subset of edges of a graph are called an edge cut set if removing them increases the number of connected components.*

An edge cut set partitions a connected graph into two *clusters* of nodes based on which side of the cut set the nodes lie. Assuming a balanced power grid and a random cut set, it is highly unlikely that the clusters are individually balanced. One of the clusters will have an excess of power generated while the other has a deficit, and the excess power must flow through the cut set. If the cut set does not have sufficient

capacity then this can lead to islanding behavior in the power grid, analogous to the synchronized clusters in the Kuramoto system below critical coupling. In equation 3.20, the quantity $\left|\omega^T x\right|$ is analogous to the total power that must be transmitted between two clusters. The assertion that $\omega^T 1_N = 0$ is equivalent to assuming the power grid is balanced.

Definition 16. *The Laplacian matrix L of a network with N nodes is defined by*

$$L_{ij} = \begin{cases} -w_{ij} & \text{if an edge exists between nodes } i \text{ and } j \\ 0 & \text{if no edge exists between } i \text{ and } j \\ -\sum_k L_{ik} & \text{if } i = j \end{cases}$$

The Laplacian matrix of a connected graph always has one zero eigenvalue corresponding to the eigenvector 1_N.

In the case where the weights w_{ij} of the graph represent the admittances of their respective electrical lines, L is known as the *admittance matrix* of the network. Given an edge cut set corresponding to a characteristic vector x, the $\left|x^T L x\right|$ term in equation (4.4) is the sum of admittances across lines in the cut set. Given a cut set, we are interested in comparing the power across that cut set with the total admittance of its corresponding edges. This is why we consider $\Lambda(x)$ to be a power flow ratio in the context of power systems.

Definition 17. *The power flow ratio $\Lambda(x)$ is defined by*

$$\Lambda(x) := \left| \frac{x^T L x}{\omega^T x} \right| \tag{5.4}$$

where x is the characteristic vector of a subset C and L is the admittance matrix.

High values of $\Lambda(x)$ (much greater than one) suggest that the edge cut set represented by x has more than enough admittance to accommodate the power that must

flow through it. If $\Lambda(x)$ is close to one, however, this suggests that the power grid is operating close to capacity across this edge set. A ratio less than one is indicative of a system beyond capacity and a fault is likely to occur. Problem 7 is analogous to finding the most critical power flow ratio in the system.

5.3 Applying Fixed Point Estimation to the Optimization Problem as Error Correction

The power flow ratio $\Lambda(x)$ assumes that each line in the cut set formed by x can individually be made to maximize the power flow across that line according to its admittance. In reality, this is often not possible due to the phase constraints of AC power. In an alternating current system, the power that flows across a line is proportional to the sine of the phase difference between the sending and receiving nodes. If this phase difference is a free variable, then the line can reach its capacity if needed. If, however, the line is part of one or more *cycles* in the network, then Kirchoff's law places a constraint on the phase difference (here we refer to a version of Kirchoff's law which states that the sum of phase differences around a cycle in the grid must sum to zero). For each edge in a cut set that is part of a cycle, there must be at least one other corresponding edge in the cut set which is part of the same cycle. Therefore, the phase differences along these two edges are dependent due to the Kirchoff's law constraint, and it may not be possible for each line to reach capacity simultaneously.

To correct for this constraint, we propose using the steady state solution of a balanced power system to approximate the relative phase differences that are achievable. This approximation entails a weighted reduction of each of the admittances in the admittance matrix L, where the reduction factor of each line is given by the cosine of the phase difference across that line in steady state. Such a strategy requires finding

the steady state, or equivalenty the fixed point ϕ^* of a Kuramoto system. This is exactly the difference between the bounds in equations (3.9) and (3.10) from chapter 3. Observations of the Braess paradox in power systems (Coletta and Jacquod, 2016) can be interpreted as situations where lines are connected between nodes with steady state phases greater than $\frac{\pi}{2}$ in difference. These edges would be assigned a negative weight and decrease the power flow ratio.

5.4 Comparing Heuristic and Optimal Approaches for a Selection of Real Power Networks

We calculated minimum values of $\Lambda(x)$ along with their critical partitions x for all of the example power systems included the the MATPOWER package (Gilg and Mittelmann, 2018). We first wanted to see if there were any interesting properties of these systems we could identify by looking at the critical partitions. For most of the test cases, the critical partition consisted of a single node in one cluster, and all the remaining nodes in the opposite cluster. This would suggest that the most probable point of failure in these systems is easily fixable, as the network splitting across such an edge set still leaves the network mostly intact. In this section, we will instead focus on the cases where the critical partition has two large clusters. Intuitively, these partitions are more serious because a failure across a large edge set is more likely to lead to a catastrophic cascade of power failure.

Secondly, we wanted to compare the heuristic solutions produced using the isoperimetric method with the optimal solutions found by traditional global optimization techniques. The isoperimetric heuristic calculation is purely linear algebra and therefore very fast to compute, whereas the global solution requires solving a discrete (binary) decision problem.

In the following cases, the power network topologies are graphed using the second

and third eigenvectors as coordinates. They should not be interpreted as geographical locations of the system nodes, only the graph topology is used. Each partition solution x is represented as a red/blue color map of the nodes, where nodes of one cluster are colored red and the other is colored blue. The choice of red or blue is arbitrary, they are used solely as indicators of the partition. It is also important to recognize that the admittances of lines and the active power required of each oscillator are not displayed in the figures, although they are used to find the partition.

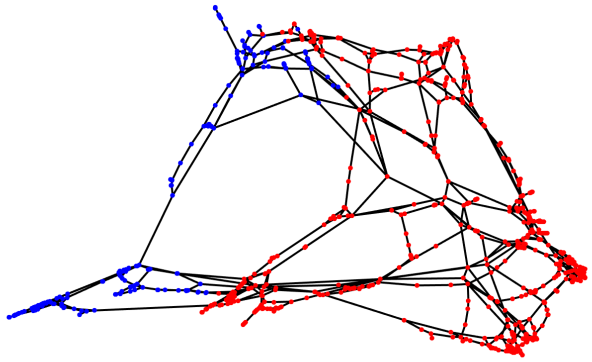

(a) Heuristic solution.

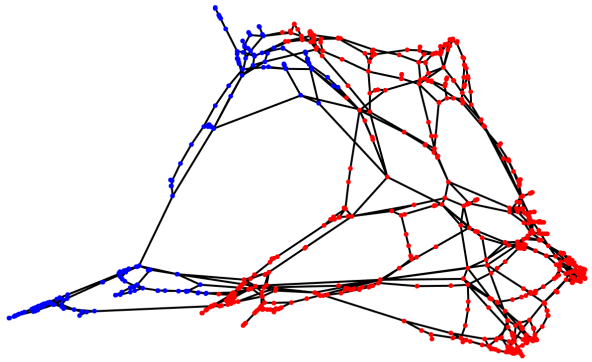

(b) Optimal solution.

Figure 5.1: A comparison of the isoperimetric heuristic algorithm calculation of clusters that minimize $\Lambda(x)$ to an optimal solver for the PEGASE 1354 test case.

The PEGASE 1354 system is a power grid of 1,354 nodes representing a condensed power system in France and the predicted critical saddle-node clusters are pictured in figure 5.1. Although there are clearly many strands of isolated nodes trailing off of various parts of the main network, the critical partition is into two relatively

large clusters which are not immediately obvious from the network topology alone. The smaller strands of nodes either have relatively low power requirements, or have relatively high admittances on their nearby lines, to the point where the most significant power constraint cut set in the system is nontrivial. The heuristic and optimal solutions are *almost* identical, differing by only a single nodes. The isoperimetric algorithm assigns 99.93% of nodes to the correct clusters. The objective value for the heuristic solution is 18% higher than the optimal.

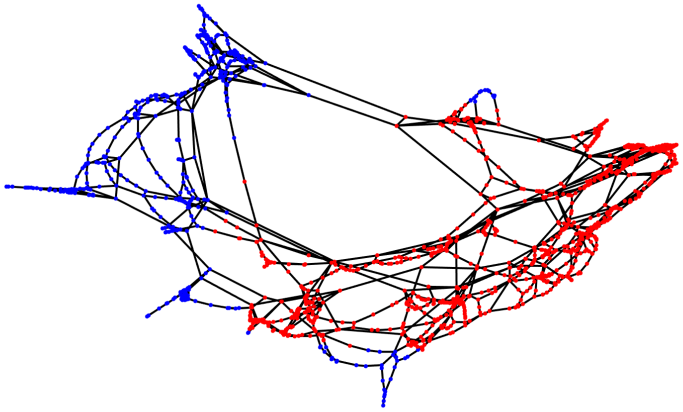

(a) Heuristic solution

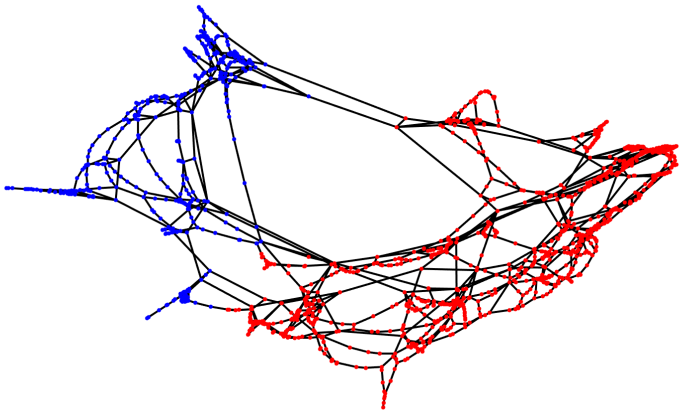

(b) Optimal solution.

Figure 5.2: A comparison of the isoperimetric heuristic algorithm calculation of clusters that minimize $\Lambda(x)$ to an optimal solver for the Polish Winter 2383 test case.

The Polish winter 2383 test case in figure 5.2 is a system of 2,383 nodes representing the power flow of a system in Poland in winter. Just as in the PEGASE case, the critical partition of the system is into two clusters of relatively similar size. Here, the optimal solution is more readily seen from the just the graph topology, the active

power requirements and line admittances are apparently not as relevant. The isoperimetric heuristic solution is significantly different than the optimal. Although they have a high percentage of nodes in common, the heuristic solution is a union of three blue clusters, while the optimal solution is only one. The isoperimetric method is not guaranteed produce a connected solution. The heuristic solution assigns 98.07% of nodes correctly and the objective for the heuristic is 34% higher than for the optimal solution.

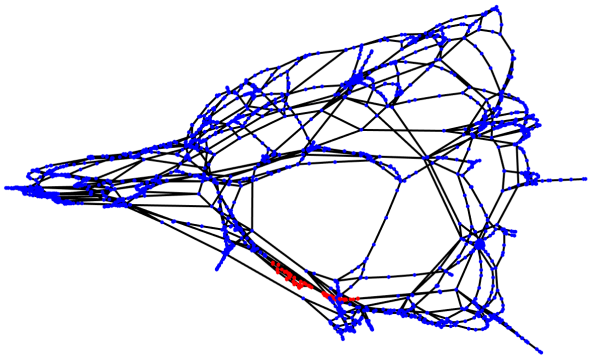

(a) Heuristic solution.

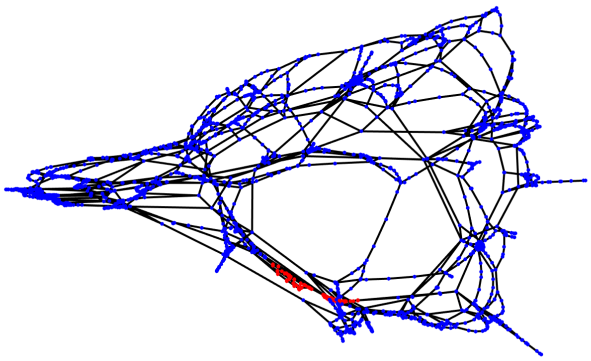

(b) Optimal solution.

Figure 5.3: A comparison of the isoperimetric heuristic algorithm calculation of clusters that minimize $\Lambda(x)$ to an optimal solver for the Polish Winter 3375 test case.

The system in figure 5.3 is another power system in Poland in the winter, this time with 3,375 nodes. The heuristic and optimal solvers in this case differ by only two nodes. 99.94% of oscillators are assigned to the correct cluster and the objective for the heuristic is 11.5% higher than for the optimal solution.

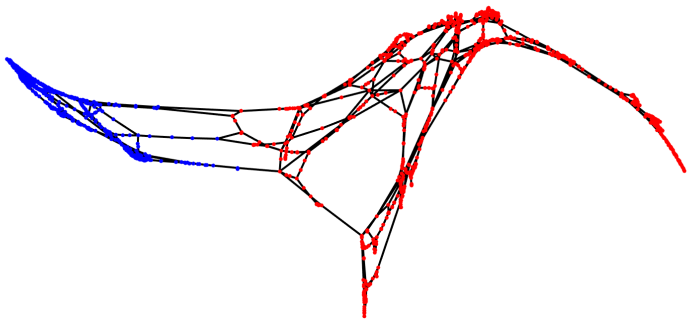

(a) Heuristic solution.

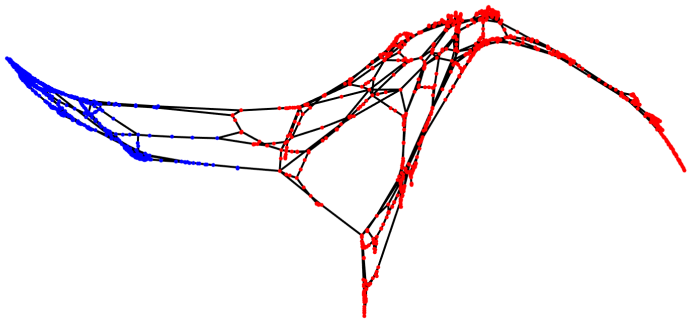

(b) Optimal solution.

Figure 5.4: A comparison of the isoperimetric heuristic algorithm calculation of clusters that minimize $\Lambda(x)$ to an optimal solver for the PEGASE 2869 test case.

Another PEGASE test system from France with 2,869 nodes is in figure 5.4. Remarkably, although the critical partition is nontrivial, both the heuristic and optimal solvers find the same solutions. This is a significant achievement considering that calculating an optimal Cheeger constant is known to be NP-complete and there are

2^{2868} possible two-cluster partitions.

Out of all of the test systems available in MATPOWER, the Polish Winter 2383 case in figure 5.2 had the most extreme difference between heuristic and optimal solutions. The isoperimetric heuristic solution is dramatically faster to compute in comparison to the global solver and assigned 100% of nodes to the correct clusters in more than half of the cases. In the cases where the solution differed, they typically were only different by a tiny percentage of nodes. A complete description of all results will appear in (Gilg and Mittelmann, 2018).

Chapter 6

FUTURE WORK

In the future, we are interested in expanding the optimization approach in problem 7 to estimate the secondary bifurcation from two to three synchronized clusters. Complementary to the network reduction interpretation in section 3.5 this would involve a calculation of the critial coupling for an arbitrary system of three oscillators embedded in a weighted, directed network. There is an enormous jump in complexity from two to three node Kuramoto systems due to the presence of cycles. As described in section 2.7, cycles force a nonlinear constraint on the oscillator phase differences and the phase offsets in coupling terms become relevant for calculating the critical coupling when cycles are present. A qualitative description of the bifurcations for an undirected three node system are found in (Maistrenko *et al.*, 2005), but a quantitative prediction is required to form an optimization problem.

A hierarchichal method could also be developed to predict the secondary bifurcations into three or more clusters. We would first calculate the split into two clusters, and then recursively subdivide each of the resulting clusters to form more. However, as evidenced by figure 3.16, there is a nontrivial chance for a random Kuramoto system to bifurcate directly from one to three or more clusters. In (Boccaletti *et al.*, 2016) these are called first-order phase transitions in contrast to the standard second-order phase transition from one cluster to two. A hierarchichal method could not possibly capture this distinction. We are interested in whether or not an optimization problem approach could.

The critical coupling estimate in problem 7 could be improved with better estimates of $r_C(\sigma)$. In section 3.2 we surveyed a few different approximations for the

standard order parameter including bounds on the curve, a numerical first-order estimate, and an asymptotic expansion. Techniques similar to these could also be used to estimate $r_C(\sigma)$ and obtain a more accurate estimate for the intercept point with $\left|\frac{\tilde{\omega}}{\sigma}\right|$ rather than assume r_C is constant at some fixed phase distribution.

We would like to find Cheeger inequality analogues for the optimization problem 7. (Shewchuk, 2016) gives a proof for a variant of the Cheeger inequalities where vertices are assigned nonnegative masses, but the proof relies on the positive definiteness of a mass-adjusted Laplacian. When ω is used for the vertex masses, some are assigned a negative mass and the Laplacian is no longer positive definite. Despite this, we still believe there exists a Cheeger inequality variation for the problem with negative masses.

One interesting statistic is the expected critical coupling for a Kuramoto system with a network chosen according to some random network type and a fixed, specified frequency vector. That expectation is difficult to compute, but perhaps the expected values of $\max_x L(x)$ or $\min_x \Lambda(x)$ are within reach. These are proxy estimates for the critical coupling, so their distributions would still be interesting. It is reasonable to expect that random matrix theory would have tools to compute statistics like these.

For the second order model in section 5.1 we assumed that all oscillators had identical damping coefficents and each line had symmetrical phase offsets. In the future we would like to drop these assumptions and find an analogue of problem 6 for a more general power systems model. We would also like to better understand the effects the second-order inertial term has on the system trajectories.

Finally, we think it would be interesting to design Kuramoto systems to promote certain synchronization qualities under constraint. One example would be to find the network with some constant number M edges with the minimum critical coupling for a fixed vector of frequencies. A proxy for this problem would be to maximize

$\min_x \Lambda(x)$ or to maximize $\Lambda(x_r)$ where x_r is the relaxed solution to the optimization problem. Optimizing a function of x_r is appealing because the relaxed solution is fast to compute, so heuristic searchers could use monte-carlo based methods like simulated annealing, genetic programming, or machine learning to search a large number of potential networks. It would be interesting to see which types of networks would maximize $\Lambda(x_r)$ or other functions of x_r such as a p-norm, and it would be interesting to see what the dynamics of the Kuramoto systems on those networks would look like.

Motivated by power failures and the phenomenon of geographical islands of AC voltage machines in power grids which oscillate with the same frequency internally but are not synchronized relative to each other, we studied the network Kuramoto model. The network Kuramoto model consists of a network of phase oscillators that experience their own inherent forcing frequency and are coupled nonlinearly to other oscillators through the phase difference between linked oscillators. It is well known that for large coupling strengths such a network will synchronize and oscillate with the mean inherent frequency of all the oscillators. As the coupling strength decreases, this synchronized state becomes unstable at a critical coupling and splits into clusters of oscillators. All oscillators in a cluster on average oscillate with the same frequency but the cluster frequencies differ from each other. In this dissertation we introduce methods to estimate the critical coupling and predict the clusters arising from a saddle node bifurcation for arbitrary and finite Kuramoto networks. We describe an approach that unifies previous approaches to estimate the critical coupling. This unified order parameter allows us to design new and better approximations that can be shown to be strict lower bounds for the critical coupling bifurcation.

Extending this approach we define new cluster order parameters leading to provable cluster-based lower bounds for the critical coupling. We show that finding the maximal lower bound is equivalent to the solution of an optimization problem over cut sets in the network. The relationship between the isoperimetric ratios and the Cheeger constant from spectral graph theory and the cluster-based lower bounds and the maximal lower bound, respectively are elucidated. Adapting the isoperimetric algorithm to approximate the solution to the optimization problem establishes a highly effective method for predicting these saddle-node clusters, confirmed by numerical simulations of clustering for tens of thousands of random networks.

Cycling back to the motivation we interpret the network Kuramoto system in

the context of power systems and perform numerical experiments on real power network test cases with thousands of nodes to assess the veracity of the critical coupling estimates and saddle-node cluster predictions. Typical simulations show correct assignment of network nodes to the bifurcating clusters for more than 95% of the nodes.

Abrams, D. M., L. M. Pecora and A. E. Motter, "Introduction to focus issue: Patterns of network synchronization", Chaos: An Interdisciplinary Journal of Nonlinear Science **26**, 9, 094601 (2016).

Almendral, J., I. Leyva, D. Li, I. Sendiña-Nadal, S. Havlin and S. Boccaletti, "Dynamics of overlapping structures in modular networks", Physical Review E **82**, 1, 016115 (2010).

Anderson, P. M. and A. A. Fouad, *Power system control and stability* (John Wiley & Sons, 2008).

Arenas, A., A. Díaz-Guilera, J. Kurths, Y. Moreno and C. Zhou, "Synchronization in complex networks", Physics reports **469**, 3, 93–153 (2008).

Biggs, N., "Algebraic potential theory on graphs", Bulletin of the London Mathematical Society **29**, 6, 641–682 (1997).

Boccaletti, S., J. Almendral, S. Guan, I. Leyva, Z. Liu, I. Sendiña-Nadal, Z. Wang and Y. Zou, "Explosive transitions in complex networks' structure and dynamics: Percolation and synchronization", Physics Reports **660**, 1–94 (2016).

Chung, F. R., "Laplacians of graphs and cheeger's inequalities", Combinatorics, Paul Erdos is Eighty **2**, 157-172, 13–2 (1996).

Chung, F. R., "Four proofs for the cheeger inequality and graph partition algorithms", in "Proceedings of ICCM", vol. 2, p. 378 (2007).

Coletta, T. and P. Jacquod, "Linear stability and the braess paradox in coupled-oscillator networks and electric power grids", Physical Review E **93**, 3, 032222 (2016).

Dörfler, F. and F. Bullo, "On the critical coupling for kuramoto oscillators", SIAM Journal on Applied Dynamical Systems **10**, 3, 1070–1099 (2011).

Dörfler, F. and F. Bullo, "Synchronization in complex networks of phase oscillators: A survey", Automatica **50**, 6, 1539–1564 (2014).

Dörfler, F., M. Chertkov and F. Bullo, "Synchronization in complex oscillator networks and smart grids", Proceedings of the National Academy of Sciences **110**, 6, 2005–2010 (2013).

Favaretto, C., D. S. Bassett, A. Cenedese and F. Pasqualetti, "Bode meets kuramoto: Synchronized clusters in oscillatory networks", in "American Control Conference (ACC), 2017", pp. 2799–2804 (IEEE, 2017a).

Favaretto, C., A. Cenedese and F. Pasqualetti, "Cluster synchronization in networks of kuramoto oscillators", IFAC-PapersOnLine **50**, 1, 2433–2438 (2017b).

FERC, "Arizona-southern california outages on september 8, 2011", http://www.ferc.gov/legal/staff-reports/04-27-2012-ferc-nerc-report.pdf (2012).

Gilg, B. and H. D. Mittelmann (in preparation, Arizona State University, 2018).

Gómez-Gardenes, J., Y. Moreno and A. Arenas, "Paths to synchronization on complex networks", Physical review letters **98**, 3, 034101 (2007).

Grabow, C., S. M. Hill, S. Grosskinsky and M. Timme, "Do small worlds synchronize fastest?", EPL (Europhysics Letters) **90**, 4, 48002 (2010).

Grady, L. and E. L. Schwartz, "Isoperimetric partitioning: A new algorithm for graph partitioning", SIAM Journal on Scientific Computing **27**, 6, 1844–1866 (2006).

Grzybowski, J., E. Macau and T. Yoneyama, "On synchronization in power-grids modelled as networks of second-order kuramoto oscillators", Chaos: An Interdisciplinary Journal of Nonlinear Science **26**, 11, 113113 (2016).

Hellmann, F., P. Schultz, C. Grabow, J. Heitzig and J. Kurths, "Survivability of deterministic dynamical systems", Scientific reports **6**, 29654 (2016).

Izumida, Y. and H. Kori, "Coarse-grained description of general oscillator networks", arXiv preprint arXiv:1311.0917 (2013).

Jadbabaie, A., N. Motee and M. Barahona, "On the stability of the kuramoto model of coupled nonlinear oscillators", in "American Control Conference, 2004. Proceedings of the 2004", vol. 5, pp. 4296–4301 (IEEE, 2004).

Kim, J. H. and V. H. Vu, "Generating random regular graphs", in "Proceedings of the thirty-fifth annual ACM symposium on Theory of computing", pp. 213–222 (ACM, 2003).

Kundur, P., J. Paserba, V. Ajjarapu, G. Andersson, A. Bose, C. Canizares, N. Hatziargyriou, D. Hill, A. Stankovic, C. Taylor *et al.*, "Definition and classification of power system stability ieee/cigre joint task force on stability terms and definitions", IEEE transactions on Power Systems **19**, 3, 1387–1401 (2004).

Kuramoto, Y., "Self-entrainment of a population of coupled non-linear oscillators", in "International symposium on mathematical problems in theoretical physics", pp. 420–422 (Springer, 1975).

Kuramoto, Y., *Chemical oscillations, waves, and turbulence*, vol. 19 (Springer Science & Business Media, 2012).

Lee, D.-S., "Synchronization transition in scale-free networks: Clusters of synchrony", Physical Review E **72**, 2, 026208 (2005).

Maistrenko, Y. L., O. Popovych and P. Tass, "Desynchronization and chaos in the kuramoto model", Dynamics of coupled map lattices and of related spatially extended systems pp. 285–306 (2005).

Mirollo, R. E., "The asymptotic behavior of the order parameter for the infinite-n kuramoto model", Chaos: An Interdisciplinary Journal of Nonlinear Science **22**, 4, 043118 (2012).

Newman, M., *Networks: an introduction* (Oxford university press, 2010).

Nishikawa, T. and A. E. Motter, "Comparative analysis of existing models for power-grid synchronization", New Journal of Physics **17**, 1, 015012 (2015).

Ottino-Löffler, B. and S. H. Strogatz, "Frequency spirals", Chaos: An Interdisciplinary Journal of Nonlinear Science **26**, 9, 094804 (2016).

Rand, W. M., "Objective criteria for the evaluation of clustering methods", Journal of the American Statistical association **66**, 336, 846–850 (1971).

Rodrigues, F. A., T. K. D. Peron, P. Ji and J. Kurths, "The kuramoto model in complex networks", Physics Reports **610**, 1–98 (2016).

Romeres, D., F. Dörfler and F. Bullo, "Novel results on slow coherency in consensus and power networks", in "Control Conference (ECC), 2013 European", pp. 742–747 (IEEE, 2013).

Schaub, M. T., N. O'Clery, Y. N. Billeh, J.-C. Delvenne, R. Lambiotte and M. Barahona, "Graph partitions and cluster synchronization in networks of oscillators", Chaos: An Interdisciplinary Journal of Nonlinear Science **26**, 9, 094821 (2016).

Schröder, M., M. Timme and D. Witthaut, "A universal order parameter for synchrony in networks of limit cycle oscillators", Chaos: An Interdisciplinary Journal of Nonlinear Science **27**, 7, 073119 (2017).

Shewchuk, J. R., "Allow me to introduce spectral and isoperimetric graph partitioning", `https://people.eecs.berkeley.edu/~jrs/papers/partnotes.pdf` (2016).

Sorrentino, F. and L. Pecora, "Approximate cluster synchronization in networks with symmetries and parameter mismatches", Chaos: An Interdisciplinary Journal of Nonlinear Science **26**, 9, 094823 (2016).

Spielman, D., "Graphs, vectors, and matrices", Bulletin of the American Mathematical Society **54**, 1, 45–61 (2017).

Stout, J., M. Whiteway, E. Ott, M. Girvan and T. M. Antonsen, "Local synchronization in complex networks of coupled oscillators", Chaos: An Interdisciplinary Journal of Nonlinear Science **21**, 2, 025109 (2011).

Strogatz, S. H., "From kuramoto to crawford: exploring the onset of synchronization in populations of coupled oscillators", Physica D: Nonlinear Phenomena **143**, 1, 1–20 (2000).

Verwoerd, M. and O. Mason, "Global phase-locking in finite populations of phase-coupled oscillators", SIAM Journal on Applied Dynamical Systems **7**, 1, 134–160 (2008).

Wikipedia, "Cluster analysis — Wikipedia, the free encyclopedia", http://en.wikipedia.org/w/index.php?title=Cluster%20analysis&oldid=797483030, [Online; accessed 01-September-2017] (2017).

Wiley, D. A., S. H. Strogatz and M. Girvan, "The size of the sync basin", Chaos: An Interdisciplinary Journal of Nonlinear Science **16**, 1, 015103 (2006).

APPENDIX A

CLUSTER ORDER PARAMETER FOR MULTIPLE CLUSTERS

Assume that the oscillators of a Kuramoto system are partitioned into sets $C_1, C_2, C_3, ...$ Define γ_p to be the mean of phases of nodes in C_p.

$$\dot{\gamma}_p = \frac{1}{|C_p|} \sum_{i \in C_p} \dot{\phi}_i$$

$$\dot{\gamma}_p = \frac{1}{|C_p|} \sum_{i \in C_p} \left[\omega_i + \sigma \sum_j A_{ij} \sin(\phi_j - \phi_i) \right]$$

Let

$$\tilde{\omega}_p = \frac{1}{|C_p|} \sum_{i \in C_p} \omega_i$$

for simplification purposes. It is convenient now that any terms in the double sums between nodes of the same cluster will cancel out (assuming the graph is undirected). We therefore only need to consider the cross-cluster connections.

$$\dot{\gamma}_p = \tilde{\omega}_p + \frac{\sigma}{|C_p|} \sum_{i \in C_p, j \notin C_p} A_{ij} \sin(\phi_j - \phi_i)$$

We then rewrite this sum to separate terms within specific clusters.

$$\dot{\gamma}_p = \tilde{\omega}_p + \frac{\sigma}{|C_p|} \sum_{l \neq p} \sum_{i \in C_p, j \in C_l} A_{ij} \sin(\phi_j - \phi_i)$$

where $l \in \{1, 2, ..., k\}$.

We want to rewrite the right hand side in terms of γ_p as much as possible. Add and subtract γ terms within the argument of the sine function.

$$\dot{\gamma}_p = \tilde{\omega}_p + \frac{\sigma}{|C_p|} \sum_{l \neq p} \sum_{i \in C_p, j \in C_l} A_{ij} \sin \left(\phi_j - \phi_i + \gamma_l - \gamma_p - \frac{1}{|C_l|} \sum_{k \in C_l} \phi_k + \frac{1}{|C_p|} \sum_{k \in C_p} \phi_k \right)$$

$$\dot{\gamma}_p = \tilde{\omega}_p + \frac{\sigma}{|C_p|} \sum_{l \neq p} \sum_{i \in C_p, j \in C_l} A_{ij} \sin \left(\gamma_l - \gamma_p - \frac{1}{|C_l|} \sum_{k \in C_l} [\phi_k - \phi_j] + \frac{1}{|C_p|} \sum_{k \in C_p} [\phi_k - \phi_i] \right)$$

Let $\Psi_{lp} = \gamma_l - \gamma_p$ and $Y_{ij} = -\frac{1}{|C_l|} \sum_{k \in C_l} [\phi_k - \phi_j] + \frac{1}{|C_p|} \sum_{k \in C_p} [\phi_k - \phi_i]$. Then,

$$\sum_{i \in C_p, j \in C_l} A_{ij} \sin \left(\Psi_{lp} + Y_{ij} \right) = r_{lp} \sin(\Psi_{lp} + Z_{lp})$$

where

$$r_{lp}^2 = \sum_{i \in C_p, j \in C_l, r \in C_p, s \in C_l} A_{ij} A_{rs} \cos(Y_{ij} - Y_{rs})$$

$$\tan(Z_{lp}) = \frac{\sum_{i\in C_p, j\in C_l} A_{ij}\sin(Y_{ij})}{\sum_{i\in C_p, j\in C_l} A_{ij}\cos(Y_{ij})}$$

$$Y_{ij} - Y_{rs} = \frac{1}{|C_l|}\sum_{k\in C_l}[\phi_k - \phi_s - \phi_k + \phi_j] + \frac{1}{|C_p|}\sum_{k\in C_p}[\phi_k - \phi_i - \phi_k + \phi_r]$$
$$Y_{ij} - Y_{rs} = \phi_j - \phi_s + \phi_r - \phi_i$$

$$r_{lp}^2 = \sum_{i\in C_p, j\in C_l, r\in C_p, s\in C_l} A_{ij}A_{rs}\cos(\phi_j - \phi_s + \phi_r - \phi_i)$$

We can also express r_{lp} using the identity $\cos(\alpha+\beta) = \cos(\alpha)\cos(\beta) - \sin(\alpha)\sin(\beta)$ with $\alpha = \phi_j - \phi_i$ and $\beta = \phi_r - \phi_s$.

$$r_{lp}^2 = \sum_{i\in C_p, j\in C_l, r\in C_p, s\in C_l} A_{ij}A_{rs}[\cos(\phi_j - \phi_i)\cos(\phi_r - \phi_s) - \sin(\phi_j - \phi_i)\sin(\phi_r - \phi_s)]$$

The summation is now separable.

$$r_{lp}^2 = \left[\sum_{i\in C_p, j\in C_l} A_{ij}\cos(\phi_j - \phi_i)\right]^2 + \left[\sum_{i\in C_p, j\in C_l} A_{ij}\sin(\phi_j - \phi_i)\right]^2$$

and

$$\dot{\gamma}_p = \tilde{\omega}_p + \frac{\sigma}{|C_p|}\sum_{l\neq p} r_{lp}\sin(\Psi_{lp} + Z_{lp})$$

Finally, r_{lp} is the cluster order parameter for clusters C_l and C_p.

APPENDIX B

NUMERICAL METHODS

Connected Erdős–Rényi networks with N nodes and M edges were generated by first creating a random spanning tree on the complete graph of size N. A random spanning tree was constructed by choosing a starting node at random and simulating a random walk on the complete graph. Each time a new node was discovered by the random walk, the last traversed edge was added to the spanning tree. This process was repeated until all nodes were visited. The remaining $M - N + 1$ edges were then chosen uniformly from all possible remaining potential pairs of nodes.

Random regular graphs were constructed using the Matlab script provided by (Kim and Vu, 2003).

Fixed points of Kuramoto systems were calculated using Newton's method with convergence assumed once the 2-norm of the residual fell below 10^{-10}.

True critical couplings for Kuramoto systems were calculated using a bisection algorithm. An initial interval was chosen sufficiently large to include the critical coupling, and coupling values at the endpoints were checked for valid fixed points. This was repeated with the interval halved at each repitition until the interval was of length 0.01 or less.

Kuramoto systems were simulated using a forward Euler solver with a timestep of 0.005 and an initial fixed point of all zero phases with inherent frequencies generated uniformly on $[-20, 20]$. To create bifurcation diagrams, systems were simulated for a minimum time of 100 and a minimum of 30% of the beginning of trajectories were thrown out to account for transients. In bifurcation diagrams, initial conditions were chosen to match the ending position of the previous simulation, to minimize transient behavior.